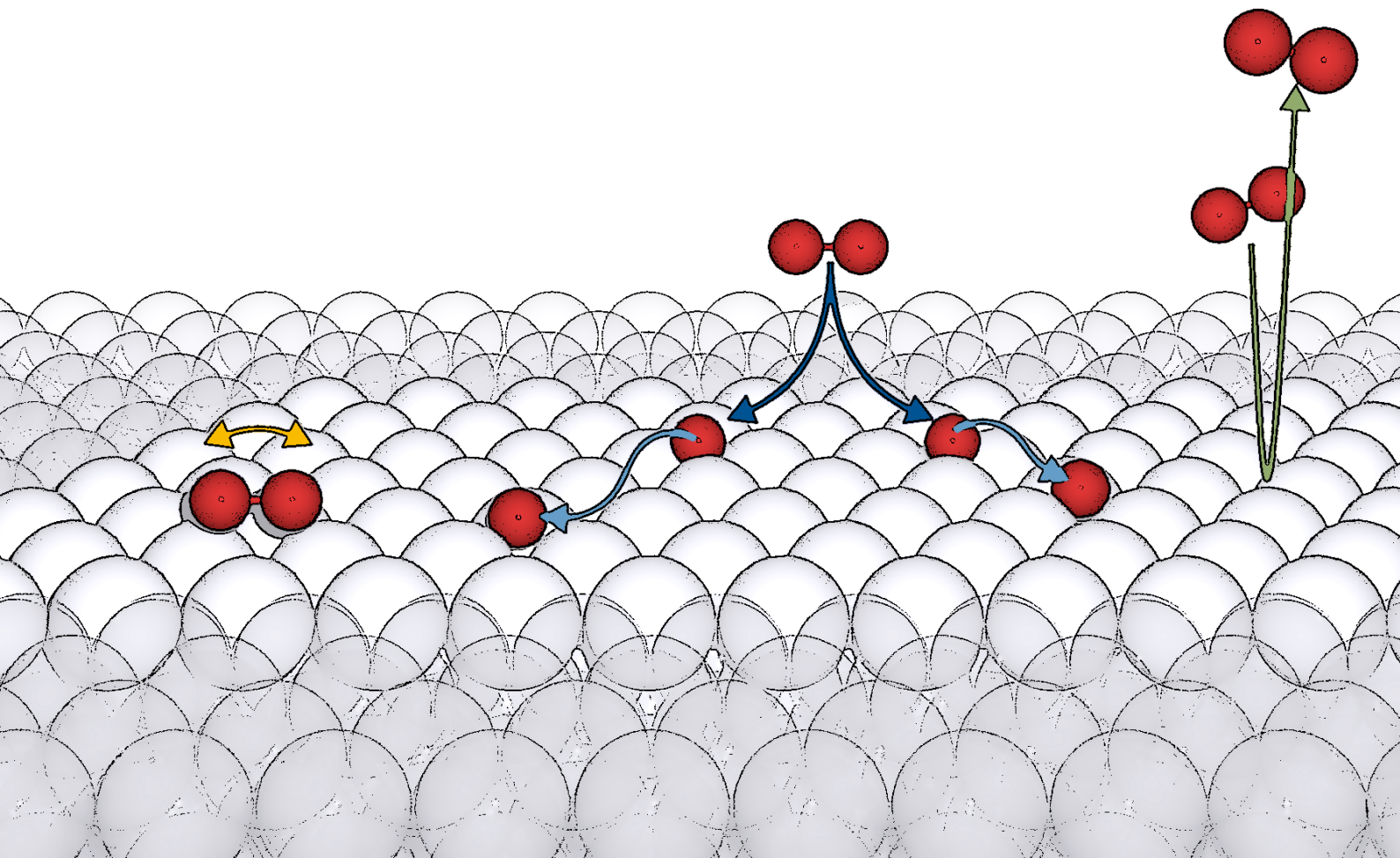**Technische Universität München**
Fakultät für Chemie
Lehrstuhl für Theoretische Chemie

Non-Adiabatic Effects in Gas-Surface Dynamics

Simon Philipp Rittmeyer

Dissertation

Technische Universität München
Fakultät für Chemie
Lehrstuhl für Theoretische Chemie

Non-Adiabatic Effects in Gas-Surface Dynamics

Simon Philipp Rittmeyer

Vollständiger Abdruck der von der Fakultät für Chemie der Technischen Universität München zur Erlangung des akademischen Grades eines

Doktors der Naturwissenschaften (Dr. rer. nat.)

genehmigten Dissertation.

Vorsitzender: Prof. Dr. Klaus Köhler

Prüfer der Dissertation:

1. Prof. Dr. Karsten Reuter

2. Prof. Dr. Ulrich Kaspar Heiz

3. Prof. Dr. Axel Groß (Universität Ulm)

Die Dissertation wurde am 20.09.2017 bei der Technischen Universität München eingereicht und durch die Fakultät für Chemie am 17.10.2017 angenommen.

Für Carolin.

Preface

This dissertation is a publication-based doctoral thesis that centers around work published in Refs. 1, 2, 3, and 4. Corresponding summaries are given in the main body of the thesis, together with a detailed assignment of individual author contributions. Moreover, all corresponding articles are attached to this thesis in form of an appendix.

The added value beyond a bare compilation of published work consists of a concise introduction embedding these manuscripts in a broader context, and thus cumulating them into a consistent piece of work. Moreover, a comprehensive review of the methods and concepts involved in Refs. 1, 2 and 4 is given, allowing for a convenient classification of the underlying level of theory.

All work which is presented was performed between January 2014 and September 2017 at the Chair of Theoretical Chemistry of the Technical University of Munich (TUM), under the supervision of Prof. Dr. Karsten Reuter. Several research stays at the Cavendish Laboratory in Cambridge and the Gorleaus Laboratories in Leiden complement the work performed locally at TUM.

Munich, September 2017

i

Abstract

Surface chemical reactions, for instance in heterogeneous catalysis, are fundamentally governed by the intricate ways in which different forms of energy are converted into each other, and transferred across the gas-solid interface. In this regard, likely dissipation channels on frequently employed metal catalysts are the adsorbate interaction with lattice vibrations, so-called substrate phonons, and the non-adiabatic excitation of electron-hole (*eh*)-pairs in the surface. Whilst important steps towards a high-level explicit modeling of the phononic degrees of freedom have recently been achieved, the quest for an accurate and numerically efficient *first-principles*-based description of electronically non-adiabatic adsorbate dynamics on metal surfaces is still ongoing.

A promising, yet disputed candidate in this regard is the concept of electronic friction within the local density friction approximation (LDFA). This cumulative thesis explicitly demonstrates the LDFA model to yield reasonable results for the vibrational damping of high-frequency adsorbate vibrations on various metal surfaces. Additionally, a simple and computationally very efficient strategy to extend the LDFA beyond the hitherto inherent independent-atom approximation is suggested, further improving upon its good performance. The role of *eh*-pair excitations in surface diffusion events is subsequently scrutinized. Here, a comparison of respective LDFA-based simulations with experimental Helium-3 spin echo measurements allows to decompose empirically obtained friction coefficients into electronic and phononic contributions. Consequently, for the thermal diffusion of Na on Cu(111) a surprisingly high degree of non-adiabaticity is found, suggesting a significant role of *eh*-pair excitations in the rapid thermalization generally relied upon in adiabatic diffusion theories.

The electronic friction approach avoids explicit electron dynamics and concomitant ultrafast time scales, but for these reasons it also precludes a more fundamental understanding of the underlying *eh*-pair excitations. Hence, using a perturbation theory-based approach rooted in time-dependent density functional theory explicit *eh*-pair excitation spectra are evaluated. For the vibrational damping of CO on several metal surfaces, a surprisingly strong influence of short electronic coherence times is thus found, ultimately verifying the Markov approximation implicitly assumed in electronic friction theory. Lastly, this thesis concludes with an extensive review on computational gas-surface dynamics, with a specific focus on theoretical models of increasing complexity to include phononic and non-adiabatic energy exchange with the surface.

Zusammenfassung

Die Dynamik von Oberflächenreaktionen, beispielsweise im Bereich der heterogenen Katalyse, wird maßgeblich von den vielfältigen darin involvierten Energieaustausch- und -umwandlungsprozessen an der Festkörperoberfläche bestimmt. Dabei findet der Energietransfer über die Grenzfläche, sogenannte Dissipation, hauptsächlich durch die Anregungen von Gitterschwingungen des Substrates statt. Im Falle metallischer Substrate konkurriert dieser phononische Dissipationskanal darüber hinaus mit der nicht-adiabatischen Anregung von Elektron-Loch-Paaren. Während jedoch eine *ab initio*-basierte explizite Beschreibung der phononischen Freiheitsgrade mittlerweile weit fortgeschritten ist, bleibt die Suche nach einer verlässlichen Modellierung nicht-adiabatischer Oberflächendynamik auf Metalloberflächen nach wie vor Gegenstand aktueller Forschung.

Ein diesbezüglich vielversprechender, wenn auch nicht unumstrittener Ansatz ist das Konzept der elektronischen Reibung im Rahmen der *local density friction approximation* (LDFA). In diesem Zusammenhang demonstriert die vorliegende publikationsbasierte Dissertation, dass auch mit diesem approximativen LDFA-Modell eine gute Beschreibung der nicht-adiabatischen Dämpfung hochfrequenter Adsorbatschwingungen für mehrere kleine Moleküle auf verschiedenen metallischen Substraten erfolgen kann. Darüber hinaus wird eine einfache und zugleich sehr effiziente Strategie vorgeschlagen, um die LDFA über die bis dato vorherrschende *independent-atom approximation* hinaus zu erweitern und so deren gute Leistung noch weiter zu verbessern. Anschließend wird sich der Rolle nicht-adiabatischer Elektron-Loch-Paar Anregungen in Diffusionsprozessen auf Metalloberflächen zugewandt. Hierzu werden experimentelle Helium-3 Spin-Echo Messungen mit Hilfe LDFA-basierter Simulationen analysiert, was eine Quantifizierung der individuellen phononischen und nicht-adiabatischen Kopplungstärken erlaubt. Für die thermische Diffusion von Na auf Cu(111) wird so überraschend hoher Einfluss nicht-adiabatischer Effekte identifiziert. Dieser legt eine bedeutende Rolle des Kontinuums von Elektron-Loch-Paar Anregungen in den unmittelbaren Thermalisierungsprozessen nahe, die vielen Diffusionstheorien zu Grunde liegen.

Der Ansatz elektronischer Reibung vermeidet eine direkte Beschreibung der zu Grunde liegenden elektronischen Anregungen und umgeht damit die Notwendigkeit einer expliziten Elektronendynamik auf der Femtosekunden Zeitskala. Diese implizite Beschreibung der elektronischen Freiheitsgrade ist maßgeblich für die numerische Effizienz, verhindert allerdings auch ein tiefer greifendes Verständnis der Ursprünge nicht-adiabatischer Effekte. Daher wird im weiteren Verlauf ein störungstheoretischer Ansatz verwendet, um die entsprechenden Elektron-Loch-Paar Anregungen explizit aufzulösen. Für die Schwingungsdämpfung von CO auf mehreren Metalloberflächen wird so ein überraschend großer Einfluss kurzer Kohärenzzeiten der elektronischen Anregungen identifiziert, was im Umkehrschluss die fundamentale Markov-Näherung im Rahmen der elektronischen Reibungstheorie validiert. Letztlich schließt diese kumulative Dissertation mit einem umfangreichen Übersichtsartikel zu Arbeiten im Bereich der Gas-Oberflächen Dynamik, wobei ein besonderer Fokus auf der Modellierung des phononischen und nicht-adiabatischen Energiedissipationskanals liegt.

Contents

List of Abbreviations

AIM	atoms-in-molecules	**LDA**	local density approximation
AIMD	*ab initio* molecular dyamics	**LDFA**	local density friction approximation
ASE	Atomic Simulation Environment	**MD**	molecular dynamics
BO	Born-Oppenheimer	**MO**	molecular orbital
BOA	Born-Oppenheimer approximation	**ODF**	orbital-dependent friction
DFT	density functional theory	**PBE**	Perdew, Burke and Ernzerhof
DOF	degree of freedom	**PES**	potential energy surface
DOS	density of states	**QM/Me**	QM/Me (embedding approach coupling a classical description of the metallic substrate with a quantum mechanical description of the adsorbate region)
eh	electron-hole (pair)		
FS	frozen surface		
GGA	generalized gradient approximation		
GLO	generalized Langevin oscillator	**SEQ**	Schrödinger equation
GSD	gas-surface dynamics	**SO**	surface oscillator
^{3}**He-SE**	Helium-3 spin echo	**TD-DFT**	time-dependent density functional theory
HEG	homogeneous electron gas		
HF	Hartree-Fock	**TDPT**	time-dependent perturbation theory
HGT	Head-Gordon and Tully		
IAA	independent-atom approximation	**TDSCF**	time-dependent self-consistent field
KS	Kohn-Sham	**xc**	exchange-correlation

1 Introduction

Dynamical processes at the gas-solid interface lie at the heart of many industrial applications of great technological value such as heterogeneous catalysis [5]. Here, different forms of energy are constantly converted into each other and the intricate ways in which this happens ultimately influence not only reaction rates but also the corresponding specificity and yield [6]. For instance, an imping-ing molecule may—in the simplest case—be reflected from a catalyst surface, thereby potentially converting parts of its initial translational energy into rotational and/or vibrational energy of the backscattered molecule or exciting vibrations in the underlying lattice [7, 8]. It may, however, as well dissociate above the surface. In this case, chemical energy stored within a molecular bond is transferred into kinetic energy of the respective fragments, resulting in fascinating phenomena such as hyperthermal diffusion [9] and immediate follow-up reactions in terms of a transient "hot" chem-istry [10]. Moreover, also the thermalization process quenching these phenomena is an interesting matter on its own, being inherently determined by the rate of energy exchange with the underlying substrate [11]. But also in case of indirect dissociation, an adsorbed molecular precursor state may first accumulate a significant amount of vibrational energy in order to dissociate. Given a suitable nano-catalyst, such a vibrational pumping can even be achieved very selectively using visible light [12, 13], yet leaving the resulting athermal mode population challenged by the rapid energy dissipation into the remaining degrees of freedom (DOFs) of the system.

Likely candidates to this end are—besides further (internal) molecular vibrations—foremost vibrational DOFs of the catalyst surface, so-called substrate phonons [14–16]. In principal, corre-sponding effects can "easily" be incorporated in computational simulations by modeling mobile substrate atoms whose equations of motion are integrated explicitly, thereby following nuclear forces as obtained from a single well-defined potential energy surface (PES). An appropriate representation of phonons and their picosecond-scale propagation distances, however, calls for system sizes that go well beyond the typical slab models required to accommodate the adsorbate-substrate chemical interaction. Adequate sampling of the phononic fine structure within an explicit treatment of the (bulk) thermal bath will therefore quickly blow up the problem's dimensionality, and hence also the computational cost that comes therewith. Initially, this mostly stimulated the development of effective theories to account for adsorbate-phonon interactions [14, 15]. With the advent and growing feasibility of explicit *ab initio* molecular dyamics (AIMD) simulations based on density functional theory (DFT) [11, 16, 17], however, the challenge of including an increasingly accurate description of the phononic energy dissipation channel in gas-surface dynamics (GSD) nowadays has emancipated from overcoming conceptual limitations of effective models, and arrived at a point that is mostly limited by computational resources [3].

On frequently employed metal catalysts, however, phonons are not the sole actor in terms of energy dissipation at the surface. An additional channel to be considered here is the adsorbate-induced excitation of typically low-energy electron-hole (*eh*)-pairs in the substrate. Emerging from a dynamical coupling of the adsorbate nuclear motion to the metallic continuum of electronic states, the mere abundance of these excitations may in principle render each dynamical process at metal surfaces electronically non-adiabatic [15, 18]. Supported by a rapidly increasing amount of

experimental evidence [19–26], this suggests a breakdown of the ubiquitous and most fundamental Born-Oppenheimer approximation (BOA) [27, 28] in many situations. In turn, these observations question the common practice description of adsorbate-substrate interactions on the level of a single, electronically adiabatic ground-state PES that is uniquely defined by the static nuclear configuration. While the latter has otherwise served to the great success of numerous dynamical studies [3], the "beyond-BOA" picture introduces an overwhelming manifold of possible excitations. Practical dynamical simulations are thus stumped by the daunting prospect of, in principle, additionally requiring an explicit quantum mechanics-based consideration of all electronic degrees of freedom fluctuating on the sub-femtosecond time scale.

In contrast to the conceptually simple addition of more and more surface DOFs in order to improve the description of the phononic channel, propagating combined nuclear-electron wave functions that would naturally include also electronic excitations is intractable for at least decades to come in the context of GSD [29]. Including electronically non-adiabatic effects in computational simulations thus inevitably requires further simplifications such as applying a mixed quantum-classical description of the system in terms of a mean field Ehrenfest [29, 30] or surface hopping framework [30–33], coarse graining the electron dynamics using time-dependent perturbation theory (TDPT) [34, 35], or entirely replacing the latter within an effective Langevin-description of the nuclear motion in terms of electronic friction [36–38]. Yet, each step further away from an exact dynamical treatment of the electronic DOFs introduces another set of approximations, the validity of which is often difficult to assess, as suitable experimental benchmark observables are scarce [3]. A shroud of uncertainty thus remains not only with respect to the validity of the effective non-adiabatic models applied, but also in a broader context regarding the relevance of the competing energy dissipation channels and their specific influence on the actual adsorbate dynamics [3, 15, 25].

This ambiguous situation sets the stage for the cumulative thesis in hand that centers around work (to be) published in Refs. 1–4. In Ref. 3 we have reviewed the current state of computational GSD with a particular focus on techniques to incorporate the competing phononic and non-adiabatic energy dissipation channels in corresponding simulations. While doing so, we specifically highlighted the persisting difficulty of gauging their performance based on experimentally accessible observables—a particular concern for the effective non-adiabatic models involved. Aiming to improve upon this situation, in Ref. 1 we assessed the accuracy of the to-date most commonly used electronic friction approach in terms of the local density friction approximation (LDFA). To this end, we compared non-adiabatic vibrational lifetimes of several diatomics on metal substrates as obtained therewith to experimental and theoretical reference values. We found a satisfying agreement for "off-the-shelf" LDFA already, and introduced a simple and computationally very efficient strategy to further improve upon this performance. With this confidence we then applied the LDFA model to atomic surface diffusion in Ref. 2. Here, combining respective simulations with Helium-3 spin echo measurements we were ultimately able to quantitatively disentangle the phononic and non-adiabatic contributions to the dynamical adsorbate-surface coupling. Lastly, in Ref. 4 we re-addressed the vibrational damping of small molecules on metal surfaces, yet this time resolving the underlying *eh*-pair excitations using a TDPT-based approach. We could thus test crucial assumptions underlying electronic friction theory, and identified a quasi Markovian-behavior of the electronic DOFs as an important reason for their good performance.

Referring to our work in Ref. 3 for an extensive literature review, the following chapters are intended to provide a broader context for the methods and concepts involved in the publications associated with this cumulative thesis. A clear focus in this regard is on a detailed discussion of non-adiabatic dynamics in chapter 2. Starting from the most fundamental time-dependent Schrödinger equation,

a concise definition of "non-adiabatic effects" will be given first, in passing also introducing the concept of molecular dynamics. Only afterwards, stepwise simplifications to the quantum many-body problem will be presented, thereby conveniently classifying the theoretical approaches used in this thesis. Chapter 3 then addresses ways to evaluate the electronic structure properties serving as a common basis for all non-adiabatic simulations, regardless of the particular effective model. Here, focus is on the ubiquitous density functional theory. A subsequent presentation of the concept of normal modes and its periodic extension to phonons in chapter 4 ultimately concludes this methodological part. The thesis is altogether completed by extensive summaries of the contained publications as well as a detailed assignment of individual author contributions in chapter 5, and a conclusive outlook in chapter 6.

2 Non-Adiabatic Dynamics

The most rigorous (yet non-relativistic) approach to any gas-surface dynamical problem lies within the solutions of the time-dependent Schrödinger equation (SEQ)

$$i\hbar \frac{\partial}{\partial t} \Psi(t) = \hat{\mathcal{H}} \Psi(t). \tag{2.1}$$

Here, the time-evolution of the many body wave function $\Psi(t)$ describing the full system is determined by the Hamilton operator $\hat{\mathcal{H}}$ (*vide infra*). Aiming for a full solution of Eq. (2.1) is a formidable goal that would yield an exact dynamical description of the nuclei on a quantum mechanical level and naturally include the multitude of possible electronic quantum transitions through, e.g., the creation of electron-hole (*eh*)-pairs. Within this framework, all degrees of freedom (DOFs) were thus treated on an equal footing, which renders non-adiabatic effects in nuclear dynamics (evolving on potential energy surfaces (PESs)) an obscure artificial concept [29]. However, such a full quantum mechanical description of the dynamical system is—even to date—limited to the complexity level of smallest gas phase molecules [39–41]. For significantly more complex systems as usually encountered in gas-surface dynamics (GSD), further approximations are thus inevitable in order to ultimately arrive at a numerically feasible (classical) description of the nuclear motion that is suitably coupled to the electronic degrees of freedom.

In a first step, one thus starts with a separation of *fast* and *slow* coordinates, r and R. Within the context of this work, the former can be thought of as electrons and the latter apply to the nuclei. The following concepts, however, are valid beyond this particular distinction. Without any loss of generality, the Hamiltonian from Eq. (2.1) is then

$$\hat{\mathcal{H}} = -\frac{\hbar^2}{2} \sum_{\alpha} M_{\alpha}^{-1} \nabla_{R_{\alpha}}^2 \underbrace{-\frac{\hbar}{2} \sum_{\beta} m_{\beta}^{-1} \nabla_{r_{\beta}}^2 + \hat{V}_{rR}(r, R)}_{:= \hat{\mathcal{H}}_r(r;R)}. \tag{2.2}$$

Here, M_{α} and m_{β} are the masses of slow and fast particle α and β. Throughout this thesis a Cartesian coordinate system is used unless stated differently. The operator $\hat{V}_{rR}(r, R)$ accounts for all interparticle interactions. In the present context, this would include electron-nuclear attraction, electron-electron and nuclear-nuclear repulsion. Separating the kinetic energy operator for the fast particles allows to define $\hat{\mathcal{H}}_r(r;R)$ as the Hamilton operator for the fast particles at a fixed slow particle-configuration R. For the present purpose, it can thus be considered as *electronic Hamiltonian*. It is further convenient to define the eigenstates of the latter as *adiabatic* or *Born-Oppenheimer (BO)* basis functions[1]

$$\hat{\mathcal{H}}_r(r;R) \phi_j^{\text{BO}}(r;R) = \mathcal{E}_j^{\text{BO}}(R) \phi^{\text{BO}}(r;R). \tag{2.3}$$

---

[1]This choice is of course not unique. Another frequently employed basis set in this context is the *diabatic* representation [29].

This choice yields a complete and orthonormal basis over $\boldsymbol{r}$ for any given (fixed) slow particle configuration $\boldsymbol{R}$. The full system wave function can thus be expanded in a Born-Huang series [28]

$$\Psi(\boldsymbol{r}, \boldsymbol{R}, t) = \sum_j \chi_j(\boldsymbol{R}, t) \phi_j^{\text{BO}}(\boldsymbol{r}; \boldsymbol{R}), \tag{2.4}$$

where the expansion coefficients $\chi_j(\boldsymbol{R}, t)$ are identified as slow particle wave functions. Lastly, the eigenvalues of $\hat{\mathcal{H}}_{\boldsymbol{r}}(\boldsymbol{r}; \boldsymbol{R})$ define the Born-Oppenheimer PESs $\mathcal{E}_j^{\text{BO}}(\boldsymbol{R})$ for fast particle state j. The evaluation of these eigenvalues can be a formidable challenge on its own already, in particular for extended systems. Chapter 3 hence deals with ways to obtain the latter by means of density functional theory. For the moment, however, the particular method used to evaluate the BO-PES is of secondary importance only.

2.1 Adiabatic and Born-Oppenheimer Approximation

When the full quantum system is separated with the ultimate goal to treat both of the remaining parts on a different level, the obviously most crucial task is to incorporate a consistent feedback or coupling between the two subsystems. Such feedback is obviously exactly incorporated for a system in which one completely excludes fast-particle quantum transitions, thus implying the slow particle motion to evolve on an ever same, single adiabatic PES (not necessarily the ground state). This assumption constitutes the so-called *adiabatic approximation*.

Inserting the exact system wave function from Eq. (2.4) into Eq. (2.1) followed by multiplication with $\phi_i^{\text{BO}*}(\boldsymbol{r}; \boldsymbol{R})$ from the left and a subsequent integration over $\boldsymbol{r}$ yields for the time evolution of the slow particle wave function

$$i\hbar \frac{\partial}{\partial t} \chi_i(\boldsymbol{R}, t) = \left[-\frac{\hbar^2}{2} \sum_\alpha M_\alpha^{-1} \nabla_{\boldsymbol{R}_\alpha}^2 - \frac{\hbar^2}{2} \sum_\alpha M_\alpha^{-1} \left(2 \sum_j \boldsymbol{d}_{ij}^\alpha \cdot \nabla_{\boldsymbol{R}_\alpha} - \sum_j D_{ij}^\alpha \right) + \mathcal{E}_i^{\text{BO}}(\boldsymbol{R}) \right] \chi_i(\boldsymbol{R}, t), \tag{2.5}$$

where $\boldsymbol{d}_{ij}^\alpha$ is the non-adiabatic coupling vector

$$\boldsymbol{d}_{ij}^\alpha = \int \phi_i^{\text{BO}*}(\boldsymbol{r}; \boldsymbol{R}) \left[\nabla_{\boldsymbol{R}_\alpha} \phi_j^{\text{BO}}(\boldsymbol{r}; \boldsymbol{R}) \right] d\boldsymbol{r} \equiv \langle \phi_i^{\text{BO}}(\boldsymbol{r}; \boldsymbol{R}) | \nabla_{\boldsymbol{R}_\alpha} | \phi_j^{\text{BO}}(\boldsymbol{r}; \boldsymbol{R}) \rangle_{\boldsymbol{r}}. \tag{2.6}$$

It should be noted that $\boldsymbol{d}_{ij}^\alpha$ is anti-Hermitian for non-degenerate wave functions and thus $\boldsymbol{d}_{ii}^\alpha = \boldsymbol{0}$ [42]. In Eq. (2.5), the second derivatives coupling has further been defined as

$$D_{ij}^\alpha = -\int \phi_i^{\text{BO}*}(\boldsymbol{r}; \boldsymbol{R}) \left[\nabla_{\boldsymbol{R}_\alpha}^2 \phi_j^{\text{BO}}(\boldsymbol{r}; \boldsymbol{R}) \right] d\boldsymbol{r} \equiv -\langle \phi_i^{\text{BO}}(\boldsymbol{r}; \boldsymbol{R}) | \left(\nabla_{\boldsymbol{R}_\alpha}^2 | \phi_j^{\text{BO}}(\boldsymbol{r}; \boldsymbol{R}) \rangle_{\boldsymbol{r}} \right). \tag{2.7}$$

An adiabatic system without $i \to j$ transitions in the fast particles' quantum state is then straightforwardly constructed by approximating the wave function from Eq. (2.4) via a simple product

$$\Psi(t) \approx \chi_i(\boldsymbol{R}, t) \phi_i^{\text{BO}}(\boldsymbol{r}; \boldsymbol{R}). \tag{2.8}$$

Equation (2.5) consequently transforms into the adiabatic SEQ

$$i\hbar \frac{\partial}{\partial t} \chi_i(\boldsymbol{R}, t) = \left[-\frac{\hbar^2}{2} \sum_\alpha M_\alpha^{-1} \nabla_{\boldsymbol{R}_\alpha}^2 + \frac{\hbar^2}{2} \sum_\alpha M_\alpha^{-1} D_{ii}^\alpha + \mathcal{E}_i^{\text{BO}}(\boldsymbol{R}) \right] \chi_i(\boldsymbol{R}, t). \tag{2.9}$$

Although obviously present in the adiabatic approximation for the wave function, the remaining term D_{ii}^α is often unwarily termed non-adiabatic correction to the BO-PES. It is, however, usually on the order of a rotational energy splitting [29] and can thus often be neglected, thereby constituting the actual Born-Oppenheimer approximation (BOA) [27]. If one choses $\phi_i^{\mathrm{BO}}(r; R)$ to be the fast particles' ground state, the physical interpretation of the adiabatic (and BO) approximation is readily at hand. The slow particles evolve on the ground state BO-PES without inducing any quantum transitions in the fast particles. Transferred to nuclei and electrons, the electronic subsystem thus instantaneously adapts to any changes in the nuclear configuration and relaxes to the respective BO ground state.

As suggested by Messiah [43] and nicely demonstrated in Refs. 29, 44 and 45, the classical limit of Eq. (2.9) can be obtained by decomposing the slow particle wave function into an amplitude and phase factor, separating real and imaginary contributions and setting $\hbar \to 0$. This ultimately yields the Hamilton-Jacobi equation which is equivalent to Newton's classical equation of motion

$$M_\alpha \ddot{\boldsymbol{R}}_\alpha = -\nabla_{\boldsymbol{R}_\alpha} \mathcal{E}_i^{\mathrm{BO}}(\boldsymbol{R}). \tag{2.10}$$

Here, the dots symbolize time derivatives, and $\boldsymbol{P}_\alpha$ is the classical mechanical momentum of slow particle α. This picture constitutes what is often (and also unwarily) referred to as Born-Oppenheimer approximation in many chemistry textbooks. It forms the conceptual basis for a plethora of intuitive concepts, most prominently that of classical nuclei evolving on a single, unique BO-PES within molecular dynamics (MD) simulations.

Regarding the validity of the adiabatic approximation, one may obtain a first guess from evaluating the probability of fast particle quantum transitions along an independent slow particle path $\boldsymbol{R}(t)$ as nicely shown by Tully [29]. In this case, non-adiabatic $i \to j$ transitions are unlikely as long as

$$\left| \frac{\pi \left(\mathcal{E}_i^{\mathrm{BO}} - \mathcal{E}_j^{\mathrm{BO}} \right)}{\hbar \dot{\boldsymbol{R}} \cdot \sum_\alpha \boldsymbol{d}_{ij}^\alpha} \right| \gg 1, \tag{2.11}$$

which is essentially the Massey criterion [46]. Thus, for systems with energetically well separated adiabatic states such as many molecules and insulators, the adiabatic approximation seems to be very reasonable. However, if energy differences between states become very small, e.g., close to an avoided crossing, or generally on a metal surface with the concomitant continuum of states at the Fermi level, the validity of the adiabatic (and Born-Oppenheimer) approximation is very questionable. In such cases, one has to consider the non-vanishing probability of non-adiabatic transitions in the fast particles' quantum system induced by the slow particle motion.

The following three sections will thus demonstrate ways that were used in the context of this work to approximately evaluate and investigate these transitions and their effect on the actual slow particle, i.e., nuclear dynamics. The obviously crucial ingredient in this regard is the *dynamical* coupling between the two subsystems[2]. This can be approximated as one-way coupling in order to efficiently obtain *eh*-pair excitation spectra along a classical nuclear path from time-dependent perturbation theory as we did in Ref. 4. It can, however, also be a mutual coupling with an implicit treatment of the electronic degree of freedom by means of a Langevin framework. Focus is then shifted towards nuclear dynamics under so-called electronic friction, as we applied in Refs. 1 and 2.

---

[2]Also within the BOA the fast and slow particles are coupled, but only statically. The slow particles evolve on the BO-PES, which is in turn the fast particles' eigenvalues for the instantaneous, fixed slow particle configuration.

2.2 Time-Dependent Perturbation Theory

Rather than ignoring any dynamical feedback between the fast and slow variables as done in the previous section, one may consider situations in which only the one way-coupling from the slow to the fast system is of interest. This assumption implies that there are ways—regardless of how complicated they may be—to evaluate a (classical) slow particle path $R(t)$ *independently* of the fast particles' dynamics (e.g., using BO-MD simulations). In such a case, a slow particle trajectory

$$R = R(t) \tag{2.12}$$

can be specified in advance. This in turn gives rise to an implicitly time-dependent fast particle Hamiltonian that determines the respective dynamics along the trajectory. Whilst of course such an approach is not completely self-consistent, it nevertheless allows for valuable insight into quantum transitions in the fast particle system. One example following this idea is the time-dependent perturbation theory-based approach to *eh*-pair excitations in the context of vibrational damping that we presented in Ref. 4.

The fundamental idea behind this approach is the assumption that the fast particles' Hamiltonian can be separated into a static and a time-dependent contribution

$$i\hbar\frac{\partial}{\partial t}\Phi(r;R(t)) = \hat{\mathcal{H}}_r(r;R(t))\Phi(r;R(t)) = \left[\hat{\mathcal{H}}_0(r) + \hat{V}_{\text{pert}}(r;R(t))\right]\Phi(r;R(t)), \tag{2.13}$$

where $\hat{V}_{\text{pert}}(r;R(t))$ is referred to as *perturbation potential*. The eigenstates of the so-gained static Hamiltonian $\hat{\mathcal{H}}_0(r)\phi_j(r) = \varepsilon_j\phi_j(r)$ then form a complete (orthonormal) basis such that one can expand the time-dependent fast particle wave function according to

$$\Phi(r;t) = \sum_j c_j(t)\phi_j(r)\exp\left(-\frac{i}{\hbar}\varepsilon_j t\right). \tag{2.14}$$

Inserting this expansion into Eq. (2.13) yields for the amplitudes (see, e.g., Ref. 47)

$$i\hbar\frac{\partial}{\partial t}c_i(t) = \sum_j c_j(t)V_{ij}(R(t))\exp\left(i\omega_{ij}t\right), \tag{2.15}$$

where $\omega_{ij} = (\varepsilon_i - \varepsilon_j)/\hbar$, and the perturbation matrix elements are

$$V_{ij}(R(t)) = \int \phi_i^*(r)\hat{V}_{\text{pert}}(r;R(t))\phi_j(r)\,dr. \tag{2.16}$$

Together with appropriate boundary conditions for the amplitudes, Eq. (2.15) yields an *exact* solution for the time-dependent wave function in Eq. (2.13). Solving this coupled differential equation would thus still not lower the computational demand. One can, however, gain a first order approximation by implying a small change in amplitudes only. Assuming that the system is in an eigenstate $\phi_i(r)$ at $t = 0$, the right hand side of Eq. (2.15) can then be replaced with the respective initial values prior to the perturbation, i.e., $c_j(t = 0) = \delta_{ij}$. This yields a first order rate for the amplitude of state j in the fast particles' system

$$\frac{\partial}{\partial t}c_j(t) = \frac{1}{i\hbar}V_{ij}(R(t))\exp\left(i\omega_{ij}t\right). \tag{2.17}$$

Equation (2.17) can be seen as the population change induced by the perturbation potential. Not asking for the actual fast particle dynamics but rather for the net effect of the perturbation after a time t lastly allows to evaluate the concomitant $i \to j$ excitation probability by integration according to

$$P_{i \to j}^{(1)}(t) = \left| \delta_{ij} + \frac{1}{i\hbar} \int_0^{t'} V_{ij}(\mathbf{R}(t')) \exp\left(i\omega_{ij}t'\right) dt' \right|^2. \tag{2.18}$$

An excitation spectrum can then be obtained by collecting all transition probabilities and sampling at energy $\hbar\omega$

$$P_{\mathrm{ex}}^{(1)}(\hbar\omega, t) = \sum_{ij} P_{i \to j}^{(1)}(t)\delta(\hbar\omega - \hbar\omega_{ij}). \tag{2.19}$$

Of course, even the evaluation of this first-order expression can be highly demanding, depending on the form of the time-dependent perturbation potential. For certain textbook models such as a constant $[V_{ij}(\mathbf{R}(t)) = V_{ij}]$ or purely harmonic perturbation $[V_{ij}(\mathbf{R}(t)) = V_{ij}\exp(\pm i\omega_{\mathrm{pert}}t)]$, however, one can readily anticipate an excitation spectrum—given that the static contributions V_{ij} can be somehow quantified at a later stage. The qualitative result in both cases are spectra with distinct peaks at $\omega = 0$ and $\omega = \pm\omega_{\mathrm{pert}}$ for the constant and harmonic perturbation, respectively. In the long-time limit ($t \to \infty$) these peaks will approach a δ-function and only resonant transitions will accumulate an appreciable excitation probability [4, 47, 48].

A common notion in textbooks [47, 48] is hence that energy conservation is recovered in the long-time limit, imposed by the δ-function. This is somewhat misleading, though, since assuming a constant amplitude V_{ij} implies a perturbation potential that is unaffected by the excitations it triggers (consistent with the assumed one-way coupling) and thus represents an infinite source of energy. There is thus no overall energy conservation but rather a *resonance* with the external perturbation. If, however, the coupling between fast and slow degrees of freedom is mutual and the perturbation is thus not external, then the δ-function indeed ensures energy conservation for the total system. This is, e.g., the case in the context of a quantum nuclear treatment of vibrational energy relaxation. Here, one considers the nuclear kinetic energy operator as non-adiabatic perturbation coupling adiabatic vibronic states [49–52].

At this point, it should further be noted that Eq. (2.18) implies a *perfect coherence* in the fast particle system over the entire integration range. This means that the phase factors contained in the integrand of Eq. (2.18) will remain as such from time $t' = 0$ to $t' = t$. It is yet these phase factors that are accountable for the long-term discrimination of off-resonant transitions. In other words, it is the fast particles' "memory" that allows for resonant-exclusive excitations in this limit. Lifting this assumption of a perfect electronic coherence—that counteracts the ideas underlying the electronic friction approach presented in section 2.4—is a centerpiece of the work we published in Ref. 4. Here, we investigated *eh*-pair excitation spectra induced by the vibrational motion of CO on different metal surfaces based on the framework presented here. Even though a harmonic model perturbation may seem like a good approximation for this problem, we rather followed a snapshot approximation [34, 35, 53] to evaluate the time-dependent perturbation potential directly from first principles. Referring to Refs. 4, 35 and 53 for details, using suitable boundary conditions this ultimately yields for the perturbation potential

$$V_{ij}(\mathbf{R}(t)) = \dot{\mathbf{R}}(t) \cdot \nabla_{\mathbf{R}} \int \phi_i^{\mathrm{KS}*}(\mathbf{r}) \hat{v}_{\mathrm{eff}}^{\mathrm{KS}}(\mathbf{R}) \phi_j^{\mathrm{KS}}(\mathbf{r}) \, d\mathbf{r}, \tag{2.20}$$

where $\phi_i^{\text{KS}}(\mathbf{r})$ are Kohn-Sham (KS) states and $\hat{v}_{\text{eff}}^{\text{KS}}(\mathbf{R})$ is the effective KS-potential (cf., chapter 3). The particular clue is that it is actually sufficient to evaluate the (static) matrix elements along the nuclear trajectory $\mathbf{R}(t)$. The latter can then be interpolated using, e.g., cubic splines thus altogether yielding a numerically highly efficient way to calculate the perturbation matrix elements [35, 53].

2.3 Ehrenfest Dynamics

The perturbation-theory based approach presented in the previous section is an efficient way to evaluate the response of the fast particles to the slow particle motion. It yet comes at the cost of a non-self consistent coupling or feedback between the two subsystems. One way to maintain such a consistent feedback is to follow time-dependent self-consistent field (TDSCF) or—in the classical limit for the slow particles—Ehrenfest dynamics. As the latter is essential to understand the concept of electronic friction, which our work in Refs. 1 and 2 is based on, the following section aims at presenting an overview of the most fundamental aspects. For further details, the interested reader is referred to the excellent reviews and book chapters by Tully [29, 30, 54], Doltsinis [42] and Drukker [44].

The fundamental assumption here is that the total time-dependent wave function from Eq. (2.4) can be approximated as a single product of a slow and fast particle wave function $\chi(\mathbf{R}, t)$ and $\Phi(\mathbf{r}, t)$, respectively

$$\Psi(t) \approx \chi(\mathbf{R}, t)\Phi(\mathbf{r}, t)\exp\left(\frac{\mathrm{i}}{\hbar}\int_0^t E_{\mathbf{r}}(t')\,\mathrm{d}t'\right). \tag{2.21}$$

Note, that in contrast to the adiabatic wave function in Eq. (2.8), the fast particle wave function is not restricted to be a single BO state and thus does not explicitly depend on $\mathbf{R}$ but carries a direct time-dependence. The additional phase factor in Eq. (2.21) is inserted for convenience in order to simplify the final equations [29, 30]. Both, $\chi(\mathbf{R}, t)$ and $\Phi(\mathbf{r}, t)$ are further assumed to be normalized over the respective coordinate subspace at each time. With an appropriate choice of the phase factor as detailed in Refs. 29 and 30 the wave function from Eq. (2.21) then yields an effective Schrödinger equation for the slow and fast particles, respectively,

$$\mathrm{i}\hbar\frac{\partial}{\partial t}\chi(\mathbf{R}, t) = \left\{-\frac{\hbar}{2}\sum_\alpha M_\alpha^{-1}\nabla_{\mathbf{R}_\alpha}^2 + \int \Phi^*(\mathbf{r}, t)\hat{\mathcal{H}}_{\mathbf{r}}(\mathbf{r}; \mathbf{R})\Phi(\mathbf{r}, t)\,\mathrm{d}\mathbf{r}\right\}\chi(\mathbf{R}, t), \tag{2.22}$$

$$\mathrm{i}\hbar\frac{\partial}{\partial t}\Phi(\mathbf{r}, t) = \left\{-\frac{\hbar}{2}\sum_\beta m_\beta^{-1}\nabla_{\mathbf{r}_\beta}^2 + \int \chi^*(\mathbf{R}, t)\hat{V}_{\mathbf{r}\mathbf{R}}(\mathbf{r}, \mathbf{R})\chi(\mathbf{R}, t)\,\mathrm{d}\mathbf{R}\right\}\Phi(\mathbf{r}, t). \tag{2.23}$$

These are the fundamental TDSCF equations that have to be solved self-consistently. The slow particles evolve in the average field of the fast particles *et vice versa*. It should be noted that the resulting mean field dynamics are a direct consequence of choosing a single-configuration wave function according to Eq. (2.21). One way to overcome this limitation is by opting for a multi-configurational approach, which—in the classical limit for the slow particles—ultimately results in surface hopping dynamics [29–31].

The classical limit for Eq. (2.22) can be obtained in a similar manner as mentioned in section 2.1 before. This ultimately yields for the slow particle equation of motion

$$M_\alpha\ddot{\mathbf{R}}_\alpha = -\nabla_{\mathbf{R}_\alpha}\left[\int \Phi^*(\mathbf{r}, \mathbf{R}, t)\hat{\mathcal{H}}_{\mathbf{r}}\Phi(\mathbf{r}, \mathbf{R}, t)\,\mathrm{d}\mathbf{r}\right]. \tag{2.24}$$

As mutual feedback between the slow and fast particles is considered here, the classical limit also has to be incorporated in Eq. (2.23). This can be done by replacing $\chi(\mathbf{R}, t)$ with a delta function at $\mathbf{R}$, resulting in

$$i\hbar \frac{\partial}{\partial t} \Phi(\mathbf{r}, \mathbf{R}, t) = \hat{\mathcal{H}}_{\mathbf{r}}(\mathbf{r}, \mathbf{R}) \Phi(\mathbf{r}, \mathbf{R}, t). \tag{2.25}$$

Following Tully's notation [29], the by now explicit dependency of the fast particle wave function on the classical coordinate $\mathbf{R}$ in this limit is indicated in Eqs. (2.24) and (2.25). The mixed quantum-classical dynamics defined in these equations constitute the so-called Ehrenfest method. The suggested physical picture are thus classical slow particles (nuclei), that evolve on a mean field potential corresponding to the expectation value of the fast particle (electronic) Hamiltonian. However, this expectation value is *not* necessarily a pure BO-PES but rather an occupation average of all BO-PES that has to be evaluated self-consistently at each step of a simulation.

The inherent mean field character of the Ehrenfest method gives rise to several deficiencies such as violated microscopic reversibility, false behavior of the wave function in the asymptotic limits of configurational space in terms of non-pure adiabatic states, and the unphysical pickup of energetically inaccessible states in the wave function. All of these deficiencies are nicely depicted in the book chapter by Doltsinis [42]. They become particularly pronounced in situations were significantly different BO-PESs with regions of strong non-adiabatic couplings are involved yielding state-specific diverging paths. For instance, a charge transfer process either occurs or not, and is definitely poorly described by a "mean" trajectory [38]. In such cases, multi-configurational surface hopping schemes [29–31] are obviously a better alternative [42]. Luckily, however, highly delocalized *eh*-pair excitations in a metal—as considered in the context of this work—are not expected to yield vastly different BO-PESs and so mean field dynamics may yield very reasonable results [29, 38].

2.4 Molecular Dynamics with Electronic Friction

Besides the conceptual deficiencies of the Ehrenfest approach, the coupled fast and slow particle dynamics still impose a high computational burden. This is particularly problematic considering the extremely small time steps—typically on the order of a few attoseconds only [55–57]—required to properly capture electron dynamics. To thus also access larger time scales on the order of several picoseconds, a nuclear dynamics scheme is desirable that on the one hand incorporates effects beyond the adiabatic and Born-Oppenheimer approximation, i.e., excitations and relaxations in the electronic system, but on the other hand does not require an explicit propagation of the electronic degrees of freedom. These demands call for a friction-like picture of the classical dynamics on an effective PES in which the coupling to the fast particles is implicitly accounted for within a generalized Langevin framework.

The motivation for such a scheme, in fact, becomes very obvious when $\Phi(\mathbf{r}, \mathbf{R}, t)$ is expanded in a BO basis according to

$$\Phi(\mathbf{r}, \mathbf{R}, t) = \sum_j c_j(t) \phi_j^{\mathrm{BO}}(\mathbf{r}, \mathbf{R}). \tag{2.26}$$

Inserting this expansion in Eq. (2.25) yields a set of coupled differential equations for the amplitudes associated with the fast particles

$$i\hbar \dot{c}_i(t) = c_i(t) \mathcal{E}_i^{\mathrm{BO}}(\mathbf{R}) - i\hbar \sum_j c_j(t) \sum_\alpha \mathbf{d}_{ij}^\alpha(\mathbf{R}) \cdot \dot{\mathbf{R}}_\alpha, \tag{2.27}$$

whereas inserting Eq. (2.26) in Eq. (2.24) results in the respective classical equation of motion for the slow particles (see Ref. 29 for a detailed derivation)

$$M_\alpha \dot{\boldsymbol{R}}_\alpha = - \underbrace{\sum_j \left| c_j(t) \right|^2 \nabla_{\boldsymbol{R}_\alpha} \mathcal{E}_j^{\mathrm{BO}}(\boldsymbol{R})}_{\text{averaged BO-PES forces}} - \underbrace{\sum_{i \neq j} c_j^*(t) c_i(t) \left[\mathcal{E}_j^{\mathrm{BO}}(\boldsymbol{R}) - \mathcal{E}_i^{\mathrm{BO}}(\boldsymbol{R}) \right] \sum_\alpha \boldsymbol{d}_{ji}^\alpha(\boldsymbol{R})}_{\text{forces due to quantum transitions}}. \qquad (2.28)$$

Obviously, the forces on the classical particles are not just the occupation averaged forces from the individual BO-PES but there is a second term that mixes in forces originating from transitions between adiabatic states. These "transition forces" thus account for changes in the mean field PES and are rigorously imposed by total energy conservation.

In a metal, excited conduction electrons are typically highly delocalized and are thus not expected to significantly alter the shape, i.e., the $\boldsymbol{R}$-dependence of the respective PESs [38]. In other words, the PESs are expected to be parallel (and continuously spaced) and thus the corresponding forces should be virtually identical. In turn this implies that the first term in Eq. (2.28) can be replaced by the ground state forces. Energy exchange between the classical and quantum system is thus only due to quantum transition between the parallel PESs. Considering adsorbate dynamics on a metal surface, Tully nicely summarized this situation as an adsorbate moving on a single (ground state BO-) PES thereby receiving small impulses of energy from the coupling to eh-pair excitations in the substrate [29]. The link of this picture with that of nuclear motion under frictional and random forces is thus not far to seek. On the other hand, it is also clear that such a description, while likely suitable to incorporate non-adiabatic effects due to delocalized eh-pair excitations in the substrate, may break down completely when also electronic transitions between adsorbate states of significantly different shape become important.

In their seminal work Head-Gordon and Tully (HGT) [38] were able show that it is indeed possible—starting from Eqs. (2.27) and (2.28)—to cast the classical nuclear equation of motion into a generalized Langevin framework (see Ref. 58 for a very instructive presentation of the latter)

$$M_\alpha \ddot{\boldsymbol{R}}_\alpha = -\nabla_{\boldsymbol{R}_\alpha} \mathcal{E}_0^{\mathrm{BO}}(\boldsymbol{R}) - \sum_\beta \int_0^t \Lambda_{\boldsymbol{R}_\alpha \boldsymbol{R}_\beta}(t, t') \dot{\boldsymbol{R}}_\beta \, \mathrm{d}t' + \mathcal{F}_{\boldsymbol{R}_\alpha}(t). \qquad (2.29)$$

Here, defining $\omega_{ji} = \left[\mathcal{E}_j^{\mathrm{BO}}(\boldsymbol{R}) - \mathcal{E}_i^{\mathrm{BO}}(\boldsymbol{R}) \right]/\hbar$ as the (constant) vertical energy difference between the BO states,

$$\Lambda_{\boldsymbol{R}_\alpha \boldsymbol{R}_\beta}(t, t') = 2\hbar \sum_j \sum_\beta \left[\boldsymbol{d}_{j0}^\alpha(\boldsymbol{R}(t)) \otimes \boldsymbol{d}_{j0}^\beta(\boldsymbol{R}(t')) \right] \omega_{j0} \cos \left[\omega_{j0}(t - t') \right] \qquad (2.30)$$

is the so-called friction kernel condensing the effects of the fast particle dynamics. The fluctuating force $\mathcal{F}_{\boldsymbol{R}_\alpha}(t)$ is related to the friction kernel and the effective system temperature T through its autocorrelation function following the fluctuation-dissipation theorem [59]

$$\langle \mathcal{F}_{\boldsymbol{R}_\alpha}(t) \mathcal{F}_{\boldsymbol{R}_\beta}(t') \rangle = k_{\mathrm{B}} T \Lambda_{\boldsymbol{R}_\alpha \boldsymbol{R}_\beta}(t, t'). \qquad (2.31)$$

At this point it should be noted that in the original derivation, HGT started from Ehrenfest dynamics and thus relied on a single-configurational approach—an insufficient description at finite temperatures [38]. This is the reason why they had to postulate Eq. (2.31) rather than consistently derive it. Very recently, Dou, Miao, and Subotnik published a more rigorous derivation of the electronic

friction approach based on a mixed quantum-classical Liouville equation including temperature and correlation effects through the electronic density matrix, yet recovering the HGT friction kernel from Eq. (2.30) under equivalent initial assumptions [60].

The replacement of the explicit electronic dynamics in Eq. (2.29) is valid within the so-called *weak coupling approximation* [38], often also referred to as *weak non-adiabaticity*. Mathematically this limit is well defined and refers to conditions at which the harmonic oscillator-like variables resulting from an action-angle transformation of the electronic amplitudes $c_i(t)$ (cf., Eqs. (2.26) to (2.28)) couple linearly rather than quadratically to the nuclear coordinates. The corresponding physical interpretation and validity, however, are somewhat intricate. Head-Gordon and Tully identified two criteria in this regard. First, the non-adiabatic energy transfer per unit time should be small, and second, one has to be able to reset the electronic system to a pure adiabatic state corresponding to the correct average energy after a characteristic time comparable to the shortest nuclear motion of interest [38]. The latter condition implies some sort of limited electronic coherence and thus "short-time memory" of the electronic degrees of freedom.

In fact, Eq. (2.29) is not the form of electronic friction that is used in actual MD simulations these days. This is mainly due to the fact that even though the electronic degrees of freedom are no longer explicitly considered, the evaluation of the friction kernel Eq. (2.30) and the concomitant non-adiabatic coupling vector at each time step still imposes a huge computational burden, in particular for extended systems [38]. Hence, one consequently follows the "short time memory"-spirit and proceeds with a Markovian approximation that localizes the friction kernel in time such that a (regular) Langevin equation of motion is recovered

$$M_\alpha \ddot{\boldsymbol{R}}_\alpha = -\nabla_{\boldsymbol{R}_\alpha} \mathcal{E}_0^{\mathrm{BO}}(\boldsymbol{R}) - \sum_\beta \boldsymbol{\eta}_{\boldsymbol{R}_\alpha \boldsymbol{R}_\beta}(\boldsymbol{R}) \cdot \dot{\boldsymbol{R}}_\beta + \boldsymbol{\mathcal{F}}_{\boldsymbol{R}_\alpha}(t), \tag{2.32}$$

where the friction tensor $\boldsymbol{\eta}_{\boldsymbol{R}_\alpha \boldsymbol{R}_\beta}$ is the Markovian limit of the friction kernel

$$\boldsymbol{\Lambda}_{\boldsymbol{R}_\alpha \boldsymbol{R}_\beta}(t, t') \xrightarrow[\text{limit}]{\text{Markovian}} 2\boldsymbol{\eta}_{\boldsymbol{R}_\alpha \boldsymbol{R}_\beta} \delta(t - t'). \tag{2.33}$$

It is still a position dependent ($N \times N$) matrix with N being the number of nuclear DOFs, yet without the explicit time-dependence of the former kernel. Thus, in a pictorial sense, non-adiabatic effects are attributed to quantum transitions within a memoryless electronic subsystem that forgets about the past immediately. The fluctuation-dissipation theorem then consequently becomes

$$\langle \boldsymbol{\mathcal{F}}_{\boldsymbol{R}_\alpha}(t) \boldsymbol{\mathcal{F}}_{\boldsymbol{R}_\beta}(t') \rangle = k_{\mathrm{B}} T \boldsymbol{\eta}_{\boldsymbol{R}_\alpha \boldsymbol{R}_\beta} \delta(t, t'), \tag{2.34}$$

which classifies the fluctuating forces as (uncorrelated) white noise.

Altogether, the trust in the electronic friction approach in the form of Eq. (2.32) lies particularly on the fact that it actually yields non-adiabatic energy dissipation rates that are consistent with a quantum-nuclear treatment of the adsorbate vibrations based on TDPT [38, 52] and linear response theory [61–63]. These, in turn, are in very good agreement with experimentally measured vibrational lifetimes [49–52, 64, 65]. One can thus consider the electronic friction formalism as a semi-classical generalization of these theories [38, 63], and in principle re-use the long standing analytical formula derived therefrom in order to evaluate individual elements of the friction tensor.

Starting from the friction kernel in Eq. (2.30), HGT derived an explicit expression of the friction tensor considering delocalized molecular orbitals (MOs) from Hartree-Fock (HF) theory as a basis for the BO states [38]. They could show that the Markov approximation is essentially equivalent

to a *constant-coupling limit* that demands a quasi-constant density of states over the energy range relevant to electronic transitions. In other words, one can conclude that the Markov approximation should be valid as long as the non-adiabatic energy losses are small compared to the energy scale on which features of the electronic structure change. The same conclusions are obtained upon deriving the friction tensor from time-dependent density functional theory (TD-DFT), where the Markov approximation corresponds to the *quasi-static limit* [62, 63]. In Ref. 4 we could further substantiate this conjecture and justify the Markovian approximation for the electronic system. Using TDPT to explicitly calculate the *eh*-pair excitation spectra, we identified short electronic coherence times as the origin of the essentially identical non-adiabatic lifetimes of the CO stretch mode on Cu(100) and Pt(111) measured from experiment, and reproduced with electronic friction theory. It is hence the (at least pseudo-) Markovian character of the electronic system that blurs influences of the vastly different band structure of the coinage and transition metal surfaces.

2.4.1 Orbital-Dependent Friction

The Hartree-Fock-MO-based expression of the friction tensor originally derived by Head-Gordon and Tully is of only little practical relevance in the context of gas-surface dynamics, because DFT is typically preferred for extended (periodic) systems (cf., chapter 3). Hence—switching to Dirac and full subscript notation for convenience, i.e., $\boldsymbol{R}_\alpha = (R_i, R_j, R_k)^T$—the representation one usually uses is given in the basis of Kohn-Sham-orbitals either via [38, 52, 65]

$$\eta_{ij}(\boldsymbol{R}) = \pi\hbar \sum_n \sum_{n'} \left(\epsilon_n^{\mathrm{KS}} - \epsilon_{n'}^{\mathrm{KS}}\right)^2 \left|\left\langle \phi_n^{\mathrm{KS}} \middle| \nabla_{R_i} \phi_{n'}^{\mathrm{KS}} \right\rangle \left\langle \phi_{n'}^{\mathrm{KS}} \middle| \nabla_{R_j} \phi_n^{\mathrm{KS}} \right\rangle\right|^2 \delta(\epsilon_n^{\mathrm{KS}} - E_{\mathrm{F}})\delta(\epsilon_{n'}^{\mathrm{KS}} - E_{\mathrm{F}}),$$

$$(2.35)$$

or, equivalently [60, 62, 63, 66],

$$\eta_{ij}(\boldsymbol{R}) = \pi\hbar \sum_n \sum_{n'} \left|\left\langle \phi_n^{\mathrm{KS}} \middle| \frac{\partial \hat{v}_{\mathrm{eff}}^{\mathrm{KS}}}{\partial R_i} \middle| \phi_{n'}^{\mathrm{KS}} \right\rangle \left\langle \phi_{n'}^{\mathrm{KS}} \middle| \frac{\partial \hat{v}_{\mathrm{eff}}^{\mathrm{KS}}}{\partial R_j} \middle| \phi_n^{\mathrm{KS}} \right\rangle\right|^2 \delta(\epsilon_n^{\mathrm{KS}} - E_{\mathrm{F}})\delta(\epsilon_{n'}^{\mathrm{KS}} - E_{\mathrm{F}}), \quad (2.36)$$

where $|\phi_n^{\mathrm{KS}}\rangle$ and ϵ_n^{KS} are the KS-states and corresponding energies, $\hat{v}_{\mathrm{eff}}^{\mathrm{KS}}$ is the effective KS-potential, and E_{F} is the Fermi energy. Both equations implicitly assume an appropriate summation over $\boldsymbol{k}$, i.e., sampling of the first Brillouin zone.

Involving electronic friction tensor elements as defined either by Eq. (2.35) or Eq. (2.36) is referred to as *orbital-dependent friction (ODF)* throughout this work. It indeed accounts for the electronic structure of the system, but condenses the effect of all addressable non-adiabatic transitions weighted by their coupling strength into a single matrix. Both, Eqs. (2.35) and (2.36) contain an explicit summation over KS-states at the Fermi level, consistent with the underlying picture of lowest energy excitations in the substrate induced by adsorbate motion. In turn, this also intuitively suggests that a high DOS at the Fermi level should be indicative of a high friction coefficient. This intuitive notion, however, can be misleading. In Ref. 4 we could show that detailed effects of the band structure are in fact washed out by the Markov approximation accompanying ODF tensors. The finite memory of the electronic system thus results in a *constant averaged-coupling limit* consistent with the original considerations by HGT, yet in reversed logical order.

Evaluating Eqs. (2.35) and (2.36) is still a formidable task in the context of gas-surface dynamics. Of particular numerical concern in this regard is the demanding evaluation of the involved gradients at

each point along the nuclear trajectory—on top of an evaluation of the PES. On the other hand, also the fragile handling of the energy-matching condition as imposed through the δ-functions within a finite sampling of reciprocal space is delicate. Here, one usually invokes a suitable broadening function (see Refs. 51, 52 and 67) which, however, can yield unphysical results if respective broadening factors are too large [68]. Altogether, this so far limited ODF calculations to at most low-dimensional model systems [63, 66, 69–75]. Only very recently, Maurer and coworkers started to tackle the full six-dimensional electronic friction tensor for diatomics on several metal surfaces [52, 65, 76], particularly allowing to assess the role of pseudo-anharmonic normal mode couplings induced through respective off-diagonal elements (cf., chapter 4).

2.4.2 *Local Density Friction Approximation*

Rather than evaluating the electronic friction tensor directly from the electronic structure of the system and consequently dealing with the concomitant numerical obscurities and efficiency issues, a much simpler embedding approach has gained considerable attention over the past few years [1, 2, 74, 75, 77–99]. Here, as first suggested by Li and Wahnström for atoms [37], and later extended to molecules by Juaristi and coworkers [77], the electronic friction tensor is pragmatically approximated from Cartesian-isotropic atomic contributions η_α, i.e.,

$$\eta_{ij}(\boldsymbol{R}) = \eta_\alpha \delta_{ij}. \tag{2.37}$$

The imposed diagonal structure of $\boldsymbol{\eta}$ thus disregards any friction-induced interatomic couplings. This, however, does not imply that the friction tensor is diagonal also in a normal mode basis. Quite in contrast, there will generally be off-diagonal contributions, yet strictly resulting only from the underlying unitary transformation of Eq. (2.37). In Ref. 4, however, we found a negligible effect of these off-diagonal contributions on the actual vibrational damping dynamics of CO on Cu(100). Remarkably enough, also the mode-coupling effect of a full ODF tensor turned out to be insignificant.

The atomic contributions in Eq. (2.37) are typically individually (and independently) evaluated from an atom-in-jellium model system [100–102]. System-specific electronic structure information thus only enters via the atomic charge determining the impurity potential, and an embedding electronic density defining the homogeneous electron gas (HEG). The respective mapping, i.e., the construction and definition of an embedding density that determines the $\boldsymbol{R}$-dependence indicated in Eq. (2.37), is of course not uniquely defined though (*vide infra*). Having said that, the functional form of the required model-friction coefficients can either be derived from TDPT for the model system [103], or from a more heuristic approach based on a combination of kinematic and quantum scattering theory [102, 104, 105]. Referring to Ref. 106 for a detailed derivation, the latter approach shall be briefly sketched here.

Starting directly with a classical description not only of the nuclear but also of the electronic dynamics, one usually considers the motion of an isotropic projectile (an atom) through a medium consisting of very light particles (jellium). Continuous momentum exchange due to collisions with the surrounding electrons will ultimately result in a loss of the projectile's kinetic energy. The respective rate of momentum transfer $p_\parallel$ parallel to the atom velocity therefore allows to define a stopping power, i.e., a differential loss of kinetic energy E per unit length x,

$$-\frac{\mathrm{d}E}{\mathrm{d}x} = -\frac{\mathrm{d}p_\parallel}{\mathrm{d}t}. \tag{2.38}$$

In order to arrive at Eq. (2.38), one has to neglect the projectile recoil for individual scattering events. This so-called *infinite mass approximation* can thus be seen as analogue to the hand-waving justification for the Born-Oppenheimer approximation often seen in textbooks, demanding a separation in time-scales due to the tremendous mass mismatch between electrons and nuclei. Further neglecting any atomic motion-induced deviation of the respective interaction potential from spherical symmetry [107], one can then evaluate the stopping power in first-order of the atomic velocity v according to

$$-\frac{\mathrm{d}E}{\mathrm{d}x} = \rho_{\mathrm{emb}} k_{\mathrm{F}} \sigma_{\mathrm{tr}}(k_{\mathrm{F}}) v = \eta v, \qquad (2.39)$$

where ρ_{emb} is the electronic density sufficiently defining the HEG, and $\sigma_{\mathrm{tr}}(k_{\mathrm{F}})$ is the transport cross section at the Fermi momentum. The latter condenses all detailed (quantum) effects of the electron-nuclear interaction (*vide infra*). In analogy to classical mechanics, the electronic friction coefficient η then combines all of these quantities into a proportionality factor for the energy dissipation. Within this *low velocity limit*, only electrons on the Fermi surface scatter with the projectile due to the Pauli exclusion principle. In this context, note the similarity with Eqs. (2.35) and (2.36), where only states directly at the Fermi level contribute to the electronic friction tensor. Moreover, the kinematic scattering approximation underlying Eq. (2.39) considers only instantaneous single projectile-electron scattering events. It can thus be interpreted as an analogue of the Markov approximation. There is no "memory" gradually building up in the HEG in terms of correlated multiple scattering events.

The key quantity to be evaluated in this regard is the transport cross section. To this end, accounting for the non-classical character of the involved electrons calls for a quantum mechanical description of the scattering event. Due to the symmetry of the problem, this ultimately boils down to solving the radial SEQ for a finite-range impurity potential in jellium. Obtained from comparing to the free particle wave functions outside the range of this potential, all relevant information about the scattering process is then encoded in the corresponding scattering phase shifts $\delta_l(k_{\mathrm{F}})$ at the Fermi momentum (see Refs. 105 and 108), such that

$$\sigma_{\mathrm{tr}}(k_{\mathrm{F}}) = \frac{4\pi}{k_{\mathrm{F}}^2} \sum_{l=0}^{\infty} (l+1) \sin^2\left[\delta_{l+1}(k_{\mathrm{F}}) - \delta_l(k_{\mathrm{F}})\right]. \qquad (2.40)$$

Here, the sum runs over the order of the underlying partial wave expansion for the electronic wave function (i.e., products of radial functions and Legendre polynomials) and can be truncated suitably in practice. In their seminal work, Puska and Nieminen tabulated the phase shifts for a wide range of impurities and different embedding electronic densities based on DFT, i.e., directly from the Kohn-Sham states [101]. These tabulated values are in fact still used these days in order to evaluate corresponding atomic electronic friction coefficients (see, e.g., Refs. 65 and 87) according to

$$\eta_\alpha = \frac{4\pi \rho_{\mathrm{emb},\alpha}}{k_{\mathrm{F}}} \sum_{l=0}^{\infty} (l+1) \sin^2\left[\delta_{l+1}(k_{\mathrm{F}}) - \delta_l(k_{\mathrm{F}})\right], \qquad (2.41)$$

where the atomic subscript α has been reintroduced for convenience[3] to comply with Eq. (2.37). Altogether, the approach sketched here yields an isotropic atomic electronic friction coefficient η_α that depends only on the electronic density of the HEG (fixing also the Fermi momentum) and—implicitly through the scattering phase shifts—on the atomic charge number of the projectile. This

---

[3]Note that also the phase shifts and the Fermi momentum implicitly depend on α.

allows to construct a convenient interpolation function prior to the dynamical simulations resulting in an invincible numerical efficiency: Once the embedding density $\rho_{\text{emb},\alpha}$ is known, the atomic electronic friction coefficient η_α is evaluated at essentially no additional cost.

Having this highly efficient formalism at hand, the obviously most crucial task is to establish an adequate procedure that maps the real adsorption system to the underlying atom-in-jellium model. To this end, one usually follows what has, in fact, already been brought up by Li and Wahnström in the context of H diffusion in Ni [37], but only later been coined *local density friction approximation* (LDFA) by Juaristi and coworkers [77]. Here, very much in the spirit of the local density approximation to the exchange-correlation-functional in DFT (cf., chapter 3), one considers only the local embedding density of the host system to define the model HEG and rigorously ignores any non-local contributions to the electronic friction coefficient. The vague phrasing of a "host system" here already implies that this is not a uniquely defined concept, not least because dividing a system quantity like the electronic density into individual atomic contributions inevitably requires further approximations. The traditional route in this context is to follow the independent-atom approximation (IAA) [74, 77, 81, 82], in which one uses the electronic density of a clean metal slab ρ_{surf} at the adsorbate atoms' positions to enter Eq. (2.41) for the individual atomic friction coefficients, i.e., $\rho_{\text{emb},\alpha} = \rho_{\text{surf}}(\boldsymbol{R}_\alpha)$.

Considering atomic adsorbates, this approximation sketches a rather intuitive physical picture of an atom being embedded into the metal surface electronic density. Even though it ignores adsorbate-surface interactions and concomitant density rearrangements due to charge transfer[4], LDFA-IAA was thus indeed shown to perform very well regarding the non-adiabatic energy losses of various ions and atoms scattered off metal surfaces [87, 88, 109] and the vibrational lifetimes of atomic adsorbates on metals [1, 79]. Turning to molecular adsorbates, however, LDFA-IAA rigorously ignores the respective molecular character and considers the adsorbate to consist of completely independent atoms—at least on the level of the non-adiabatic treatment. The friction tensor from Eq. (2.37) is consequently composed of independent sub-matrices

$$\eta_{ij}^{\text{IAA}}(\boldsymbol{R}) = \eta_\alpha \left(\rho_{\text{surf}}(\boldsymbol{R}_\alpha) \right) \delta_{ij}. \tag{2.42}$$

There have been attempts to overcome this limitation and to evaluate friction coefficients from the sketched embedding model beyond atomic impurities [110]. However, these naturally break with the radial symmetry of the problem. Consequently suffering from severe performance losses they are thus no practical alternative to LDFA-IAA.

Of course, the assumption of independent atoms is very restrictive in the context of molecular adsorbates and thus lacks, e.g., the steep increase of friction coefficients at dissociative transition states predicted from ODF [71, 73, 111]. This obvious shortcoming raised a heated debate in literature [77, 111, 112] questioning the validity of the LDFA-IAA-based results *per se*. The most controversial point in this regard was the argument that immanently low nuclear velocities close to a transition state may effectively suppress any non-adiabatic energy dissipation according to Eq. (2.39) and thus supersede an accurate description of the friction coefficient in these relevant regions [77, 112]. There was hence a prevalent uncertainty in how far conceptual shortcomings of the LDFA-IAA approach actually carry over to experimentally accessible observables.

This unclear situation was the motivation for our work in Ref. 1. Comparing corresponding dynamically evaluated vibrational lifetimes for several diatomic molecules on metal surfaces with

---

[4]To some extent density rearrangements are accounted for also in the LDFA-IAA approach through the self-consistent evaluation of scattering phase shifts, yielding a screened effective potential. Yet, this is done on the model system-level only and not on the full Hamiltonian level [1, 2].

accurate experimental reference data, we found that LDFA-IAA performs on an almost equal level with previous ODF calculations published in literature. Even beyond the inherent lack of the molecular adsorbate character this is highly surprising, given that information on the electronic structure of the system only enters the LDFA formalism on the level of a (not even uniquely defined) embedding electronic density, whereas ODF accounts for the actual KS-states and respective non-adiabatic couplings through Eqs. (2.35) and (2.36). Moreover, following an atoms-in-molecules (AIM) approach to introduce molecular information in the atomic embedding densities, we could further improve upon this good performance while retaining the great numerical efficiency of the LDFA approach. This new method coined LDFA-AIM constructs the respective atomic embedding densities via a suitable Hirshfeld-partitioning [113] of the full self-consistent system electronic density evaluated at the respective atomic positions. In contrast to the IAA, these in turn carry an implicit dependence on the full system configuration vector $\boldsymbol{R}$ and the friction tensor does not decompose into independent sub-matrices as in Eq. (2.42).

Lastly, the results from Ref. 1 essentially verifying the LDFA-IAA/AIM approximation for the electronic friction tensor were a cornerstone of our work in Ref. 2 addressing the thermal diffusion of Na on Cu(111). Whilst the overall adsorbate-surface coupling to the surface was fixed by fitting to experimental measurements, an analysis of respective trajectories based on LDFA friction coefficients ultimately allowed to disentangle the role of non-adiabatic and phononic couplings, revealing a surprisingly high degree of non-adiabaticity in this case.

3 Electronic Structure Theory

The previous chapter on non-adiabatic dynamics focused on transitions in the electronic subsystem that are induced by the nuclear kinetic energy operator, and the respective feedback to the nuclear degrees of freedom. These effects may appear to be some complex augmentation to "regular" molecular dynamics, where solving Eq. (2.3) for Born-Oppenheimer states and eigenvalues is actually the most simple and straightforward task. This notion, however, is wrong in two aspects. First, non-adiabatic effects are not just an external supplement, but they are naturally included in a consistent quantum mechanical treatment of the full electron-nuclear system. Instead, they only become an augmentation that has to be re-introduced once the adiabatic and Born-Oppenheimer approximation break down. Second, given the approximate methods to include non-adiabatic effects into a BO-framework of the dynamics sketched in the previous section, typically most of the computational effort is in fact spent on solving the electronic Schrödinger equation corresponding to Eq. (2.3). The most intriguing problem in this regard stems from the exceedingly large dimensionality of essentially all chemically relevant systems that eludes an exact solution for the (many-body) electronic wave function. This calls for further approximations giving rise to two competing paradigms.

On the one hand, there are so-called wave function-based approaches originating from quantum chemistry. Here, one tries to find approximate solutions to the respective eigenvalue problem involving the *exact* electronic Hamiltonian. Consequently, approximations to the functional form of the many-body wave function have to be made. These start with a simple single-particle product leading to a mean field description in Hartree theory, over a single Slater determinant introducing quantum mechanical exchange effects due to the Pauli principle in Hartree-Fock theory, to multi-configurational approaches including correlation effects such as Coupled Clusters and Configuration Interaction. Excellent overviews in this regard can be found in Refs. 114, 115 and 116. Even though in particular this last class of methods can yield astonishing accuracy and a reliable description of excited states, their application is often limited to small systems only.

On the other hand, originating more from solid state physics, there are approaches solving the eigenvalue problem for an *approximate* electronic Hamiltonian. These are most prominently exemplified by the ubiquitous density functional theory—the most widespread approach to solve for the electronic energy of extended metal systems that also has been heavily made use of in Refs. 1, 2 and 4.

3.1 Density Functional Theory

For a system of interacting electrons in an external potential constituted by the nuclei there is a one-to-one mapping between the ground state electronic density $\rho(\boldsymbol{r})$ and the external potential. In other words, the electronic density uniquely determines the external potential and hence the electronic Hamiltonian with its eigenvalues—*et vice versa*. This seminal statement is known as the first Hohenberg-Kohn theorem stated in 1964 [117]. Its importance lies in the fact that it replaces the quest for a high-dimensional many-body wave function with searching for a three dimensional quantity only, i.e., the electronic density. This theorem thus constitutes the foundation of density functional theory (DFT). Moreover, Hohenberg and Kohn also gave a hint at how to use it in order

to solve the many-body SEQ by demonstrating that the exact ground state electronic density $\rho_0(\boldsymbol{r})$ minimizes the (electronic) energy functional, resulting in a variational principle known as the second Hohenberg-Kohn theorem [117]

$$E_0 = E\left[\rho_0(\boldsymbol{r})\right] < E\left[\rho(\boldsymbol{r})\right]. \tag{3.1}$$

If the energy functional was known, a direct minimization of the latter would thus yield the exact solution for the many-body problem. Unfortunately, this is not the case. Hence, in a first step separating known from unknown contributions, one can (assuming immobile, classical nuclei) divide the energy functional into

$$E\left[\rho(\boldsymbol{r})\right] = \underbrace{V_{\text{ext}}\left[\rho(\boldsymbol{r})\right] + V_{\text{H}}\left[\rho(\boldsymbol{r})\right] + T_{\text{S}}\left[\rho(\boldsymbol{r})\right]}_{\text{known}} + \underbrace{E_{\text{xc}}\left[\rho(\boldsymbol{r})\right]}_{\text{unknown}}. \tag{3.2}$$

Here, the exact electron-nuclear interaction V_{ext} and the classical Coulomb (or Hartee) energy for the electron-electron interaction V_{H} are straightforward functionals of the electronic density (see, e.g., Ref. 16). The exact functional for the kinetic energy of the interacting electrons in turn is unknown. However, its counterpart for a system of non-interacting electrons T_{S} can actually be found (*vide infra*). All thus unknown remaining quantum many-body effects not captured by V_{H} and T_{S} are consequently contained in the so-called exchange-correlation (xc) functional E_{xc}, a universal functional of the electron density only, for which adequate approximations need to be found. Note that the DFT xc-energy indeed contains the exchange and correlation energy as known from wave function-based theories, but beyond that also accounts for kinetic correlation energy, i.e., the part of the kinetic energy that is not accounted for by T_{S}. Approximate xc-functionals further effectively contain corrections for the non-vanishing electron self-interaction that remains from an approximate treatment of the exchange energy.

3.1.1 Kohn-Sham Approach

There are so-called orbital-free models that directly target an electronic density functional of the kinetic energy such that the partitioning from above is not even necessary. However, whilst those retain the low dimensionality of the target function (the electronic density), they usually suffer from a poor representation of the kinetic energy [115]. Hence, a far more widespread method is based on a procedure suggested by Kohn and Sham in 1965 [118]. The main underlying idea here is that for a non-interacting system, the exact solution to the SEQ is given as a Slater determinant of single particle states ϕ_i obtained from HF theory. Hence, the exact kinetic energy for such a system system can be straightforwardly evaluated. If one therefore constructs a fictitious non-interacting system that is as similar as possible to the real system, the correspondingly evaluated kinetic energy T_{S} may already account for most of the kinetic energy of the interacting system. In turn, the remaining contributions to the xc-functional should be small, facilitating the quest for good approximations.

Kohn and Sham established such an ideal one-to-one mapping of the real system to a reference system of non-interacting single particle states ϕ_i^{KS} within an effective potential such that its corresponding electronic density

$$\rho(\boldsymbol{r}) = \sum_i \phi_i^{\text{KS}}(\boldsymbol{r}) \tag{3.3}$$

is equal to that of the real interacting system. The KS-equations that actually determine the reference system can be found using Eq. (3.3) and minimizing the energy functional with respect to the KS-states thereby demanding their normalization

$$\left[-\frac{\hbar^2}{2m_\mathrm{e}} \nabla^2_{\boldsymbol{r}_i} + \hat{v}_\mathrm{eff}(\boldsymbol{r}) \right] \phi_i^\mathrm{KS}(\boldsymbol{r}) = \epsilon_i^\mathrm{KS} \phi_i^\mathrm{KS}(\boldsymbol{r}). \tag{3.4}$$

Note that what is identified as KS-eigenenergies ϵ_i^KS in principle just enters the formalism as Lagrange multipliers. The effective KS-potential $\hat{v}_\mathrm{eff}$ is determined by the external and Hartree potential, as well as the functional derivative of the xc-functional. It hence depends on the entire electronic density $\rho(\boldsymbol{r})$, which demands the KS-equations to be solved self-consistently. By introducing the reference system, the KS-approach ultimately allows for a reliable evaluation of large parts of the kinetic energy. However, this comes at the cost of increasing the complexity from a 3-dimensional equation for the electronic density to N coupled 3-dimensional single particle equations. It should further be noted that the underlying one-to-one mapping to a non-interacting reference system can also be extended to time-dependent problems. This is ensured by the Runge-Gross theorem [119] and forms the foundation of TD-DFT which in turn provides the basis for the perturbation-theory based treatment of *eh*-pair excitations we used in Ref. 4.

The KS-approach is free of any approximations. That is, if the exact xc-functional was known, KS-DFT would yield the exact ground state energy. However, apart from representing the electronic density that minimizes the energy functional, the converged KS-states and their associated eigenvalues in principle lack any further physical meaning. Their sole purpose is to gain a good guess for the kinetic energy thus minimizing the remaining contributions in the xc-functional. As such, there is, e.g., no Koopman's theorem (unless the exact xc-functional is found) [115]. In general, the KS-states should not be confused with the single particle states, i.e., the MOs obtained from wave function-based approaches. Still—depending on the respective approximation for the xc-functional— the KS-eigenvalue spectrum $\{\epsilon_i^\mathrm{KS}\}$ often gives a very reasonable guess for the latter [16, 120–122]. This empirical fact is implicitly relied on in the DFT-based implementations of the ODF and LDFA method, and has also been made use of in the evaluation of the *eh*-pair excitation spectra in the context of Ref. 4.

3.1.2 *Approximations for the Exchange-Correlation Functional*

Density functional theory is *in principle* exact. However, although its existence is assured, the exact closed form of the xc-functional in Eq. (3.2) is not known—and probably never will be [16, 123]. Hence, accurate approximations for E_xc can be seen as the "holy grail" of electronic structure theory [123], the quest for which continues ever since the seminal paper by Hohenberg-Kohn was published in 1965 [117]. Complications in this regard arise in particular from the fact that, unlike in the case of wave function-based theory, there is no systematic way of improving upon existing approximations. Practical xc-functionals will thus always be empirical to some extent, resulting in a plethora of different approaches and parametrization strategies. To still be able to classify the various approximations for E_xc, Perdew suggested a scheme coined *Jacob's ladder* [124]. Referring to the biblical narrative, each rung further up the ladder symbolizes a conceptual step towards the exact xc-functional.

The first rung in this ladder consists of the so-called local density approximation (LDA), that was proposed by Hohenberg and Kohn themselves already [117]. The underlying idea here is very similar

to that of the LDFA approach for the electronic friction coefficient (cf., section 2.4). Also here, the problem is locally mapped on a simple system that can be solved (almost) exactly. In the LDA it is assumed that the electronic density is an only slowly varying function. Hence, at each point in space, it is suitably approximated by a corresponding HEG for which the xc-energy can be calculated to almost arbitrary precision by quantum Monte Carlo methods [125]. Whilst the LDA performs rather well for extended systems with more delocalized electronic states such as metals, it yields unsatisfactory results for molecular systems where non-local effects resulting from a much more inhomogeneous electronic density cannot be captured by construction [16, 115].

Improving over the LDA in the spirit of a local Taylor expansion, functionals on the second rung correspondingly take into account also the (local) gradient of the electronic density, constituting the family of generalized gradient approximation (GGA)-functionals. This leads to an enormous improvement in performance for molecular and slab systems [123, 126–128] with moderate additional computational cost. Consequently, despite further improvements on succeeding rungs of Jacob's ladder, GGA-functionals are still widely used in solid state applications [129], particularly in the context of gas-surface dynamics [3]. An important representative of this rung is the functional by Perdew, Burke and Ernzerhof (PBE) [130, 131] that has also been used in all DFT-calculations underlying Refs. 1, 2 and 4. Recently, a questionable trend of intermixing different GGA functionals within a so-called specific reaction parameter approach has emerged also in the field of gas-surface dynamics [17, 132].

Developing xc-functionals beyond the GGA is a highly active field where in particular the addition of non-local van-der-Waals dispersion corrections has gained considerable attention [123]. The next logical step in the expansion spirit to improved upon the LDA is to include not just the gradient, but also the Laplacian of the electronic density (or, alternatively, the kinetic energy density in an orbital expansion), thereby advancing to the third rung on Jacob's ladder. These kinds of functionals are referred to as meta-GGA functionals. A different route is taken on the fourth rung. These so-called hybrid functionals rely on the fact that the exchange energy is exactly accounted for within HF theory. Hence, the idea is to evaluate the exchange energy from the (occupied) KS-orbitals in order to augment the xc-functional. The often occurring notion of an added "exact" HF-exchange in this context is, however, misleading as the KS-orbitals generally do not correspond to the HF-orbitals. Prominent hybrid functionals are for instance B3LYP [133, 134] and PBE0 [135, 136]. The latter mixes PBE and HF-exchange in a 3:1 ratio, while retaining the full PBE correlation energy.

4 Normal Modes and Phonons

The concept of normal modes and their periodic counterpart, so-called phonons, is ubiquitous throughout all publications associated with this thesis [1–4]. Both are qualitatively fundamentally different to the non-adiabatic effects focused on in chapter 2, even though in particular the "interaction with phonons" is often discussed in the same context as the latter. In fact, however, normal modes and phonons are (in the lingo of chapter 2) essentially just a suitable set of slow particle coordinates conveniently representing molecular and lattice vibrations. It is important to keep in mind that these are completely accounted for within the adiabatic and Born-Oppenheimer approximation. Whilst we have given an extensive overview on different techniques to incorporate the coupling of an adsorbate to lattice vibrations—also referred to as phononic DOFs—in the context of GSD in Ref. 3, focus in this chapter is more on a short presentation of the underlying mathematical concept. Excellent more comprehensive introductions to this matter can be found in Ref. 137, and Refs. 138 and 139 for normal modes and phonons, respectively.

In an MD-spirit assuming that the nuclear motion on a (non-periodic) PES V is captured by classical mechanics, the corresponding Newton's equations of motion read as

$$m_i \ddot{R}_i = -\left(\frac{\partial V}{\partial R_i}\right),\qquad(4.1)$$

where R_i refers to Cartesian nuclear coordinates with associated mass m_i. It is convenient in this context to remove the explicit mass-dependence by introducing a set of mass-weighted Cartesian displacement coordinates $y_i = \sqrt{m_i}(R_i - R_{i,0})$, where $\mathbf{R}_0$ is a local minimum of the PES. Equation (4.1) thus transforms to

$$\ddot{y}_i = -\left(\frac{\partial V}{\partial y_i}\right).\qquad(4.2)$$

Upon locally approximating the PES by a second-order Taylor expansion around the local minimum $\mathbf{R}_0$, i.e., $\mathbf{y} = \mathbf{0}$, one can define a *harmonic potential* according to

$$V_{\text{harm}}(\mathbf{y}) = V(\mathbf{y}) - V(\mathbf{0}) = \underbrace{\sum_i \left(\frac{\partial V}{\partial y_i}\right)_{\mathbf{0}} y_i}_{=0} + \frac{1}{2} \sum_i \sum_j \left(\frac{\partial^2 V}{\partial y_i \partial y_j}\right)_{\mathbf{0}} y_i y_j,\qquad(4.3)$$

where the first derivatives contribution vanishes at $\mathbf{y} = \mathbf{0}$ by definition. Within this harmonic potential, Eq. (4.2) is given by

$$\ddot{y}_i = -\left(\frac{\partial V_{\text{harm}}}{\partial y_i}\right) = -\sum_j \left(\frac{\partial^2 V}{\partial y_i \partial y_j}\right)_{\mathbf{0}} y_j,\qquad(4.4)$$

or, in matrix-vector notation

$$\ddot{\mathbf{y}} = -\mathbf{\Phi}\mathbf{y}.\qquad(4.5)$$

The (mass-weighted) force constants matrix $\boldsymbol{\Phi}$ is thus the (mass-weighted) Hessian of the PES at the equilibrium configuration, coupling the individual DOFs through the second derivatives from Eq. (4.3), i.e.,

$$\Phi_{ij} = \left(\frac{\partial^2 V}{\partial y_i \partial y_j} \right)_0 = \frac{1}{\sqrt{m_i m_j}} \left(\frac{\partial^2 V}{\partial R_i \partial R_j} \right)_{R_0} . \tag{4.6}$$

The force constants matrix is symmetric by construction. Hence, there is a similarity transformation using the *orthogonal* matrix $\boldsymbol{Q}$ (where $\boldsymbol{Q}^T \boldsymbol{Q} = 1$, i.e. $\boldsymbol{Q}^{-1} = \boldsymbol{Q}^T$) such that $\boldsymbol{Q}^T \boldsymbol{\Phi} \boldsymbol{Q} = \boldsymbol{\Omega}$ is a diagonal matrix with elements $\Omega_{ij} = \omega_i^2 \delta_{ij}$. Upon defining $\boldsymbol{Q}^T \boldsymbol{y} = \boldsymbol{q}$, a straightforward transformation of Eq. (4.5) into the eigenbasis of $\boldsymbol{\Phi}$ then yields

$$\ddot{\boldsymbol{q}} = \boldsymbol{Q}^T \ddot{\boldsymbol{y}} \overset{(4.5)}{=} -\boldsymbol{Q}^T \boldsymbol{\Phi} \boldsymbol{y} = -\boldsymbol{Q}^T \boldsymbol{\Phi} \boldsymbol{Q} \boldsymbol{Q}^T \boldsymbol{y} = -\boldsymbol{\Omega} \boldsymbol{q}, \tag{4.7}$$

or in component notation,

$$\ddot{q}_i = - \sum_j \Omega_{ij} q_j = -\omega_i^2 q_i. \tag{4.8}$$

In this basis of *normal modes* (i.e. the eigenvectors of $\boldsymbol{\Phi}$) there is hence no potential-induced coupling between the individual DOFs. In contrast, they rather separate into independent harmonic oscillators q_i with frequency ω_i as obvious from Eqs. (4.7) and (4.8).

Altogether, normal modes (and associated frequencies) are eigenvectors (and eigenvalues) of the force constants matrix defining a convenient basis to describe vibrational motion within a harmonic approximation of the PES. They form a complete orthogonal basis such that any molecular vibrational motion can be conveniently decomposed into a superposition of these independent fundamental vibrations. This has been made use of, e.g., in the context of Refs. 1 and 4, where certain normal modes were "pumped" in order to initialize underlying MD simulations. To this end, one constructs a suitable $\dot{\boldsymbol{q}}$ vector such that $q^2 = 2E_{\text{kin}}$, and yields the (mass-weighted) Cartesian velocities via the straightforward back transformation $\boldsymbol{Q} \dot{\boldsymbol{q}} = \dot{\boldsymbol{y}}$. Whilst such a decomposition of the kinetic energy is always possible, a corresponding decomposition of the potential energy to yield (mass-weighted) Cartesian displacements can in turn only be done for strictly harmonic potentials. However, once the nuclear elongation from the equilibrium position increases, higher-order terms in the respective expansion of the PES may become relevant. In these cases, normal modes are still a convenient orthogonal basis, but the potential energy can no longer be decomposed into individual mode-specific contributions. Moreover, the corresponding equations of motion become coupled through so-called anharmonic effects.

In passing it should be noted, that within an electronic friction-like description of nuclear dynamics, also the frictional (and fluctuating) forces may couple between normal modes even if the harmonic approximation is valid. In the 0 K case, the corresponding Langevin equation reads

$$\ddot{\boldsymbol{q}} = -\boldsymbol{\Omega} \boldsymbol{q} - \boldsymbol{Q}^T \tilde{\boldsymbol{\Lambda}} \boldsymbol{Q} \dot{\boldsymbol{q}}. \tag{4.9}$$

In general the mass-weighted friction tensor $\tilde{\boldsymbol{\Lambda}}$ ($\tilde{\Lambda}_{ij} = \eta_{ij}/\sqrt{m_i m_j}$, cf. section 2.4) and the force constants matrix do not share a common set of eigenvectors. Hence, $\boldsymbol{Q}^T \tilde{\boldsymbol{\Lambda}} \boldsymbol{Q}$ is not diagonal and but rather couples between individual components of $\boldsymbol{q}$. This friction-induced mode coupling has gained considerable attention with first calculations of the full electronic friction tensor popping up

very recently [52, 65, 76]. As to which extent it is comparable to potential-related anharmonic effects, however, is still unclear.

The concept of normal modes also carries over to periodic structures. However, the respective bookkeeping of indices becomes significantly more complex and shall thus be omitted here (see Ref. 53 for a very refined presentation). When the potential energy of a periodic structure is approximated analogous to Eq. (4.3), one usually refers to a *harmonic solid*. The normal modes of such a harmonic solid (or, any solid approximated therewith) are often termed phonons [138]. Owing to the infinite extent of the system, however, the number of DOFs coupled through the corresponding dynamical matrix (the periodic counterpart of the force constants matrix) is, in principle, of likewise infinite dimensionality yielding an infinite number of normal modes. In contrast to the molecular case, the solutions for the corresponding equations of motion are not harmonic oscillator-like functions but rather plane waves with a characteristic wave vector $\boldsymbol{k}$. In principle, any value of $\boldsymbol{k}$ that is part of the reciprocal lattice yields one of infinitely many plane wave solutions. By virtue of translational symmetry, however, unique solutions are restricted to $\boldsymbol{k}$-vectors in the first Brillouin zone, ultimately yielding a phononic band structure.

Having said that, the "interaction with phonons" in the context of GSD essentially refers to the dynamical coupling between the nuclear adsorbate DOFs and the normal modes of the underlying substrate. As we have reviewed in great detail in Ref. 3, different models to (effectively) account for the latter exist. These start from coupling to a single oscillator mimicking rigid shifts of the substrate, range over an effective (generalized) Langevin-like treatment and peak in approaches that resolve an increasing amount of phononic DOFs by explicitly incorporating the dynamics of more and more substrate atoms. For instance, the latter allow to identify individual phonon excitations upon dissociation events [11, 53, 140–142] by using very refined methods to transform obtained Cartesian displacements and velocities of the substrate atoms to the basis of corresponding normal modes. The state-of-the-art of accounting for phononic interactions in GSD has thus arrived at a point where no more effective models are required and an increasingly accurate description is solely bound to the number of substrate DOFs that can be afforded in corresponding dynamical simulations. Such a systematic improvability contrasts the phononic energy dissipation channel from its non-adiabatic counterpart, whose description is and will be bound to effective models for the foreseeable future [3].

5 Publications

The thesis in hand is publication-based and centers around work (to be) published in Refs. 1–4. With the original articles and accepted/submitted manuscripts being included in the appendix, the following sections aim at giving a concise summary of the work presented therein. Moreover, a detailed assignment of individual author contributions is given for each publication.

5.1 Electronic Friction-Based Vibrational Lifetimes of Molecular Adsorbates: Beyond the Independent-Atom Approximation

5.1.1 Content

This work addressed an ongoing debate in literature as to which extent the popular and conceptually simple LDFA is capable to describe non-adiabatic effects in the context of gas-surface dynamics. As detailed in section 2.4.2, the LDFA relies on an isotropic embedding model in order to evaluate individual atomic friction coefficients, which are then successively combined to approximate the electronic friction tensor. Information about the electronic structure of the adsorbate-substrate system thus enters only on the level of a local embedding density. This allows for a numerically highly efficient evaluation of respective non-adiabatic contributions. However, in particular the concomitant prevalent IAA decomposing molecular adsorbates into (on the level of the friction tensor) isolated atoms raised serious concern about the accuracy of this method.

In this regard, the vibrational lifetimes of high-frequency adsorbate modes on metal surfaces are valuable experimental observables accurately accessible through pump-probe spectroscopy. With a vibrational frequency well above the highest optical phonons these short-lived modes are assumed to decay most dominantly through the excitation of *eh*-pairs in the substrate. Hence, comparison to this well-defined key observable is a crucial ingredient in order to arrive at an informed assessment of any non-adiabatic theory. We thus set out to first compare the performance of the "off-the-shelf" LDFA-IAA model for the vibrational lifetimes of the CO stretch mode on Cu(100) and Pt(111) with experimental data and values predicted from the more refined ODF model (cf., section 2.4.1). Altogether, we found all values to fall within the same order of magnitude, which is very surprising given the conceptual simplicity of the LDFA-IAA approach. Trying to improve over deficiencies within the latter, we further introduced an alternative way of determining the LDFA embedding density. To this end, we suitably constructed the atomic embedding density following an AIM approach from the electronic density of the full (adsorbate + substrate) system relying on Hirshfeld's partitioning scheme. The so-introduced computational overhead is negligibly small, such that also this modified LDFA-AIM approach is characterized by a superb numerical efficiency. Thus also accounting for the molecular character of the adsorbate, vibrational lifetimes evaluated using LDFA-AIM were spot on with experimental reference values for CO on Cu(100) and Pt(111). Moreover, also for H_2 on Ru(0001) and CN on Pt(111) we found lifetimes that were fully consistent with ODF reference calculations from literature, but at a fraction of the respective numerical cost. Altogether, this work significantly consolidated the trust in the approximate LDFA model and pointed towards potential improvements over prevalent assumptions relied on in this context.

5.1.2 Individual Contributions

The idea underlying the LDFA-AIM model was first formulated during my master thesis [106] together with Jörg Meyer, who is now at Leiden University (The Netherlands). He provided an early version of the Hirshfeld partitioning code used to apply the LDFA-AIM model, and an interface to the JuNoLo code [143] to check the influence of dispersion corrections on the vibrational PES. Lastly,

he contributed in co-editing the manuscript. J. Iñaki Juaristi from the Departamento & Centro de Física de Materiales (CSIC-UPV/EHU) in San Sebastián (Spain) introduced me to the concept of the LDFA and contributed in several fruitful discussions during the development of the LDFA-AIM model. Moreover, he provided the interpolation functions for the respective LDFA electronic friction coefficients and proofread the manuscript. Karsten Reuter supervised the project during its entire course and played a significant part in co-editing the manuscript.

I evaluated the vibrational PESs, embedding electronic densities and electronic friction coefficients for all systems using Castep [144] and a modified code for the Hirshfeld partitioning scheme originally written by Jörg Meyer [53, 145], all conveniently interfaced using the Atomic Simulation Environment (ASE) [146, 147]. I further wrote a Python-based MD code from scratch to allow for simulations with varying forms of the (position-dependent) friction tensor—also in internal or normal mode coordinates—and to implement the LDFA-IAA/AIM models. This, among others, also included the analytical representation of the PESs and electronic friction coefficients in terms of cubic bivariate splines, and tools for a respective normal mode analysis. In this context, particular use was made of the SciPy [148, 149] and NumPy [150] packages. Lastly, I ran all simulations, did the respective analysis, wrote the manuscript and created all figures using the matplotlib package [151].

5.2 Energy Dissipation during Diffusion at Metal Surfaces: Disentangling the Role of Phonons versus Electron-Hole Pairs

S.P. Rittmeyer, D.J. Ward, P. Gütlein, J. Ellis, W. Allison, and K. Reuter

5.2.1 Content

In this work we followed a top-down approach to disentangle the relative importance of the competing phononic and non-adiabatic energy dissipation channels for the thermal diffusion of Na on Cu(100). To this end, we presented a novel approach using computational simulations in order to analyze experimental Helium-3 spin echo (^{3}He-SE) measurements. This technique provides direct time-resolved access to the surface (auto-)correlation function. Since corresponding decay rates are very sensitive to the adsorbate-substrate coupling and the underlying diffusion mechanism, ^{3}He-SE measurements encode highly valuable microscopic insight. Assessing these signatures from simulations to decode this information, however, demands numerically highly efficient methods due to the large ensemble size and time scales required for an adequate stochastic averaging. We hence set up a Langevin framework relying on an analytical representation of the PES in order to reproduce these characteristic experimental signatures. All parameters entering the underlying model were either evaluated from *first principles* or obtained from experimental measurements—except for the friction coefficient. Being the only unknown, the latter was then obtained from fitting the resulting simulated signatures to the experimental measurements.

First aiming for a combined apparent friction coefficient, our approach consequently treats the dynamical adsorbate interaction with phonons and non-adiabatic *eh*-pairs on an equal footing in terms of an implicit coupling to two independent additive heat baths. Further non-self consistently evaluating the non-adiabatic contributions for the best-fit simulations within the LDFA approach in a second step, we found an unexpectedly high degree of non-adiabaticity of about (20±5)% for this system. Given the relatively small adsorbate-substrate mass mismatch and the generally low electronic friction coefficients for Na on Cu(111) (both suggesting a dominant phononic coupling), we thus generally inferred a more pronounced role of *eh*-pair excitations than hitherto assumed by classical textbook notion. In this regard, extending our approach to the vast experimental database of ^{3}He-SE measurements that has accumulated over the years may perspectively help to gain more insight into this matter.

5.2.2 Individual Contributions

This work emerged from a collaboration with experimental colleagues from the Cavendish Laboratory, University of Cambridge (United Kingdom). David J. Ward conducted the ^{3}He-SE measurements and wrote the corresponding experimental parts of the supporting information ensuing the publication. Together with William Allison and John Ellis he further contributed in many fruitful discussions considering the calculation of ^{3}He-SE signatures from simulated particle trajectories and the extraction of corresponding decay rates. All three finally proofread the manuscript. Patrick Gütlein contributed to this work in the context of his master thesis which was performed under my direct supervision at the Chair of Theoretical Chemistry of the Technical University of Munich. He worked out an early version of the analytical representation of the PES (and the electronic friction coefficients) and

evaluated a respective parametrization from DFT. This included comprehensive convergence checks that were relied on in the PES/electronic friction coefficients ultimately used for the simulations. Lastly, Patrick Gütlein did extensive tests regarding the Langevin-MD simulations and concomitant evaluation of ^{3}He-SE signatures. Karsten Reuter supervised the project during its entire course and played a significant part in editing the manuscript.

I initiated the project and created all code necessary to conduct and analyze the MD simulations. To this end, I significantly extended the MD code initially created in the context of Ref. 1 to allow for the required Langevin simulations and the concomitant analysis. Among others, this includes Fortran [152]/Cython [153]-based extensions to allow for numerically efficient calls to the analytical representation of the PES and electronic friction coefficients, and a toolbox to extract intermediate scattering functions from simulated trajectories as well as to fit respective decay rates. In this regard, all code development heavily relied on the SciPy [148, 149] and NumPy [150] packages. I further re-parametrized the analytical PES and electronic friction coefficient through DFT calculations in the aftermath of Patrick Gütlein's master thesis using CASTEP [144] and a modified version of the Hirshfeld partitioning code originally written by Jörg Meyer [53, 145], all conveniently interfaced using the ASE [146, 147]. In this context, I further used an interpolation function for the electronic friction coefficient of Na (as a function of the embedding density) as liberally provided by J. Iñaki Juaristi. Lastly, I performed all simulations, did the corresponding analysis steps, wrote the manuscript including the methodological and computational parts of the supplemental material, and created all corresponding figures using the matplotlib package [151].

5.3 Energy Dissipation at Metal Surfaces

S.P. Rittmeyer, V.J. Bukas, and K. Reuter

5.3.1 Content

In this article we presented a state-of-the-art review on the field of gas-surface dynamics, with a particular focus on theoretical and computational models to account for energy dissipation into the phononic and non-adiabatic channel. This is an extremely challenging problem and a microscopically detailed theoretical understanding has not been achieved. We drew this conclusion by illuminating different approaches to incorporate dissipative effects, from coarse-grained effective theories to increasingly sophisticated methods. In detail, we started with adiabatic frozen surface (FS) models and proceeded from a rigidly coupled surface oscillator (SO) over the generalized Langevin oscillator (GLO) approach to full-dimensional *ab initio* molecular dyamics (AIMD) simulations, and finally arrived at a classical pair potential-based embedding scheme extending thereon (QM/Me). In the context of non-adiabatic energy dissipation, we mainly focused on the electronic friction approach, both within the LDFA and ODF, and discussed the relative importance of effects beyond the Born-Oppenheimer approximation in combination with models for the phononic energy dissipation.

We illustrated the application of these methods to include energy dissipation in computational simulations for different elementary processes such as inelastic scattering, vibrational damping, and surface diffusion. In this regard, particular focus was on the persisting difficulty of gauging the performance of the respective (effective) theoretical treatment based on experimentally accessible observables. We concluded that—while often targeted in both theoretical and experimental studies—stochastic measures such as sticking coefficients and diffusion constants are rather ill-suited benchmark observables in this regard. They inherently convolute many elementary processes which renders them very insensitive towards microscopic details—a shortcoming that ultimately complicates establishing a profound and detailed understanding of the energy transfer mechanisms involved in GSD.

5.3.2 Individual Contributions

This review article emerged from a very close collaboration with Vanessa J. Bukas, who is affiliated with Stanford University (California, USA). Together we sketched the logical structure of the article, discussed the relevant literature cited therein and wrote the introduction and conclusions. Being more detailed about the main body of the review, Vanessa J. Bukas predominantly contributed to the parts on (effective) models for phononic energy dissipation in the context of inelastic scattering, and the section on hot diffusion. In turn, I mostly wrote the section on vibrational damping, thermal diffusion, as well as on non-adiabatic effects in the context of inelastic scattering. I further created the graphical abstract and all figures contained in the article using the ASE [146, 147] and the open source tools Inkscape, GIMP, and POV-ray. In general, however, both Vanessa J. Bukas and I edited each part of the manuscript. Lastly, Karsten Reuter contributed in discussions about the review structure, co-edited the introduction part, and played a significant part in proofreading the overall manuscript.

5.4 Nonadiabatic Vibrational Damping of Molecular Adsorbates: Insights into Electronic Friction and the Role of Electronic Coherence

5.4.1 Content

In this work we addressed a persisting obscurity encountered in the non-adiabatic vibrational damping of molecular adsorbates, particularly CO, on metal surfaces. Even though the underlying coinage and transition metal substrates exhibit a vastly different DOS in the region around the Fermi level, the lifetime of the CO stretch mode on both Cu(100) and Pt(111) as obtained from experiments and confirmed by electronic friction theory is virtually identical (cf., our previous work in Ref. 1). Such a finding is rather surprising, given the notion that dominant low-energy non-adiabatic transitions in the metal should be between electronic states energetically located close around the Fermi level. Not the least, this physical picture is reflected in the analytical formula for the friction coefficients in both ODF and LDFA (cf., section 2.4). One would thus naively expect a correlation between the DOS at the Fermi level and the strength of the effective non-adiabatic coupling—opposed to experimental and electronic friction-based findings.

To shed light into this enigmatic behavior, we pursued a first order TDPT-based approach rooted in TD-DFT that allows to explicitly evaluate the *eh*-pair excitations (and their initial and final states, respectively) underlying the non-adiabatic vibrational damping (cf., section 2.2). We found that correspondingly evaluated spectra indeed show characteristic differences for CO on Cu(100) and Pt(111) in the long-time or perfect coherence limit. These intuitively correlate with the underlying DOS and differ significantly between the two substrates. Accordingly, we found the non-adiabatic energy dissipation rate to be much lower on Cu(100) than on Pt(111). Whilst the latter was spot-on with experimental measurements (and simulations based on electronic friction theory) our results for the coinage metal substrate, however, obviously were not. Only upon approaching a limit of very short electronic coherence times, we could reconcile the energy dissipation rate also on Cu(100) with the experimental evidence.

We thus could show that a finite electronic coherence time—as implicitly assumed in electronic friction theory within the Markov approximation—is fundamental to rationalize the hitherto enigmatic similarity of measured vibrational lifetimes of CO on Pt(111) and Cu(100). At the same time, shortening the electronic coherence had a very distinct effect also on the underlying spectra, essentially washing out the pronounced band structure effects observed before. In this pseudo-Markovian limit the resulting broad spectra for both substrates were—without being imposed—in line with the constant coupling limit from electronic friction theory. We were thus able to touch (and verify) very basic assumptions underlying this approach. Our work thus ultimately explains the good performance of this effective theory in reproducing the experimental vibrational lifetimes.

5.4.2 Individual Contributions

The analytical extension of the TDPT approach to vibrational motion was initiated as part of my master thesis [106] together with Jörg Meyer, who is now affiliated with Leiden University (The Netherlands). He further provided an earlier version of a Castep-based code to evaluate *eh*-pair

spectra, parts of which I later stripped and modified to extract the required KS-matrix elements in the basis of the unperturbed KS-orbitals. Jörg Meyer further hosted me during my research stay in Leiden where together we devised the application of this approach as presented here. He was also involved in fruitful discussions thereafter and lastly co-edited the manuscript. Karsten Reuter supervised the project during its entire course and played a significant part in co-editing the manuscript.

I evaluated the vibrational properties of all systems using CASTEP [144] and further calculated all trajectories based thereon in normal mode coordinates with the MD code I created in the context of Refs. 1 and Ref. 2. Among others, this demanded the implementation of a propagation scheme for the Langevin equation of motion with an actual friction tensor rather than a friction coefficient. Moreover, I extracted the required KS-effective potential matrix elements using modified parts of a CASTEP-based routine initially written by Jörg Meyer in the context of previous work on elastic scattering [35, 53]. In addition, I re-wrote and greatly extended a Python-based code I started to work on during my master thesis [106] to evaluate *eh*-pair excitation spectra starting from the corresponding matrix elements. In this regard, the SciPy [148, 149] and NumPy [150] packages were again heavily relied on. The multiprocessing module included in the Python standard library as of version 2.6 was further used in order to parallelize the computationally demanding parts of the calculation. Moreover, the resultant program includes symmetry-based acceleration schemes, parts of which were originally formulated together with Jörg Meyer in the context of my master thesis [106]. These schemes significantly reduce the number of required integrals in order to efficiently evaluate the respective *eh*-pair excitation spectra, also in the long-time limit. A detailed description of these algorithms will be published elsewhere. Lastly, I evaluated all spectra, did the respective analysis, wrote the manuscript and the supplemental material, and created all figures therein using the matplotlib package [151].

6 Summary, Conclusions and Outlook

A plethora of highly successful concepts in physics and chemistry, such as molecular dynamics simulations, force fields, transition state and kinetic rate theory or the Bell-Polanyi-Evans principle are inevitably connected to the concept of a unique potential energy surface that governs the dynamics of the underlying system. Scientifically growing up with these concepts in mind, it is stunning to realize that there is actually a whole new level of complexity arising with the simple fact that electronic and nuclear motion cannot always be decoupled in the sense of the adiabatic and Born-Oppenheimer approximation. Whilst for gas phase molecules these non-adiabatic effects translate to a rather intuitive picture of nuclei evolving on and switching between several well-separated PESs, the continuous distribution of excitations in a metal surface essentially blurs out the entire concept of potential energy surfaces. Even within the BOA, accurately evaluating the electronic structure of (realistic) molecules and solids has kept an entire scientific community busy for more than the past 50 years. It is thus altogether not surprising that brilliant minds such as John C. Tully built their career on ways to account for non-adiabatic dynamics, yet still leaving us limited to approximate effective models. Going beyond the Born-Oppenheimer approximation for the dynamical description of metal-adsorbate interactions thus continues to be an emerging field of *first principles*-based modeling. In this regard, electronic friction-based MD is—despite many limitations—the best shot we currently have to address non-adiabatic energy dissipation in high-dimensional gas-surface simulations.

This work started with a heated yet unresolved debate about the validity of the LDFA method [77, 111, 112], and a rough idea on how to introduce some more "chemical intuition" than accounted for within the concomitant IAA. Realizing that this effective model will never be qualified for a most accurate and complete account of non-adiabatic effects but in turn foremost requires a pragmatic validation, we chose to straightforwardly compare its performance for vibrational lifetimes with experimental measurements and ODF calculations in Ref. 1. Certainly, LDFA does not account for the tensorial character of the electronic friction and may thus miss out some details of the underlying dynamics. Still, given its conceptual simplicity the resulting performance when comparing to these benchmark observables was stunning. Consequently, our work has ever since been recognized and established as advocate for the LDFA method in literature. The straightforward extension beyond the IAA that we introduced with the AIM scheme, moreover, allows to easily incorporate the method into AIMD simulations thereby superseding the evaluation of the clean surface electronic density at each time step. In fact, significant development effort on combining LDFA-AIM with a QM/Me-based description of the nuclear dynamics [11, 53, 140–142] was spent during the work on this thesis, with a first application of this combined QM/Me+EF approach to the dissociation of O_2 on Pd(100) already in the making. This will allow to combine an accurate description of the phononic fine structure with electronic friction theory-based non-adiabatics for the first time, and thus constitute a further important step towards disentangling these competing energy exchange mechanisms in GSD.

In our extensive review on computational gas-surface dynamics in Ref. 3 we concluded that, despite all detailed mechanistic understanding that has grown over the years, a general assessment of the relative importance of the phononic and non-adiabatic energy dissipation channel has still not been achieved. The apparent pronounced dependence on the specific systems and the prevalent

uncertainty associated with effective models prevents the establishment of "simple" rules of thumb in this regard. In this context, we highlighted the importance of going beyond stochastic experimental measures such as sticking coefficients and diffusion constants in order to gauge the computational tools available. One such target observable are [3]He-SE signatures in the context of surface diffusion [154]. These are very sensitive to the adsorbate-substrate coupling and the underlying diffusion mechanism, and thus encode highly valuable microscopic information [155, 156]. In Ref. 2 we thus reproduced corresponding experimental measurements for thermal adatom diffusion using *ab inito*-based Langevin-MD simulations. This first resulted in combined adiabatic/non-adiabatic friction coefficients that quantified the overall adsorbate-surface coupling. A subsequent analysis of underlying trajectories using the LDFA model then allowed to further quantify the non-adiabatic contributions to the latter—a newly established procedure that can be easily applied to the vast database of [3]He-SE measurements for various systems that has accumulated over the years [157]. For the specific system under investigation, Na on Cu(111), we found a surprisingly large contribution of non-adiabatic coupling conflicting with the common textbook notion of purely adiabatic thermal diffusion. It will be interesting to see whether this is just a coincidence, or transfers also to other systems.

As surprising and fundamental our findings in Ref. 2 are, they simultaneously highlight one of the major issues of the electronic friction approach. Being an effective theory that coarse-grains the electron dynamics up to an implicit Langevin-treatment, it precludes a more profound understanding of the underlying *eh*-pair excitations. That is to say, this method yields a net non-adiabatic effect without offering the chance to further scrutinize its origins. One of the prominent obscurities in this regard are the virtually identical non-adiabatic vibrational lifetimes for CO on Cu(100) and Pt(111) [158, 159]. Electronic friction theory, both within the ODF and LDFA model, reproduces these lifetimes rather accurately [1, 51, 52, 64]—a baffling finding given the pronounced band structure-differences of the underlying coinage and transition metal substrates. We hence had a second look at these systems in Ref. 4, this time however equipped with a TDPT-approach rooted in TD-DFT. By correlating resulting *eh*-pair excitation spectra with respective electronic coherence times, we finally identified a pseudo-Markovian behavior of the electronic DOFs to wash out effects of the differing band structures. Such an assumption is implicitly included in the electronic friction approach, which in turn explains its great success in this regard.

Altogether, the work underlying this thesis has contributed significantly towards further establishing the electronic friction approach, and particularly the LDFA method, as a go-to-model for non-adiabatic gas-surface dynamics. Its performance has been validated on a sound basis by comparing to experimental benchmark observables, and crucial assumptions were tested using higher-level methods. Moreover, the seeds were sown to combine the latter with an accurate description of the substrate nuclear degrees of freedom in terms of a QM/Me+EF model as well as to extend the disentanglement of phononic and non-adiabatic contributions in the context of surface diffusion in systematic studies.

However, electronic friction theory is not a universal remedy for all instances. It may yield a pragmatic and efficient description of non-adiabatic effects, but to understand the latter on a broader scope, going beyond electronic friction seems necessary at several points. For instance, the TDPT method we adapted for molecular adsorbate vibrations can straightforwardly be extended also to diffusive motion. Large parts of the necessary code infrastructure were in fact already created. This would then allow to further scrutinize and potentially rationalize the surprisingly high non-adiabaticity we found for Na diffusion on Cu(111) on the level of individual *eh*-pair excitations. Moreover, respective excitation spectra, potentially combined with their phononic counterpart, may

be of great value in order to devise the friction kernel in generalized Langevin-MD simulations [160, 161].

As a concluding remark, it should be mentioned that the simulation of non-adiabatic gas-surface dynamics is still far away from being a black-box procedure. Although electronic friction may appear as a straightforward concept, one has to keep in mind the assumptions it is built on. In particular, this refers to the assumptions of highly delocalized electronic excitations in the metal substrate that do not significantly alter the shape of the corresponding PESs. In this case it is reasonable to replace the forces on the nuclei by those of the ground state BO-PES and to add some frictional coupling. However, as soon as the field of weak non-adiabaticity is abandoned and this Ehrenfest-inspired picture breaks down, i.e., as soon as individual electronic excitations lead to pronounced differences in the corresponding PESs, electronic friction theory is no longer an adequate tool. This prominently applies to situations involving transient electron-transfer between adsorbate and substrate as, e.g., observed in the scattering of vibrationally excited NO from Au(111) [26, 33, 162–167]. But also more generally, situations with massive rearrangements of the system's electronic structure such as spin transitions or the making and breaking of chemical bonds are envisioned to be problematic. Here, respective excitations undoubtedly have to be taken into account explicitly and it will be interesting to see if corresponding novel and efficient approaches will emerge in the future.

Acknowledgments / Danksagung

First and foremost I want to thank Karsten Reuter for his continuous support and motivation throughout all the years we have been working together. Thank you for letting me "do my thing", yet setting boundaries and giving advice—scientific and strategic—wherever and whenever I needed it. I guess this is what excellent leadership feels like. Moreover, thank you for making me realize that doing a PhD is not just all about science, hard work and having good ideas. Equally important, it is also about growing up, getting things done and taking over responsibility. Independence is a state of mind...

Moreover, I want to particularly acknowledge Jörg Meyer. He introduced me to the field of non-adiabatic dynamics, and I undoubtedly benefited significantly from his impressively deep knowledge. I further very much enjoyed several research stays in Leiden and the passionate scientific spirit I felt there. Our continuous fruitful discussions beyond my stays in Leiden were priceless.

I further want to express my gratitude to my former "team mate" Vanessa Jane Bukas for countless discussions about science, but also about completely unrelated non-sense. Actually, I am very excited that we could conclude our mini-subgroup with a joint review article. I am also thankful for carefully proofreading this thesis, and the steady language-wise counsel over the past years.

Moreover, I owe thanks to many other great scientists. I am grateful to David J. Ward and Bill Allison for working with me in a fascinating project on surface diffusion, and for inviting me to their lab in Cambridge twice. I also want to thank Alec Wodtke for inviting me to his group's retreat on Schloss Ringberg, and Geert-Jan Kroes for inviting me to his group in Leiden. For many fruitful and enjoyable discussions at conferences, workshops, and during visits I further want to acknowledge (in alphabetical order) John Ellis, Gernot Füchsel, J. Iñaki Juaristi, Alexander Kandratsenka, Reinhard Maurer, Francesco Nattino, Eckhard Pehlke, Matt Probert, and John Tully. I also appreciate Patrick Gütlein's endurance and achievements during his internships and master thesis. Together we entered unchartered territory, yet returned quite successfully. Lastly, a heartfelt thank you goes to Axel Groß for getting me enthusiastic about computational chemistry.

From the very first moment I entered the Theoretical Chemistry group in Munich I felt highly welcome and enjoyed a very friendly and supportive atmosphere. It is fascinating to see that even though fluctuations are part of the business, this spirit keeps going on. In this regard, I owe sincere thanks to many current and former group members, too many to name them all. However, Ruth Mösch's endless efforts in defending us from bureaucracy should not remain nameless. Also, our IT-guys Christoph Scheurer, Max Hoffmann, Christoph Schober, Georg Michelitsch and Matthias Kick are to be explicitly appreciated, spending an enormous amount of their precious time to ensure a stable working environment for the entire group. Moreover, I am particularly grateful to Christoph Schober for and bearing with my endless bureaucratic questions during the final days of this thesis, and acknowledge countless memorable discussions about and beyond science with him, Patrick Gütlein, Hendrik Heenen, Georg Michelitsch, Harald Oberhofer, Christoph Scheurer, Markus Sinstein, Thomas Stecher and many more. You know who you are. Lastly, a big thank you goes to our running crew, as well as everyone participating in our morning coffee breaks.

Furthermore, I greatly appreciate Kai Sanwald's steady companionship over the past years in Ulm

and Munich. Even though our scientific ways diverged as PhD students, I am happy we still manage to keep in touch and very much enjoyed our weekly lunch breaks together. I also thank Martin Eberhardt for an undying friendship ever since we met in elementary school.

Last, but actually above all, I want to thank my wife, my family and my in-laws from the bottom of my heart. Danke für das gemeinsame Lächeln, den Zusammenhalt und die bedingungslose Geborgenheit von Kindesbeinen an. Danke, Carolin, für all deine Unterstützung, deine unendliche Herzenswärme und dein Verständnis dafür, dass eine Promotion manchmal auch Entbehrungen erfordert.

Munich, September 2017

Bibliography

[1]   S. P. Rittmeyer, J. Meyer, J. I. Juaristi, and K. Reuter, Phys. Rev. Lett. **115**, 046102 (2015) (cit. on pp. i, 2, 7, 10, 15, 17–19, 22–24, 27, 32, 35–38).

[2]   S. P. Rittmeyer, D. J. Ward, P. Gütlein, J. Ellis, W. Allison, and K. Reuter, Phys. Rev. Lett. **117**, 196001 (2016) (cit. on pp. i, 2, 7, 10, 15, 17–19, 22, 23, 27, 36, 38).

[3]   S. P. Rittmeyer, V. J. Bukas, and K. Reuter, accepted for publication in Adv. Phys. X (2017) 10.1080/23746149.2017.1381574 (cit. on pp. i, 1, 2, 22, 23, 25, 27, 37).

[4]   S. P. Rittmeyer, J. Meyer, and K. Reuter, Phys. Rev. Lett. **119**, 176808 (2017) (cit. on pp. i, 2, 7–9, 14, 15, 19, 21–24, 27, 38).

[5]   G. Ertl, Angew. Chem. Int. Ed. **47**, 3524 (2008) (cit. on p. 1).

[6]   G. Ertl, Adv. Catal. **45**, 1 (2000) (cit. on p. 1).

[7]   G.-J. Kroes, Science **321**, 794 (2008) (cit. on p. 1).

[8]   A. C. Luntz, "Dynamics of Gas-Surface Interactions," in *Surface and Interface Science* (Wiley-VCH, 2016) Chap. 47, pp. 1255–1314 (cit. on p. 1).

[9]   J. Barth, Surf. Sci. Rep. **40**, 75 (2000) (cit. on p. 1).

[10] A. Carley, P. Davies, and M. Roberts, Catal. Lett. **80**, 25 (2002) (cit. on p. 1).

[11] J. Meyer, and K. Reuter, Angew. Chem. Int. Ed. **53**, 4721 (2014) (cit. on pp. 1, 25, 37).

[12] S. Linic, P. Christopher, and D. Ingram, Nature Mat. **10**, 911 (2011) (cit. on p. 1).

[13] P. Christopher, H. Xin, and S. Linic, Nature Chem. **3**, 467 (2011) (cit. on p. 1).

[14] J. C. Tully, Annu. Rev. Phys. Chem. **31**, 319 (1980) (cit. on p. 1).

[15] J. C. Tully, Annu. Rev. Phys. Chem. **51**, 153 (2000) (cit. on pp. 1, 2).

[16] A. Groß, *Theoretical Surface Science: A Microscopic Perspective*, 2nd ed. (Springer, 2009) (cit. on pp. 1, 20–22).

[17] G.-J. Kroes, and C. Díaz, Chem. Soc. Rev. **45**, 3658 (2016) (cit. on pp. 1, 22).

[18] J. C. Tully, J. Chem. Phys. **137**, 22A301 (2012) (cit. on p. 1).

[19] H. Nienhaus, Surf. Sci. Rep. **45**, 1 (2002) (cit. on p. 2).

[20] A. M. Wodtke, J. C. Tully, and D. J. Auerbach, Int. Rev. Phys. Chem. **23**, 513 (2004) (cit. on p. 2).

[21] E. Hasselbrink, Curr. Opin. Solid St. M. **10**, 192 (2006) (cit. on p. 2).

[22] E. Hasselbrink, Surf. Sci. **603**, 1564 (2009) (cit. on p. 2).

[23] I. Rahinov, R. Cooper, D. Matsiev, C. Bartels, D. J. Auerbach, and A. M. Wodtke, Phys. Chem. Chem. Phys. **13**, 12680 (2011) (cit. on p. 2).

[24] H. Arnolds, Prog. Surf. Sci. **86**, 1 (2011) (cit. on p. 2).

[25] K. Golibrzuch, N. Bartels, D. J. Auerbach, and A. M. Wodtke, Annu. Rev. Phys. Chem. **66**, 399 (2015) (cit. on p. 2).

[26] A. M. Wodtke, Chem. Soc. Rev. **45**, 3641 (2016) (cit. on pp. 2, 39).

[27] M. Born, and R. Oppenheimer, Ann. Phys, **389**, 457 (1927) (cit. on pp. 2, 7).

[28] M. Born, and K. Huang, *Dynamical Theory of Crystal Lattices* (Oxford University Press, 1954) (cit. on pp. 2, 6).

[29] J. C. Tully, "Nonadiabatic Dynamics," in *Modern Methods for Multidimensional Dynamics Computations in Chemistry*, edited by D. L. Thompson, (World Scientific, 1998) Chap. 2, pp. 34–72 (cit. on pp. 2, 5, 7, 10–12).

[30] J. C. Tully, Faraday Discuss. **110**, 407 (1998) (cit. on pp. 2, 10, 11).

[31] J. C. Tully, J. Chem. Phys. **93**, 1061 (1990) (cit. on pp. 2, 10, 11).

[32] M. D. Hack, and D. G. Truhlar, J. Phys. Chem. A **104**, 7917 (2000) (cit. on p. 2).

[33] N. A. Shenvi, S. Roy, and J. C. Tully, J. Chem. Phys. **130**, 174107 (2009) (cit. on pp. 2, 39).

[34] M. Timmer, and P. Kratzer, Phys. Rev. B **79**, 165407 (2009) (cit. on pp. 2, 9).

[35] J. Meyer, and K. Reuter, New J. Phys. **13**, 085010 (2011) (cit. on pp. 2, 9, 10, 36).

[36] E. G. d'Agliano, P. Kumar, W. Schaich, and H. Suhl, Phys. Rev. B **11**, 2122 (1975) (cit. on p. 2).

[37] Y. Li, and G. Wahnström, Phys. Rev. Lett. **68**, 3444 (1992) (cit. on pp. 2, 15, 17).

[38] M. Head-Gordon, and J. C. Tully, J. Chem. Phys. **103**, 10137 (1995) (cit. on pp. 2, 11–14).

[39] A. Abedi, N. T. Maitra, and E. K. U. Gross, Phys. Rev. Lett. **105**, 123002 (2010) (cit. on p. 5).

[40] A. Abedi, N. T. Maitra, and E. K. U. Gross, J. Chem. Phys. **137**, 22A530 (2012) (cit. on p. 5).

[41] A. Abedi, F. Agostini, Y. Suzuki, and E. K. U. Gross, Phys. Rev. Lett. **110**, 263001 (2013) (cit. on p. 5).

[42] N. Doltsinis, "Molecular dynamics beyond the Born-Oppenheimer approximation: mixed quantum-classical approaches," in *Computational nanoscience: do it yourself!* Edited by J. Grotendorst, S. Blügel, and D. Marx, (NIC FZ Jülich, 2006), pp. 389–409 (cit. on pp. 6, 10, 11).

[43] A. Messiah, *Quantum Mechanics* (Dover Publications Inc., 1961) (cit. on p. 7).

[44] K. Drukker, J. Comput. Phys. **153**, 225 (1999) (cit. on pp. 7, 10).

[45] C. Carbogno, "Non-adiabatic Effects in the Dissociative Adsorption of O_2 on Aluminium (111) Surfaces," PhD thesis (Universität Ulm, 2009) (cit. on p. 7).

[46] H. S. W. Massey, Rep. Prog. Phys. **12**, 248 (1949) (cit. on p. 7).

[47] G. Schatz, and M. Ratner, *Quantum Mechanics in Chemistry*, Dover Books on Chemistry Series (Dover Publications, 2002) (cit. on pp. 8, 9).

[48] J. Sakurai, and J. Napolitano, *Modern Quantum Mechanics*, 2nd ed. (Prentice Hall, 2007) (cit. on p. 9).

[49] M. Head-Gordon, and J. C. Tully, J. Chem. Phys. **96**, 3939 (1992) (cit. on pp. 9, 13).

[50] M. Head-Gordon, and J. C. Tully, Phys. Rev. B **46**, 1853 (1992) (cit. on pp. 9, 13).

[51] V. Krishna, and J. C. Tully, J. Chem. Phys. **125**, 054706, 054706 (2006) (cit. on pp. 9, 13, 15, 38).

[52] R. J. Maurer, M. Askerka, V. S. Batista, and J. C. Tully, Phys. Rev. B **94**, 115432 (2016) (cit. on pp. 9, 13–15, 25, 38).

[53] J. Meyer, "Ab initio Modeling of Energy Dissipation during Chemical Reactions at Transition Metal Surfaces," PhD thesis (Freie Universität Berlin, 2012) (cit. on pp. 9, 10, 25, 30, 32, 36, 37).

[54] J. C. Tully, Int. J. Quantum Chem. **40**, 299 (1991) (cit. on p. 10).

[55] M. Lindenblatt, and E. Pehlke, Phys. Rev. Lett. **97**, 216101 (2006) (cit. on p. 11).

[56] M. Lindenblatt, and E. Pehlke, Surf. Sci. **600**, 5068 (2006) (cit. on p. 11).

[57] M. Grotemeyer, and E. Pehlke, Phys. Rev. Lett. **112**, 043201 (2014) (cit. on p. 11).

[58] M. E. Tuckerman, *Statistical Mechanics: Theory and Molecular Simulation* (Oxford University Press, 2010) (cit. on p. 12).

[59] R. Kubo, Rep. Prog. Phys. **29**, 255 (1966) (cit. on p. 12).

[60] W. Dou, G. Miao, and J. E. Subotnik, Phys. Rev. Lett. **119**, 046001 (2017) (cit. on pp. 13, 14).

[61] M. Persson, and B. Hellsing, Phys. Rev. Lett. **49**, 662 (1982) (cit. on p. 13).

[62] B. Hellsing, and M. Persson, Phys. Scr. **29**, 360 (1984) (cit. on pp. 13, 14).

[63] J. R. Trail, D. M. Bird, M. Persson, and S. Holloway, J. Chem. Phys. **119**, 4539 (2003) (cit. on pp. 13–15).

[64] M. Forsblom, and M. Persson, J. Chem. Phys. **127**, 154303 (2007) (cit. on pp. 13, 38).

[65] M. Askerka, R. J. Maurer, V. S. Batista, and J. C. Tully, Phys. Rev. Lett. **116**, 217601 (2016) (cit. on pp. 13–16, 25).

[66] N. Lorente, and M. Persson, Faraday Discuss. **117**, 277 (2000) (cit. on pp. 14, 15).

[67] J. Trail, M. Graham, and D. Bird, Comp. Phys. Comm. **137**, 163 (2001) (cit. on p. 15).

[68] D. Novko, M. Alducin, M. Blanco-Rey, and J. I. Juaristi, Phys. Rev. B **94**, 224306 (2016) (cit. on p. 15).

[69] J. T. Kindt, J. C. Tully, M. Head-Gordon, and M. A. Gomez, J. Chem. Phys. **109**, 3629 (1998) (cit. on p. 15).

[70] J. R. Trail, M. C. Graham, D. M. Bird, M. Persson, and S. Holloway, Phys. Rev. Lett. **88**, 166802 (2002) (cit. on p. 15).

[71] A. C. Luntz, and M. Persson, J. Chem. Phys. **123**, 074704 (2005) (cit. on pp. 15, 17).

[72] A. C. Luntz, M. Persson, and G. O. Sitz, J. Chem. Phys. **124**, 091101 (2006) (cit. on p. 15).

[73] A. C. Luntz, M. Persson, S. Wagner, C. Frischkorn, and M. Wolf, J. Chem. Phys. **124**, 244702 (2006) (cit. on pp. 15, 17).

[74] G. Füchsel, T. Klamroth, S. Monturet, and P. Saalfrank, Phys. Chem. Chem. Phys. **13**, 8659 (2011) (cit. on pp. 15, 17).

[75] G. Füchsel, S. Schimka, and P. Saalfrank, J. Phys. Chem. A **117**, 8761 (2013) (cit. on p. 15).

[76] R. J. Maurer, B. Jiang, H. Guo, and J. C. Tully, Phys. Rev. Lett. **118**, 256001 (2017) (cit. on pp. 15, 25).

[77] J. I. Juaristi, M. Alducin, R. Díez Muiño, H. F. Busnengo, and A. Salin, Phys. Rev. Lett. **100**, 116102 (2008) (cit. on pp. 15, 17, 37).

[78] I. Goikoetxea, J. I. Juaristi, M. Alducin, and R. Díez Muiño, J. Phys. Condens. Matter **21**, 264007 (2009) (cit. on p. 15).

[79] J. C. Tremblay, S. Monturet, and P. Saalfrank, Phys. Rev. B **81**, 125408 (2010) (cit. on pp. 15, 17).

[80] A. S. Muzas, J. I. Juaristi, M. Alducin, R. Díez Muiño, G. J. Kroes, and C. Díaz, J. Chem. Phys. **137**, 064707 (2012) (cit. on p. 15).

[81] L. Martin-Gondre, M. Alducin, G. A. Bocan, R. Díez Muiño, and J. I. Juaristi, Phys. Rev. Lett. **108**, 096101 (2012) (cit. on pp. 15, 17).

[82] L. Martin-Gondre, M. Alducin, G. A. Bocan, R. Díez Muiño, and J. I. Juaristi, Phys. Rev. Lett. **108**, 139901(E) (2012) (cit. on pp. 15, 17).

[83] L. Martin-Gondre, G. Bocan, M. Alducin, J. Juaristi, and R. Díez Muiño, Comput. Theor. Chem. **990**, 126 (2012) (cit. on p. 15).

[84] L. Martin-Gondre, G. A. Bocan, M. Blanco-Rey, M. Alducin, J. I. Juaristi, and R. Díez Muiño, J. Phys. Chem. C **117**, 9779 (2013) (cit. on p. 15).

[85] M. Blanco-Rey, J. I. Juaristi, R. Díez Muiño, H. F. Busnengo, G. J. Kroes, and M. Alducin, Phys. Rev. Lett. **112**, 103203 (2014) (cit. on p. 15).

[86] P. Saalfrank, J. I. Juaristi, M. Alducin, M. Blanco-Rey, and R. Díez Muiño, J. Chem. Phys. **141**, 234702, 234702 (2014) (cit. on p. 15).

[87] O. Bünermann, H. Jiang, Y. Dorenkamp, A. Kandratsenka, S. M. Janke, D. J. Auerbach, and A. M. Wodtke, Science **350**, 1346 (2015) (cit. on pp. 15–17).

[88] S. M. Janke, D. J. Auerbach, A. M. Wodtke, and A. Kandratsenka, J. Chem. Phys. **143**, 124708, 124708 (2015) (cit. on pp. 15, 17).

[89] O. Galparsoro, R. Pétuya, J. I. Juaristi, C. Crespos, M. Alducin, and P. Larrégaray, J. Phys. Chem. C **119**, 15434 (2015) (cit. on p. 15).

[90] D. Novko, M. Blanco-Rey, J. I. Juaristi, and M. Alducin, Phys. Rev. B **92**, 201411 (2015) (cit. on p. 15).

[91] B. Jiang, M. Alducin, and H. Guo, J. Phys. Chem. Lett. **7**, 327 (2016) (cit. on p. 15).

[92] I. Lončarić, M. Alducin, P. Saalfrank, and J. I. Juaristi, Nucl. Instrum. Meth. B **382**, 114 (2016) (cit. on p. 15).

[93] D. Novko, M. Blanco-Rey, J. Juaristi, and M. Alducin, Nucl. Instrum. Meth. B **382**, 26 (2016) (cit. on p. 15).

[94] X. Luo, B. Jiang, J. I. Juaristi, M. Alducin, and H. Guo, J. Chem. Phys. **145**, 044704 (2016) (cit. on p. 15).

[95] D. Novko, M. Blanco-Rey, M. Alducin, and J. I. Juaristi, Phys. Rev. B **93**, 245435 (2016) (cit. on p. 15).

[96] R. Scholz, G. Floß, P. Saalfrank, G. Füchsel, I. Lončarić, and J. I. Juaristi, Phys. Rev. B **94**, 165447 (2016) (cit. on p. 15).

[97] G. Füchsel, M. del Cueto, C. Díaz, and G.-J. Kroes, J. Phys. Chem. C **120**, 25760 (2016) (cit. on p. 15).

[98] O. Galparsoro, R. Petuya, F. Busnengo, J. I. Juaristi, C. Crespos, M. Alducin, and P. Larrégaray, Phys. Chem. Chem. Phys. **18**, 31378 (2016) (cit. on p. 15).

[99] G.-J. Kroes, J. I. Juaristi, and M. Alducin, J. Phys. Chem. C **121**, 13617 (2017) (cit. on p. 15).

[100] E. Zaremba, J. H. Rose, L. M. Sander, and H. B. Shore, J. Phys. F **7**, 1763 (1977) (cit. on p. 15).

[101] M. J. Puska, and R. M. Nieminen, Phys. Rev. B **27**, 6121 (1983) (cit. on pp. 15, 16).

[102] P. Echenique, and M. Uranga, in *Interaction of Charged Particles with Solids and Surfaces*, Vol. 271, edited by A. Gras-Marti, H. Urbassek, N. R. Arista, and F. Flores, Nato ASI Series (Plenum Press, 1991), pp. 39–71 (cit. on p. 15).

[103] L. Bönig, and K. Schönhammer, Phys. Rev. B **39**, 7413 (1989) (cit. on p. 15).

[104] E. Bonderup, "Lecture Notes on: Penetration of Charged Particles through Matter," 1978 (cit. on p. 15).

[105] L. I. Schiff, *Quantum Mechanics*, 3rd ed. (McGraw-Hill, 1968) (cit. on pp. 15, 16).

[106] S. P. Rittmeyer, "Non-Adiabatic Vibrational Damping of O_2 on Ag(100): Implications for Light-Enhanced Catalysis?" Master thesis (Technische Universität München, 2013) (cit. on pp. 15, 29, 35, 36).

[107] E. Zaremba, A. Arnau, and P. Echenique, Nucl. Instrum. Meth. B **96**, 619 (1995) (cit. on p. 16).

[108] B. H. Bransden, and C. J. Joachain, *Physics of Atoms and Molecules*, 2nd ed. (Prentice Hall, 2003) (cit. on p. 16).

[109] H. Winter, J. I. Juaristi, I. Nagy, A. Arnau, and P. M. Echenique, Phys. Rev. B **67**, 245401 (2003) (cit. on p. 17).

[110] R. Díez Muiño, and A. Salin, Phys. Rev. B **62**, 5207 (2000) (cit. on p. 17).

[111] A. C. Luntz, I. Makkonen, M. Persson, S. Holloway, D. M. Bird, and M. S. Mizielinski, Phys. Rev. Lett. **102**, 109601 (2009) (cit. on pp. 17, 37).

[112] J. I. Juaristi, M. Alducin, R. Díez Muiño, H. F. Busnengo, and A. Salin, Phys. Rev. Lett. **102**, 109602 (2009) (cit. on pp. 17, 37).

[113] F. Hirshfeld, Theor. Chim. Acta **44**, 129 (1977) (cit. on p. 18).

[114] A. Szabo, and N. S. Ostlund, *Modern Quantum Chemistry: Introduction to Advanced Electronic Structure Theory* (Dover Publications Inc., 1996) (cit. on p. 19).

[115] F. Jensen, *Introduction to Computational Chemistry*, 2nd ed. (Wiley, Dec. 2006) (cit. on pp. 19–22).

[116] C. J. Cramer, *Essentials of Computational Chemistry: Theories and Models*, 2nd ed. (Wiley, 2005) (cit. on p. 19).

[117] P. Hohenberg, and W. Kohn, Phys. Rev. **136**, B864 (1964) (cit. on pp. 19–21).

[118] W. Kohn, and L. J. Sham, Phys. Rev. **140**, A1133 (1965) (cit. on p. 20).

[119] E. Runge, and E. K. U. Gross, Phys. Rev. Lett. **52**, 997 (1984) (cit. on p. 21).

[120] R. Stowasser, and R. Hoffmann, J. Am. Chem. Soc. **121**, 3414 (1999) (cit. on p. 21).

[121] D. P. Chong, O. V. Gritsenko, and E. J. Baerends, J. Chem. Phys. **116**, 1760 (2002) (cit. on p. 21).

[122] R. van Meer, O. V. Gritsenko, and E. J. Baerends, J. Chem. Theo. Comp. **10**, 4432 (2014) (cit. on p. 21).

[123] A. D. Becke, J. Chem. Phys. **140**, 18A301 (2014) (cit. on pp. 21, 22).

[124] J. P. Perdew, and K. Schmidt, AIP Conference Proceedings **577**, 1 (2001) (cit. on p. 21).

[125] D. M. Ceperley, and B. J. Alder, Phys. Rev. Lett. **45**, 566 (1980) (cit. on p. 22).

[126] J. P. Perdew, J. A. Chevary, S. H. Vosko, K. A. Jackson, M. R. Pederson, D. J. Singh, and C. Fiolhais, Phys. Rev. B **46**, 6671 (1992) (cit. on p. 22).

[127] J. L. D. Silva, C. Stampfl, and M. Scheffler, Surf. Sci. **600**, 703 (2006) (cit. on p. 22).

[128] H. S. Yu, S. L. Li, and D. G. Truhlar, J. Chem. Phys. **145**, 130901 (2016) (cit. on p. 22).

[129] P. J. Hasnip, K. Refson, M. I. J. Probert, J. R. Yates, S. J. Clark, and C. J. Pickard, Phil. Trans. R. Soc. **372**, 20130270 (2014) (cit. on p. 22).

[130] J. P. Perdew, K. Burke, and M. Ernzerhof, Phys. Rev. Lett. **77**, 3865 (1996) (cit. on p. 22).

[131] J. P. Perdew, K. Burke, and M. Ernzerhof, Phys. Rev. Lett. **78**, 1396 (1997) (cit. on p. 22).

[132] C. Díaz, E. Pijper, R. A. Olsen, H. F. Busnengo, D. J. Auerbach, and G. J. Kroes, Science **326**, 832 (2009) (cit. on p. 22).

[133] C. Lee, W. Yang, and R. G. Parr, Phys. Rev. B **37**, 785 (1988) (cit. on p. 22).

[134] A. D. Becke, J. Chem. Phys. **98**, 5648 (1993) (cit. on p. 22).

[135] J. P. Perdew, M. Ernzerhof, and K. Burke, J. Chem. Phys. **105**, 9982 (1996) (cit. on p. 22).

[136] C. Adamo, and V. Barone, J. Chem. Phys. **110**, 6158 (1999) (cit. on p. 22).

[137] E. B. Wilson, J. C. Decius, and P. C. Cross, *Molecular Vibrations* (Dover Publications Inc., 1980) (cit. on p. 23).

[138] N. Ashcroft, and N. Mermin, *Solid State Physics* (Cengage Learning, 1976) (cit. on pp. 23, 25).

[139] C. Kittel, *Introduction to Solid State Physics*, 8th ed. (John Wiley and Sons Ltd, 2004), 704 pp. (cit. on p. 23).

[140] V. J. Bukas, and K. Reuter, Phys. Rev. Lett. **117**, 146101 (2016) (cit. on pp. 25, 37).

[141] V. J. Bukas, "Dissociation and dissipation dynamics of adsorbates at solid surfaces," PhD thesis (Technische Universität München, 2016) (cit. on pp. 25, 37).

[142] V. J. Bukas, and K. Reuter, J. Chem. Phys. **146**, 014702 (2017) (cit. on pp. 25, 37).

[143] P. Lazić, N. Atodiresei, M. Alaei, V. Caciuc, S. Blügel, and R. Brako, Comp. Phys. Comm. **181**, 371 (2010) (cit. on p. 29).

[144] S. J. Clark, M. D. Segall, C. J. Pickard, P. J. Hasnip, M. I. J. Probert, K. Refson, and M. C. Payne, Z. Kristallogr. **220**, 567 (2005) (cit. on pp. 30, 32, 36).

[145] E. R. McNellis, J. Meyer, and K. Reuter, Phys. Rev. B **80**, 205414 (2009) (cit. on pp. 30, 32).

[146] S. R. Bahn, and K. W. Jacobsen, Comput. Sci. Eng. **4**, 56 (2002) (cit. on pp. 30, 32, 33).

[147] A. H. Larsen, J. J. Mortensen, J. Blomqvist, I. E. Castelli, R. Christensen, M. Dułak, J. Friis, M. N. Groves, B. Hammer, C. Hargus, E. D. Hermes, P. C. Jennings, P. B. Jensen, J. Kermode, J. R. Kitchin, E. L. Kolsbjerg, J. Kubal, K. Kaasbjerg, S. Lysgaard, J. B. Maronsson, T. Maxson, T. Olsen, L. Pastewka, A. Peterson, C. Rostgaard, J. Schiøtz, O. Schütt, M. Strange, K. S. Thygesen, T. Vegge, L. Vilhelmsen, M. Walter, Z. Zeng, and K. W. Jacobsen, J. Phys. Condens. Matter **29**, 273002 (2017) (cit. on pp. 30, 32, 33).

[148] T. E. Oliphant, Comput. Sci. Eng. **9**, 10 (2007) (cit. on pp. 30, 32, 36).

[149] K. J. Millman, and M. Aivazis, Comput. Sci. Eng. **13**, 9 (2011) (cit. on pp. 30, 32, 36).

[150] S. van der Walt, S. C. Colbert, and G. Varoquaux, Comput. Sci. Eng. **13**, 22 (2011) (cit. on pp. 30, 32, 36).

[151] J. D. Hunter, Comput. Sci. Eng. **9**, 90 (2007) (cit. on pp. 30, 32, 36).

[152] P. Peterson, Int. J. Comp. Sci. Eng. **4**, 296 (2009) (cit. on p. 32).

[153] S. Behnel, R. Bradshaw, C. Citro, L. Dalcin, D. S. Seljebotn, and K. Smith, Comput. Sci. Eng. **13**, 31 (2011) (cit. on p. 32).

[154] A. Jardine, H. Hedgeland, G. Alexandrowicz, W. Allison, and J. Ellis, Prog. Surf. Sci. **84**, 323 (2009) (cit. on p. 38).

[155] A. P. Jardine, J. Ellis, and W. Allison, J. Chem. Phys. **120**, 8724 (2004) (cit. on p. 38).

[156] A. P. Jardine, G. Alexandrowicz, H. Hedgeland, W. Allison, and J. Ellis, Phys. Chem. Chem. Phys. **11**, 3355 (2009) (cit. on p. 38).

[157] A. P. Jardine, J. Ellis, and W. Allison, J. Phys. Condens. Matter **14**, 6173 (2002) (cit. on p. 38).

[158] M. Morin, N. J. Levinos, and A. L. Harris, J. Chem. Phys. **96**, 3950 (1992) (cit. on p. 38).

[159] J. D. Beckerle, R. R. Cavanagh, M. P. Casassa, E. J. Heilweil, and J. C. Stephenson, J. Chem. Phys. **95**, 5403 (1991) (cit. on p. 38).

[160] M. Ceriotti, G. Bussi, and M. Parrinello, Phys. Rev. Lett. **102**, 020601 (2009) (cit. on p. 39).

[161] M. Ceriotti, G. Bussi, and M. Parrinello, J. Chem. Theo. Comp. **6**, 1170 (2010) (cit. on p. 39).

[162] Y. Huang, A. M. Wodtke, H. Hou, C. T. Rettner, and D. J. Auerbach, Phys. Rev. Lett. **84**, 2985 (2000) (cit. on p. 39).

[163] Y. Huang, C. T. Rettner, D. J. Auerbach, and A. M. Wodtke, Science **290**, 111 (2000) (cit. on p. 39).

[164] S. Li, and H. Guo, J. Chem. Phys. **117**, 4499 (2002) (cit. on p. 39).

[165] N. A. Shenvi, S. Roy, and J. C. Tully, Science **326**, 829 (2009) (cit. on p. 39).

[166] S. Roy, N. A. Shenvi, and J. C. Tully, J. Chem. Phys. **130**, 174716 (2009) (cit. on p. 39).

[167] R. Cooper, C. Bartels, A. Kandratsenka, I. Rahinov, N. Shenvi, K. Golibrzuch, Z. Li, D. J. Auerbach, J. C. Tully, and A. M. Wodtke, Angew. Chem. Int. Ed. **51**, 4954 (2012) (cit. on p. 39).

Appendices

Electronic Friction-Based Vibrational Lifetimes of Molecular Adsorbates: Beyond the Independent-Atom Approximation

S.P. Rittmeyer, J. Meyer, J.I. Juaristi, and K. Reuter

Electronic Friction-Based Vibrational Lifetimes of Molecular Adsorbates: Beyond the Independent-Atom Approximation

Simon P. Rittmeyer,[1,*] Jörg Meyer,[2,†] J. Iñaki Juaristi,[3,4,5] and Karsten Reuter[1]

[1]*Chair for Theoretical Chemistry and Catalysis Research Center, Technische Universität München, Lichtenbergstrasse 4, 85747 Garching, Germany*
[2]*Leiden Institute of Chemistry, Gorlaeus Laboratories, Leiden University, P.O. Box 9502, 2300 RA Leiden, Netherlands*
[3]*Departamento de Física de Materiales, Facultad de Químicas, UPV/EHU, Apartado 1072, 20080 San Sebastián, Spain*
[4]*Centro de Física de Materiales CFM/MPC (CSIC-UPV/EHU), Paseo Manuel de Lardizabal 5, 20018 San Sebastián, Spain*
[5]*Donostia International Physics Center (DIPC), Paseo Manuel de Lardizabal 5, 20018 San Sebastián, Spain*

We assess the accuracy of vibrational damping rates of diatomic adsorbates on metal surfaces as calculated within the local-density friction approximation (LDFA). An atoms-in-molecules (AIM) type charge partitioning scheme accounts for intramolecular contributions and overcomes the systematic underestimation of the nonadiabatic losses obtained within the prevalent independent-atom approximation. The quantitative agreement obtained with theoretical and experimental benchmark data suggests the LDFA-AIM scheme as an efficient and reliable approach to account for electronic dissipation in *ab initio* molecular dynamics simulations of surface chemical reactions.

A central challenge in energy and catalysis applications is to transfer energy specifically into those degrees of freedom that actually drive a desired surface chemical reaction—and to keep this energy in these degrees of freedom for a sufficiently long time. In this transfer of energy, losses due to electronic nonadiabaticity can be an important dissipation channel [1,2]. In aiming to assess this channel for systems of technological interest, predictive-quality calculations would be a valuable addition to experimental endeavors. Especially for chemical reactions at frequently employed metal substrates, however, a corresponding methodology has not yet been well established.

To date, most accurate solutions of the full nuclear-electron wave function are restricted to systems of the complexity level of gas-phase H_2^+ [3]. In the limit of weak nonadiabaticity as pertinent to electron-hole (eh) pair excitations during adsorbate dynamics on metal surfaces, less rigorous approaches rely on mixed quantum-classical dynamics. The imposed computational burden nevertheless still restricts their practical use to simple metals and subpicosecond time scales [4,5], to symmetric adsorbate trajectories [6,7], or to only qualitative accounts of the metal electronic structure [8,9]. Presently, it is thus only the concept of electronic friction [10–13] and its incorporation into classical molecular dynamics (MD) simulations on the Born-Oppenheimer potential energy surface (PES) V_{PES} [14–21] that promises predictive-quality and material-specific trajectory calculations over an extended period of time.

Particularly the local-density friction approximation (LDFA) [16,22] and for molecular adsorbates an additional independent-atom approximation (IAA) [16–18] provide a

further decrease in computational cost. This has allowed for first accounts of electronic nonadiabaticity in large-scale MD simulations based on a first-principles and high-dimensional description of the underlying PES—either interpolated [16–19] or even evaluated on-the-fly within *ab initio* MD simulations [20,21]. However, due to the drastic simplifications introduced with the IAA, the validity of the LDFA formalism for molecular adsorbates *per se* has been controversially discussed [16,23,24]. By construction, the IAA does not resolve the electronic structure of the interacting molecule-surface system and in particular the location of the molecular frontier orbitals in the surface band structure. It can thus, for instance, not reproduce the enhancement of friction coefficients close to the transition state of a molecular dissociation event on metal surfaces [23]. On the other hand, the necessity of an accurate description of such regions of enhanced friction for the overall nonadiabatic energy dissipation has been questioned, as the typically low velocities in these regions effectively suppress the contribution of the friction term within the dynamics [16].

Despite the success in recent applications, it thus remains elusive to which extent the limitations of the prevalent IAA carry over to actual observables. In this situation, the vibrational lifetimes of high-frequency adsorbate modes can provide a sensitive measure, as they are largely governed by energy dissipation in the electronic nonadiabatic channel [25–27]. Accurate experimental reference data then allow for a substantiated assessment of the quality of the nonadiabatic description. In this study, we perform such an assessment, primarily focusing on the internal stretch mode of two systems which have been

studied most extensively and conclusively by experiments: CO adsorbed on Cu(100) and Pt(111) [26]. Despite the largely different surface frontier orbital locations and concomitant hybridizations at the transition and noble metal surface, we find the LDFA-IAA to already exhibit a good qualitative performance with respect to experimental [28,29] and theoretical [30,31] benchmark data. Rather than an explicit account of the surface band structure, our analysis suggests missing intramolecular contributions as reason for the remaining differences. Approximately incorporating such contributions through a numerically efficient atoms-in-molecules (AIM) charge partitioning indeed yields consistent lifetimes for a range of diatomic adsorbate systems.

In friction theory, all nonadiabatic effects due to the excitation of eh pairs in the metal substrate are condensed into a single velocity-dependent dissipative force that augments the classical equations of motion,

$$m_i \frac{d^2 R_{i\alpha}}{dt^2} = -\frac{\partial V_{\mathrm{PES}}}{\partial R_{i\alpha}} - \sum_{j=1}^{N}\sum_{\beta=1}^{3} \eta_{i\alpha j\beta} \frac{dR_{j\beta}}{dt} + \mathcal{F}_{i\alpha}(T). \quad (1)$$

Here, small latin and greek subscripts denote atoms and Cartesian degrees of freedom, respectively, and N is the total number of atoms of mass m_i and position $\mathbf{R}_i$ in the system. The fluctuating white noise force $\mathcal{F}_{i\alpha}(T)$ becomes negligible at very low temperatures and vanishes exactly at 0 K. Every element of the friction tensor $\boldsymbol{\eta}$ is, in principle, a function of all nuclear coordinates. Within the spirit of weak coupling, the focus is usually on the diagonal contributions describing the electronic friction felt by each atom [13,27].

These atomic friction coefficients $\eta_{i\alpha j\beta} = \eta_{i\alpha}\delta_{ij}\delta_{\alpha\beta}$ can e.g., be calculated within the quasi-static regime building on time-dependent density-functional theory (DFT) as suggested by Persson and Hellsing [11,32]. While insightful and generally in good agreement with experiments, the accurate numerical evaluation of this approach is challenging in practice and has hitherto been limited to low-dimensional potentials describing the adsorbate-metal interaction [14,15,31,33,34]. This shifts interest to more effective schemes and there in particular to the local-density friction approximation. The LDFA introduces isotropic scalar atomic friction coefficients η_i^{LDFA}, such that $\eta_{i\alpha j\beta}^{\mathrm{LDFA}} = \eta_i^{\mathrm{LDFA}}\delta_{ij}\delta_{\alpha\beta}$. These coefficients can be calculated very efficiently from the scattering properties of an atomic impurity embedded in a free electron gas (FEG) [10,12,35]. In order to relate this model to the actual motion of adsorbates, the embedding density of the FEG ρ_{emb} is then chosen as the electron density value of the clean metal surface ρ_{surf} at the position of the adsorbate atoms. In its application to molecular adsorbates, this implies an independent-atom approximation—which has been regarded and discussed as being inherently included in the LDFA formalism in this context [16,23,24]. As a result of the IAA,

the employed atomic friction coefficients are insensitive to the molecular nature of the adsorbate, yet can be evaluated very efficiently. The only input variable is the clean surface electronic density, which, assuming a frozen surface, has to be calculated only once in advance.

We obtain the two-dimensional PES $V_{\mathrm{PES}}(d_{\mathrm{CO}}, Z_{\mathrm{c.m.}})$ of an adsorbed CO molecule as a function of its bond length d_{CO} and center-of-mass (c.m.) height $Z_{\mathrm{c.m.}}$ above the frozen surface through DFT calculations. Each PES is supported by 442 data points that are calculated with the CASTEP plane-wave pseudopotential code [36] and subsequently interpolated using bivariate cubic splines. Electronic exchange and correlation (xc) is treated on the generalized gradient approximation (GGA) level in terms of the Perdew-Burke-Ernzerhof (PBE) functional [37]. The metal surfaces are modeled by five layer slabs with a separating 20 Å vacuum distance. We consider top-site adsorbed CO molecules on one side of the slab within a $c(2 \times 2)$ and $(\sqrt{3} \times \sqrt{3})R30°$ surface unit cell on Cu(100) and Pt(111), respectively. In both cases, the molecular axis is perpendicular to the surface, with the C atom coordinated to the metal atom. At the employed computational settings [600 eV cutoff energy, ultrasoft pseudopotentials [38], $(10 \times 10 \times 1)$ and $(11 \times 11 \times 1)$ Monkhorst-Pack **k**-point grids [39] for Cu(100) and Pt(111), respectively], the PES data points are converged to < 5 meV. Our investigation is not affected by the well-known CO adsorption puzzle and the concomitant wrong absolute depth of the adsorption well [40]. This is confirmed by essentially identical lifetimes we obtain when using PESs generated with a van der Waals-xc-functional [41] that leads to a stabilization of the top site [42].

Vibrational lifetimes τ are extracted from classical MD simulations on the interpolated PESs by numerically solving Eq. (1). Within the LDFA the atomic friction coefficients η_i^{LDFA} are calculated from the scattering phase shifts of the Kohn-Sham orbitals at the Fermi momentum $\delta_l^F = \delta_l(k_F)$ for an atomic impurity embedded in a FEG of density $\rho_{\mathrm{emb},i}$ [10,12,35],

$$\eta_i^{\mathrm{LDFA}}(\rho_{\mathrm{emb},i}) = \frac{4\pi\rho_{\mathrm{emb},i}}{k_F} \sum_{l=0}^{\infty} (l+1)\sin^2[\delta_l^F - \delta_{l+1}^F], \quad (2)$$

where $\rho_{\mathrm{emb},i}^{\mathrm{IAA}} = \rho_{\mathrm{surf}}(\mathbf{R}_i)$ within the IAA as described before. Assuming a constant energy dissipation rate and thus an exponential decay of the vibrational energy E_{vib}, the lifetime τ can be extracted from the simulations by a logarithmic fit of E_{vib} versus time t. To initialize our simulations, we assign the adsorbate stretch-mode a projected kinetic energy of $\hbar\omega$, where ω is the normal mode frequency. Higher initial kinetic energies up to $5\hbar\omega$ result in minute lifetime changes of less than 0.1 ps.

Figure 1 shows the vibrational lifetimes that result from our simulations. We compare them to experimental values obtained from pump-probe spectroscopy [28,29] and
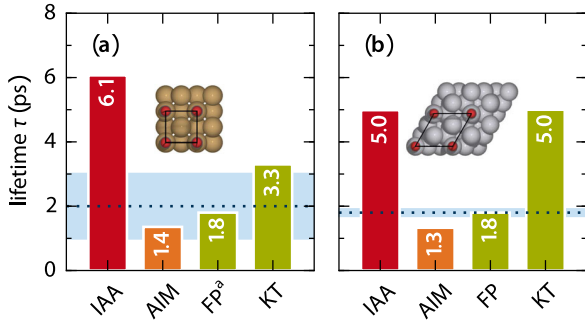
FIG. 1 (color online). Vibrational lifetimes for CO on (a) Cu(100) and (b) Pt(111). Values as obtained within the independent-atom approximation (IAA) and the atoms-in-molecules (AIM) approach from Eq. (3) are contrasted to corresponding predicted lifetimes published by Forsblom and Persson (FP) [30] and Krishna and Tully (KT) [31]. For comparison, experimental values as obtained from pump-probe spectroscopy by Morin *et al.* for CO on Cu(100) [29] and Beckerle *et al.* for CO on Pt(111) [28] are shown as a dotted line and a blue stripe further indicating the reported experimental uncertainty. ^{a}CO on Cu(100).

theoretical values as published by Forsblom and Persson (FP) [30], and Krishna and Tully (KT) [31]. The latter two values are both based on the orbital-dependent Persson-Hellsing expression mentioned above [11,32], albeit obtained from different derivations and relying on slightly different numerical treatment. For both systems, the LDFA-IAA lifetimes agree fairly well with the theoretical values from FP and KT, as well as with experiment. With all numbers falling within one order of magnitude, the current data thus does not further support the harsh criticism the LDFA-IAA was faced with before [23]. Generally, they are instead consistent with the good LDFA-IAA performance reported in earlier studies on nonadiabatic energy losses of various ions scattered off metal surfaces [43] and on the vibrational damping of atoms on metal surfaces [11,32,44]. Conspicuously, however, in these studies on adsorbate atoms the agreement was even more quantitative and lacked the systematic underestimation (overestimation) of LDFA-IAA nonadiabatic energy losses (lifetimes) apparent in Fig. 1.

Rather than from a generally insufficient account of the electronic structure of the interacting adsorbate-surface system, this suggests that LDFA-IAA deficiencies arise particularly in the treatment of molecular adsorbates as isolated adatoms. In this respect—within the underlying atomic embedding model—systematic shortcomings lie in the complete neglect of both adsorbate-substrate as well as intramolecular contributions to ρ_{emb}. Considering only the density of the clean surface, ρ_{emb} is systematically underestimated, consistent with the underestimated energy losses observed in Fig. 1. Even more, by construction a thus defined ρ_{emb} is also blind to dynamical changes of intramolecular bond distances and characters. Figure 2 illustrates this for the vibrational motion of CO at Cu(100).
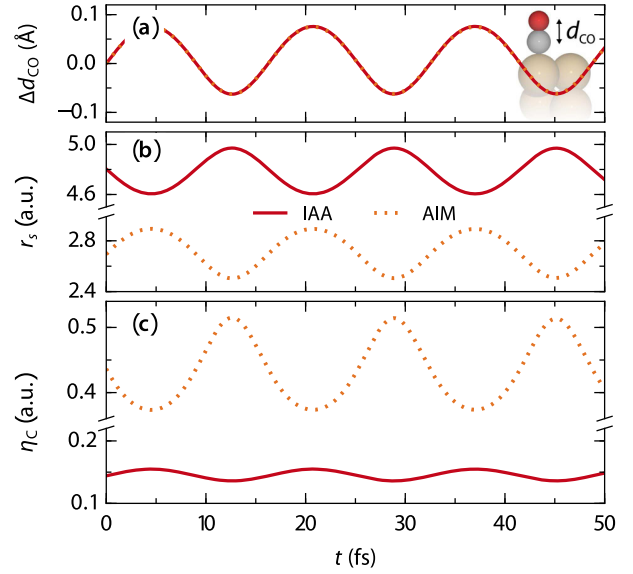

FIG. 2 (color online). (a) Change of the C–O bond length Δd_{CO} on Cu(100) over the first few periods of the stretch mode. (b) Embedding density $\rho_{emb,C}$ of the C atom represented by the Wigner-Seitz radius $r_s = [3/(4\pi\rho_{emb,C})]^{1/3}$ in atomic units (a.u.). (c) Corresponding carbon friction coefficient. Solid red lines refer to the IAA, dotted orange lines to an AIM embedding density according to Eq. (3).

The LDFA-IAA friction coefficient of the carbon atom decreases with smaller C–O bond lengths d_{CO} and thus larger distances Z_C of the C atom from the metal surface. This is due to the fact that the IAA only accounts for changes of ρ_{surf} along the vibrational coordinate. The LDFA-IAA thus effectively decomposes the molecular vibration into two independent adatom vibrations. Yet, even without any intramolecular bonding there will be an increasing overlap of the O and C atomic densities with decreasing d_{CO}. This intramolecular contribution to ρ_{emb} at the position of every constituent atom is thus completely missed in the LDFA-IAA approximation.

A straightforward way to account for such contributions is to perform a charge decomposition through a projection scheme like Hirshfeld's analysis [45]. For any given adsorbate configuration this provides the projected density of any adsorbate atom ρ_i^{Hirsh}, and corresponding sharing function w_i^{Hirsh} at any position $\mathbf{R}$ [46]. Within an AIM picture, we can then define as embedding density for atom i at position $\mathbf{R}_i$,

$$\rho_{emb,i}^{AIM} = \rho_{SCF}(\mathbf{R}_i) - \rho_i^{Hirsh}(\mathbf{R}_i)$$
$$= [1 - w_i^H(\mathbf{R}_i)]\rho_{SCF}(\mathbf{R}_i). \qquad (3)$$

We thus consider as embedding density the full self-consistently calculated density ρ_{SCF} of the entire interacting adsorbate-surface system just without the contribution associated with atom i. This naturally contains density

contributions from all other atoms in the system (both substrate and adsorbate) and consequently carries an implicit dependence $\rho_{emb,i}^{AIM}(\{\mathbf{R}_{i\neq j}\})$. Figure 2(b) contrasts the correspondingly obtained $\rho_{emb,C}^{AIM}$ to $\rho_{emb,C}^{IAA}$ during the CO vibrational motion. Intriguingly, the two quantities differ not only quantitatively, but even exhibit a reversed phase behavior. The account of the density contribution of the O atom in $\rho_{emb,C}^{AIM}$ thus outweighs the influence of the clean surface density seen by the IAA: At the largest vertical heights of the carbon atom Z_C, where $\rho_{emb,C}^{IAA}$ is smallest, also d_{CO} is smallest. Already in the simple diatomic this leads to such a large intramolecular density contribution that the overall $\rho_{emb,C}^{AIM}$ is largest.

These new features also carry over to the corresponding friction coefficients, and in turn to the calculated lifetimes. As apparent from Fig. 1 the LDFA-AIM approach cures the systematic overestimation of lifetimes and yields values that are now *en par* with the FP calculations and experiments. Similar findings have been obtained when applying the LDFA-AIM to two further systems [47] for which reference lifetimes have been reported from orbital-dependent theories, CN on Pt(111) [30] and H_2 on Ru(0001) [17]. With $\tau^{AIM} = 0.9$ ps vs $\tau^{FP} = 2.4$ ps and $\tau^{AIM} = 210$ fs vs $\tau^{[17]} = 215$ fs, respectively, LDFA-AIM yields in both cases lifetimes that are fully consistent with the reference numbers, yet at a fraction of the numerical cost of the orbital-dependent theories.

Adjusting ρ_{emb} to also take into account influences from atoms other than only the clean metal surface hence seems to provide a simple, but effective correction for a molecular treatment within the LDFA. The idea underlying Eq. (3) is thereby similar to the subtraction of a free atom density as suggested in the context of vibrational damping of adatoms [44]. However, employing Hirshfeld sharing functions [45] offers the advantage that the embedding densities are guaranteed to be within physically well defined boundaries $0 \leq \rho_{emb,i}^{AIM} \leq \rho_{SCF}(\mathbf{R}_i)$. This way, our proposed scheme also preserves the molecular dissociation limit by construction: At large bond distances, the respective friction coefficients smoothly go over into friction coefficients virtually identical to the ones obtained for independent atoms. This is nicely illustrated by essentially identical vibrational lifetimes obtained within the IAA and AIM for the H_2 on Ru(0001) system, where the individual atoms are separated by about 2.7 Å on the surface. Furthermore, a Hirshfeld analysis typically requires only a minute computational effort compared to achieving self-consistency for electronic energies and forces (or compared to the multiple self-consistent calculations required to obtain derivatives from finite differences in the FP or KT approaches). The LDFA-AIM scheme proposed here can thus be easily carried out at every time step of *ab initio* MD simulations, allowing surface motion to be explicitly taken into account. In this respect, Eq. (3) defines an embedding density not only for

adsorbate but also for bulk atoms. Friction coefficients derived therefrom could thus, in principle, as well be invoked to evaluate energy losses due to electron-phonon coupling in the bulk.

In conclusion, we have shown that the vibrational damping of high-frequency adsorbate modes on metal surfaces can be added to the list of nonadiabatic phenomena that are reasonably well described by means of electronic friction. The complete neglect of intramolecular effects in the prevalent LDFA-IAA approximation is thereby likely to underestimate the electronic energy dissipation. The here presented AIM alternative instead accounts for them approximately through a charge partitioning scheme. As it thus effectively treats the molecular electrons as part of the metallic substrate, we expect the AIM friction concept to generally rather overestimate nonadiabatic energy losses and to perform best for chemisorbed adsorbates at close distances to the surface. Being a direct descendant of the LDFA, our scheme is, of course, also unlikely to overcome fundamental limitations that come with its heritage. As such it is unlikely to properly capture the strong enhancement of friction coefficients directly at the transition state leading to molecular dissociation. However, as important as it may be, this actual dissociation event only constitutes a fraction of the dynamics that is relevant to chemical surface reactions. Other important aspects like a vibrational pre-excitation or an ensuing hot adatom motion may dominate the overall (nonadiabatic) energy dissipation [20,48], yet take place over much longer time scales. They can thus only be assessed with a numerically highly efficient method like the LDFA. In this respect, our results further consolidate the trust in LDFA-based results for these important long-term events.

---

*Corresponding author.
simon.rittmeyer@tum.de
†j.meyer@chem.leidenuniv.nl

[1] A. M. Wodtke, J. C. Tully, and D. J. Auerbach, Int. Rev. Phys. Chem. **23**, 513 (2004).
[2] H. Nienhaus, Surf. Sci. Rep. **45**, 1 (2002).
[3] A. Abedi, N. T. Maitra, and E. K. U. Gross, Phys. Rev. Lett. **105**, 123002 (2010).
[4] M. Lindenblatt and E. Pehlke, Phys. Rev. Lett. **97**, 216101 (2006).
[5] M. Grotemeyer and E. Pehlke, Phys. Rev. Lett. **112**, 043201 (2014).

[6] M. Timmer and P. Kratzer, Phys. Rev. B **79**, 165407 (2009).

[7] J. Meyer and K. Reuter, New J. Phys. **13**, 085010 (2011).

[8] N. Shenvi, S. Roy, and J. C. Tully, Science **326**, 829 (2009).

[9] N. Shenvi, S. Roy, and J. C. Tully, J. Chem. Phys. **130**, 174107 (2009).

[10] P. Echenique, R. Nieminen, and R. Ritchie, Solid State Commun. **37**, 779 (1981).

[11] B. Hellsing and M. Persson, Phys. Scr. **29**, 360 (1984).

[12] P. M. Echenique, R. M. Nieminen, J. C. Ashley, and R. H. Ritchie, Phys. Rev. A **33**, 897 (1986).

[13] M. Head-Gordon and J. C. Tully, J. Chem. Phys. **103**, 10137 (1995).

[14] J. R. Trail, D. M. Bird, M. Persson, and S. Holloway, J. Chem. Phys. **119**, 4539 (2003).

[15] A. C. Luntz and M. Persson, J. Chem. Phys. **123**, 074704 (2005).

[16] J. I. Juaristi, M. Alducin, R. Díez Muiño, H. F. Busnengo, and A. Salin, Phys. Rev. Lett. **100**, 116102 (2008).

[17] G. Füchsel, T. Klamroth, S. Monturet, and P. Saalfrank, Phys. Chem. Chem. Phys. **13**, 8659 (2011).

[18] L. Martin-Gondre, M. Alducin, G. A. Bocan, R. Díez Muiño, and J. I. Juaristi, Phys. Rev. Lett. **108**, 096101 (2012).

[19] G. Füchsel, S. Schimka, and P. Saalfrank, J. Phys. Chem. A **117**, 8761 (2013).

[20] M. Blanco-Rey, J. I. Juaristi, R. Díez Muiño, H. F. Busnengo, G. J. Kroes, and M. Alducin, Phys. Rev. Lett. **112**, 103203 (2014).

[21] P. Saalfrank, J. I. Juaristi, M. Alducin, M. Blanco-Rey, and R. Díez Muiño, J. Chem. Phys. **141**, 234702 (2014).

[22] Y. Li and G. Wahnström, Phys. Rev. Lett. **68**, 3444 (1992).

[23] A. C. Luntz, I. Makkonen, M. Persson, S. Holloway, D. M. Bird, and M. S. Mizielinski, Phys. Rev. Lett. **102**, 109601 (2009).

[24] J. I. Juaristi, M. Alducin, R. Díez Muiño, H. F. Busnengo, and A. Salin, Phys. Rev. Lett. **102**, 109602 (2009).

[25] J. C. Tully, M. Gomez, and M. Head-Gordon, J. Vac. Sci. Technol. A **11**, 1914 (1993).

[26] H. Arnolds, Prog. Surf. Sci. **86**, 1 (2011).

[27] P. Saalfrank, Chem. Rev. **106**, 4116 (2006).

[28] J. D. Beckerle, R. R. Cavanagh, M. P. Casassa, E. J. Heilweil, and J. C. Stephenson, J. Chem. Phys. **95**, 5403 (1991).

[29] M. Morin, N. J. Levinos, and A. L. Harris, J. Chem. Phys. **96**, 3950 (1992).

[30] M. Forsblom and M. Persson, J. Chem. Phys. **127**, 154303 (2007).

[31] V. Krishna and J. C. Tully, J. Chem. Phys. **125**, 054706 (2006).

[32] M. Persson and B. Hellsing, Phys. Rev. Lett. **49**, 662 (1982).

[33] N. Lorente and M. Persson, Faraday Discuss. **117**, 277 (2000).

[34] A. C. Luntz, M. Persson, S. Wagner, C. Frischkorn, and M. Wolf, J. Chem. Phys. **124**, 244702 (2006).

[35] M. J. Puska and R. M. Nieminen, Phys. Rev. B **27**, 6121 (1983).

[36] S. J. Clark, M. D. Segall, C. J. Pickard, P. J. Hasnip, M. I. J. Probert, K. Refson, and M. C. Payne, Z. Kristallogr. **220**, 567 (2005).

[37] J. P. Perdew, K. Burke, and M. Ernzerhof, Phys. Rev. Lett. **77**, 3865 (1996); **78**, 1396 (1997).

[38] D. Vanderbilt, Phys. Rev. B **41**, 7892 (1990).

[39] H. J. Monkhorst and J. D. Pack, Phys. Rev. B **13**, 5188 (1976).

[40] P. J. Feibelman, B. Hammer, J. K. Nørskov, F. Wagner, M. Scheffler, R. Stumpf, R. Watwe, and J. Dumesic, J. Phys. Chem. B **105**, 4018 (2001).

[41] M. Dion, H. Rydberg, E. Schröder, D. C. Langreth, and B. I. Lundqvist, Phys. Rev. Lett. **92**, 246401 (2004).

[42] P. Lazić, M. Alaei, N. Atodiresei, V. Caciuc, R. Brako, and S. Blügel, Phys. Rev. B **81**, 045401 (2010).

[43] H. Winter, J. I. Juaristi, I. Nagy, A. Arnau, and P. M. Echenique, Phys. Rev. B **67**, 245401 (2003).

[44] J. C. Tremblay, S. Monturet, and P. Saalfrank, Phys. Rev. B **81**, 125408 (2010).

[45] F. Hirshfeld, Theor. Chim. Acta **44**, 129 (1977).

[46] E. R. McNellis, J. Meyer, and K. Reuter, Phys. Rev. B **80**, 205414 (2009).

[47] Consistent with the theoretical work by FP [30], we consider perpendicular CN adsorption with the C atom coordinated to the metal on a top site within a (2×2) surface unit cell. The H_2 on Ru(0001) system is modeled by analogy with the equilibrium configuration mentioned by Füchsel *et al.* [19], i.e., using a (2×2) surface unit cell with two H atoms adsorbed in adjacent fcc hollow sites. For both systems, we use a $(9 \times 9 \times 1)$ Monkhorst-Pack **k**-point grid [39]. All remaining computational details are the same as outlined for CO on Cu(100) and Pt(111), respectively.

[48] J. Meyer and K. Reuter, Angew. Chem. Int. Ed. **53**, 4721 (2014).

Energy Dissipation during Diffusion at Metal Surfaces: Disentangling the Role of Phonons versus Electron-Hole Pairs

S.P. Rittmeyer, D.J. Ward, P. Gütlein, J. Ellis, W. Allison, and K. Reuter

P H Y S I C A L   R E V I E W   L E T T E R S

Energy Dissipation during Diffusion at Metal Surfaces: Disentangling the Role of Phonons versus Electron-Hole Pairs

Simon P. Rittmeyer,[1,*] David J. Ward,[2] Patrick Gütlein,[1] John Ellis,[2] William Allison,[2] and Karsten Reuter[1]

[1]*Chair for Theoretical Chemistry and Catalysis Research Center, Technische Universität München,
Lichtenbergstr. 4, 85747 Garching, Germany*
[2]*Cavendish Laboratory, University of Cambridge, Madingley Road, Cambridge CB3 0HE, United Kingdom*

Helium spin echo experiments combined with *ab initio* based Langevin molecular dynamics simulations are used to quantify the adsorbate-substrate coupling during the thermal diffusion of Na atoms on Cu(111). An analysis of trajectories within the local density friction approximation allows the contribution from electron-hole pair excitations to be separated from the total energy dissipation. Despite the minimal electronic friction coefficient of Na and the relatively small mass mismatch to Cu promoting efficient phononic dissipation, about $(20 \pm 5)\%$ of the total energy loss is attributable to electronic friction. The results suggest a significant role of electronic nonadiabaticity in the rapid thermalization generally relied upon in adiabatic diffusion theories.

Energy dissipation during surface dynamical processes at solid surfaces has been extensively studied, both due to its paramount technological importance and intriguing fundamental richness. Scattering or adsorption of molecules, diffusion, and chemical reactions are all known to be intricately governed by the detailed ways in which chemical and kinetic energy is transferred into and out of substrate degrees of freedom. On insulating or semiconducting surfaces the dynamical coupling to the surface can be attributed to the excitation of and interaction with lattice vibrations with some confidence. In contrast, on metal surfaces the role of competing electronic nonadiabatic effects such as electron-hole (*eh*) pair excitations is a continuing topic of debate. In fact, there is growing experimental evidence that can only be rationalized by breaking with the prevalent Born-Oppenheimer view [1,2]. It may even be argued that due to the continuum of substrate electronic states at the Fermi edge, no dynamical process can strictly be adiabatic at metal surfaces at all [3,4]. On the other hand, many phenomena still seem to be very well described using purely adiabatic theories [5–9].

Recent *ab initio* calculations of dynamical phenomena beyond the Born-Oppenheimer approximation have attempted to resolve some of this ambiguity [10–14]. In particular the numerically appealing concept of electronic friction [10,15–17] within the local density friction approximation (LDFA) [18,19] has become a popular approach in this regard [14,18,20–24]. Scattering processes [8,14,18,25,26] and (dissociative) adsorption events [10,14,23,27] have gained the most attention in this context and with the high incident energies, short contact times, and massive charge rearrangements such processes are likely to be good candidates for a high degree of electronic nonadiabaticity.

In comparison to scattering and adsorption processes, the situation is less clear for surface diffusion. On the one hand, diffusing adsorbates are necessarily close to the surface and in regions of high electronic density, with a concomitant amount of electronic friction. On the other hand, the comparably low velocities that are involved may suppress the nonadiabatic channel and thus favor a coupling to the phononic degrees of freedom to finally render surface diffusion electronically adiabatic. Interestingly, a significant contribution of nonadiabatic energy dissipation in the transient H-atom diffusive motion following H_2 dissociation over Pd(100) has been reported by Blanco-Rey and coworkers only recently [20,21,24]. The results are consistent with a similar prediction by Wahnström made for H diffusion on Ni(100) in the late 1980s [28]. Hydrogen diffusion is, however, a somewhat special case given that competing phononic couplings are small for this very light adsorbate [21,24].

In order to obtain a more comprehensive insight into the relative importance of lattice vibrations and *eh*-pair excitations for the energy dissipation during surface diffusion we therefore address the thermal motion of Na on Cu(111). Alkali metal systems have long been used as prototypical systems due to the relative simplicity of their surface chemistry [29,30] and the Na/Cu combination chosen for the current work benefits from having a much higher adsorbate-substrate mass ratio in comparison to H/Pd. Together with the thermally distributed adsorbate velocities, the coupling to phononic degrees of freedom might be expected to be significantly stronger. Simultaneously, the electronic friction coefficient is a material property that exhibits the well known Z_1 oscillations as a function of the atomic number [17,31,32]. At any embedding density of interest for surface diffusion, the electronic friction is found

196001-1

to be particularly low for light alkali metals. We might, therefore, expect minimal *eh*-pair excitations during the diffusive dynamics of sodium on a free-electron-like metal such as copper. As a consequence one would expect phononic coupling to dominate the overall dynamic interaction with the substrate for Na/Cu(111). Analyzing helium spin echo signatures for surface diffusion with *ab initio* based Langevin molecular dynamics (MD) simulations we nevertheless find that the energy loss due to electronic friction contributes approximately $(20 \pm 5)\%$ of the total energy dissipation, thus reinforcing the view that diffusion is an important class of dynamical processes in which electronic nonadiabaticity is anything but negligible.

The helium spin echo technique utilizes the ^{3}He nuclear spin as an internal timer, providing direct access to the intermediate scattering function (ISF) $I(\Delta \mathbf{K}, t)$ at a momentum transfer $\Delta \mathbf{K}$ specified by the scattering geometry [33]. As a result of surface adsorbate motion the (auto) correlation determined through the ISF decays in time, and for processes where the adsorbate couples to the degrees of freedom of the substrate would typically exhibit an exponential decay. The decay rate $\alpha(\Delta \mathbf{K})$ is highly sensitive to the frictional adsorbate-substrate coupling, with a functional dependence on $\Delta \mathbf{K}$ characteristic of the detailed diffusion mechanism [34,35]. In the present study experiments were conducted at a surface temperature of 155 K with measurements along the $[11\bar{2}]$ azimuth of a Cu(111) crystal dosed to a coverage of $\Theta = 0.025$ monolayer (ML) of sodium [36].

The form of $\alpha(\Delta \mathbf{K})$ extracted from the data is shown in Fig. 1. At large values of $|\Delta \mathbf{K}|$ the behavior is indicative of single-jump diffusion, consistent with the Chudley-Elliott model [37], while at smaller values below about 0.6 Å^{-1} there is an obvious deviation from the ideal sinusoidal signature that is consistent with "de Gennes narrowing" [38] and observed for previous works on repulsive interacting adsorbates [35], notably sodium diffusing on the Cu (100) surface [39].

A quantification of the adsorbate-substrate frictional coupling can be achieved within the kinematic scattering approximation [35]. As further detailed in the Supplemental Material [40], the ISF is directly related to the real-space motion $\mathbf{R}_j(t)$ of an ensemble of N_{atoms} adsorbates j through the autocorrelation function of the coherent intermediate amplitudes

$$A(\Delta \mathbf{K}, t) = \sum_{j}^{N_{\text{atoms}}} \exp \left[-i\Delta \mathbf{K} \cdot \mathbf{R}_j(t) \right]. \quad (1)$$

The corresponding trajectories $\mathbf{R}_j(t)$ are conveniently obtained from Langevin MD simulations, in which the overall friction coefficient η is varied until optimum agreement with the experimental decay rates is obtained [34,35,58]. Specifically, in the current work we employed a system of $N_{\text{atoms}} = 200$ adatoms in a supercell consisting of
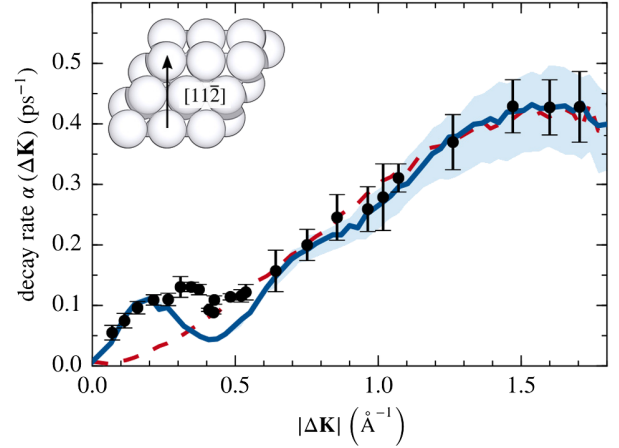

FIG. 1. Experimentally measured decay rates $\alpha(\Delta \mathbf{K})$ along the $[11\bar{2}]$ surface direction as opposed to those extracted from simulations with a best-fit friction coefficient of $\eta = 10$ amu ps^{-1} (solid blue line). The blue-shaded region indicates the sensitivity when varying the free parameter η by $\pm 30\%$. Simulations using an optimum value for η, but without adsorbate-adsorbate interaction potentials, yield the dashed sinusoidal red line. This line lacks the de Gennes narrowing peak at small $|\Delta \mathbf{K}|$, but is unaffected in the region sensitive to the frictional coupling.

a (49×82) array of rectangular Cu(111) unit cells and used $T = 155$ K to match the experimental Na coverage and temperature. Appropriate averaging over 100 MD runs accumulated over 1.6 ns (2^{14} steps) each ensured converged decay rates $\alpha(\Delta \mathbf{K})$.

To minimize the number of free parameters the two-dimensional adsorbate-substrate potential energy surface (PES) employed in the Langevin MD simulations was determined by density-functional theory (DFT) calculations using CASTEP [59] at the generalized gradient level in terms of the Perdew-Burke-Ernzerhof (PBE) functional [60]. As detailed in the Supplemental Material [40] these calculations are used to parametrize an analytical Fourier representation of the PES, which faithfully reproduces the DFT PES with a root-mean-square deviation of < 2 meV. As indicated by the de Gennes narrowing feature at small $|\Delta \mathbf{K}|$ in Fig. 1, we additionally account for repulsive adsorbate-adsorbate interactions through pairwise repulsive dipole-dipole interaction potentials according to Kohn and Lau [61]. The required (coverage-dependent) dipole moments of the respective adatoms are obtained by fitting experimental work function–change measurements [62] to the Topping model of surface depolarization [63], as had already been done successfully for Na on Cu(100) [64].

The resulting analysis exhibits only one remaining free parameter, the friction coefficient η. As shown in Fig. 1 an optimized value of $\eta = 10$ amu ps^{-1} achieves an overall excellent agreement with the experimental measurements. All prominent features in the experimental curve, i.e., the modulation corresponding to the de Gennes narrowing at

small values of $|\Delta \mathbf{K}|$ as well as the sinusoidal line shape for larger values are qualitatively reproduced with the major contributory factors to diffusion quantitatively reproduced to a large extent. To obtain an estimate of the sensitivity of our results, we additionally indicate in Fig. 1 the range of $\alpha(\Delta \mathbf{K})$ values we obtain when varying the best-fit friction coefficient within $\pm 30\%$. It is obviously only the region at $|\Delta \mathbf{K}| > 0.7$ Å^{-1} that is increasingly sensitive to this friction coefficient, and the $\pm 30\%$ uncertainty safely brackets the experimental error bars. The small but apparently systematic deviations in the lower $|\Delta \mathbf{K}|$ region are instead attributed to a conceivably insufficient treatment of adsorbate-adsorbate interactions. When completely switching off the dipole interactions in our simulations, the changes to the sinusoidal shape predicted by the single jump model [37] are exclusively restricted to this low $|\Delta \mathbf{K}|$ region, cf. Fig. 1. Thus, the friction value we obtain is completely robust with respect to these aspects of our model. A similar robustness is obtained with respect to the PES topology. As detailed in the Supplemental Material [40], variations of the diffusion barrier over the bridge sites by $\pm 30\%$, to account for inaccuracies of the DFT PBE functional we use, also lead to a variation of decay rates that falls almost exactly within the shaded region in Fig. 1.

The friction coefficient has contributions from both phononic and electronically nonadiabatic dissipation [65]. In a two-bath model for diffusion, contributions have been shown to be additive [66] so we can write

$$\eta \approx \eta_{\text{phonons}} + \eta_{eh\text{-pairs}}. \qquad (2)$$

To disentangle the two dissipation channels approximately, we calculate the ensemble-averaged electronic friction experienced over the Langevin-MD trajectories within the LDFA [15,17–19]. For this we first determine an analytic Fourier representation of the position-dependent electronic friction coefficient of a diffusing Na atom $\eta_{eh\text{-pairs}}(\mathbf{R}_j)$ using a procedure analogous to that employed for the PES. At each DFT point $\mathbf{R}_{\text{DFT}}$ calculated for the PES parametrization, the embedding density required in the LDFA ansatz is extracted from the self-consistent total electronic density through an atoms-in-molecules scheme based on a Hirshfeld decomposition [22]. The resulting grid of $\eta_{eh\text{-pairs}}(\mathbf{R}_{\text{DFT}})$ is subsequently expanded in a Fourier series as further detailed in the Supplemental Material [40]. Figure 2 illustrates the resulting continuous electronic friction coefficient along two high symmetry lines along the Cu(111) surface. Obviously, $\eta_{eh\text{-pairs}}(\mathbf{R}_j)$ correlates with the inverse height profile of the Na adsorbate; the closer the adsorbate is to the Cu(111) surface, the higher the embedding density and the larger the friction coefficient becomes.

The average electronic friction experienced by the entire Langevin ensemble of adatoms j is then approximated non-self-consistently at each MD time step as $\eta_{eh\text{-pairs,av}}(t) = \sum_j^{N_{\text{atoms}}} \eta_{eh\text{-pairs}}(\mathbf{R}_j(t))/N_{\text{atoms}}$ for each trajectory generated
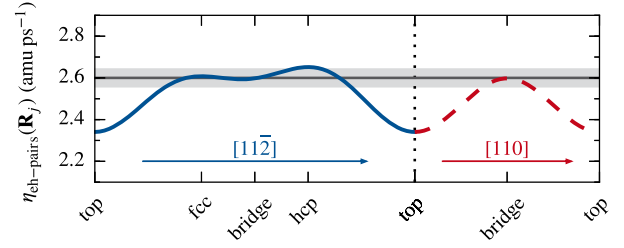

FIG. 2. Interpolated electronic friction coefficient $\eta_{eh\text{-pairs}}(\mathbf{R}_j)$ experienced by a Na atom along the $[11\bar{2}]$ (solid blue) and $[1\bar{1}0]$ (dashed red) surface direction. The horizontal dark gray line indicates the determined ensemble- and time-averaged electronic friction $\eta_{eh\text{-pairs}}$, with the light-gray corridor indicating the standard deviation over all time steps and trajectories.

in our best-fit simulations. Averaging over all trajectories and time steps we finally arrive at an estimate of the electronically nonadiabatic dissipation contribution to the overall η of $\eta_{eh\text{-pairs}} = 2.60$ amu ps^{-1}. As apparent from Fig. 2 this average value is somewhere between the friction coefficients experienced at the most stable fcc and hcp adsorption sites and the lowest-energy diffusion barrier over the bridge sites. As also shown in the figure, the standard deviation resulting from this average $\eta_{eh\text{-pairs}}$ is very small (± 0.04 amu ps^{-1}), consistent with the fact that the thermalized Na atoms spend the predominant time in the corresponding (meta)stable basins of the PES. In terms of the motion through the surface electron density, the situation is thus highly comparable to vibrational dynamics, an area where the LDFA has been shown to perform quantitatively [22]. Correspondingly, we expect this level of theory to provide a reliable assessment of the relative amount of electronic friction, even though it would be conceptually interesting to compare to higher-level theories that for instance account for tensorial aspects of friction [67] or that additionally provide the explicit eh-pair excitation spectra [12,68]. We further note that similar to the findings for adsorbate vibrations [22], a key element in the use of the simple LDFA scheme is the appropriate determination of the host embedding density experienced by the adsorbate. For the analysis so far, we used the atoms-in-molecules approach based on Hirshfeld's projection scheme [22]. The corresponding integrated Hirshfeld charges indicate a charge transfer of $0.3e$ from a Na atom adsorbed in the fcc or hcp sites to the Cu substrate, which naturally enhances the embedding density and thus the electronic friction coefficient. Use of the independent-atom-approximation as originally employed within the LDFA context [18] does not account for such a charge transfer in constructing the embedding density but relies on the self-consistent screening of the underlying isotropic model system. This would then predict an $\eta_{eh\text{-pairs}}$ that is just about 63% of the value determined here. Because of the ambiguous choice of the embedding density, both methods

P H Y S I C A L   R E V I E W   L E T T E R S

can be considered to yield an upper and lower limit of the LDFA approach, respectively [22].

Given these considerations and comparing the determined $\eta_{eh\text{-pairs}}$ with the total friction coefficient, we arrive at the surprising result that electronic nonadiabaticity amounts to about $(20 \pm 5)\%$ of the total energy dissipation, and this in a system that was selectively chosen to minimize this dissipation channel. Tentatively, we would thus expect even more pronounced influences of eh-pair excitations in the diffusive motion of adsorbates like potassium atoms, i.e., elements that correspond to a maximum of the Z_1 oscillations of the electronic friction coefficient. As had been shown in the previous work on H diffusion [20,21,24,28], the relative contribution will, of course, also be increased at smaller adsorbate-substrate mass ratios by the concomitant suppression of phononic dissipation. All in all, the picture that emerges is of surface diffusion in which electronic nonadiabaticity plays a much more prominent role than hitherto anticipated. Indeed, one could conjecture that it is in fact electronic nonadiabaticity that ensures rapid thermalization in adsorbate systems with a large frequency mismatch and that explains the long-term success of adiabatic theories to determine diffusion constants and other kinetic parameters for growth and catalysis applications.

---

*Corresponding author.
simon.rittmeyer@tum.de

[1] J. C. Tully, J. Chem. Phys. **137**, 22A301 (2012).
[2] A. M. Wodtke, Chem. Soc. Rev. **45**, 3641 (2016).
[3] J. C. Tully, Annu. Rev. Phys. Chem. **51**, 153 (2000).
[4] A. M. Wodtke, J. C. Tully, and D. J. Auerbach, Int. Rev. Phys. Chem. **23**, 513 (2004).
[5] P. Nieto, E. Pijper, D. Barredo, G. Laurent, R. A. Olsen, E.-J. Baerends, G.-J. Kroes, and D. Farías, Science **312**, 86 (2006).
[6] C. Díaz, J. K. Vincent, G. P. Krishnamohan, R. A. Olsen, G. J. Kroes, K. Honkala, and J. K. Nørskov, Phys. Rev. Lett. **96**, 096102 (2006).
[7] I. Goikoetxea, J. Beltrán, J. Meyer, J. I. Juaristi, M. Alducin, and K. Reuter, New J. Phys. **14**, 013050 (2012).
[8] A. S. Muzas, J. I. Juaristi, M. Alducin, R. Díez Muiño, G. J. Kroes, and C. Díaz, J. Chem. Phys. **137**, 064707 (2012).
[9] P. M. Hundt, B. Jiang, M. E. van Reijzen, H. Guo, and R. D. Beck, Science **344**, 504 (2014).
[10] A. C. Luntz and M. Persson, J. Chem. Phys. **123**, 074704 (2005).
[11] N. A. Shenvi, S. Roy, and J. C. Tully, Science **326**, 829 (2009).
[12] J. Meyer and K. Reuter, New J. Phys. **13**, 085010 (2011).
[13] M. Grotemeyer and E. Pehlke, Phys. Rev. Lett. **112**, 043201 (2014).
[14] S. M. Janke, D. J. Auerbach, A. M. Wodtke, and A. Kandratsenka, J. Chem. Phys. **143**, 124708 (2015).
[15] P. Echenique, R. Nieminen, and R. Ritchie, Solid State Commun. **37**, 779 (1981).
[16] B. Hellsing and M. Persson, Phys. Scr. **29**, 360 (1984).
[17] P. M. Echenique, R. M. Nieminen, J. C. Ashley, and R. H. Ritchie, Phys. Rev. A **33**, 897 (1986).
[18] J. I. Juaristi, M. Alducin, R. Díez Muiño, H. F. Busnengo, and A. Salin, Phys. Rev. Lett. **100**, 116102 (2008).
[19] Y. Li and G. Wahnström, Phys. Rev. Lett. **68**, 3444 (1992).
[20] M. Blanco-Rey, J. I. Juaristi, R. Díez Muiño, H. F. Busnengo, G. J. Kroes, and M. Alducin, Phys. Rev. Lett. **112**, 103203 (2014).
[21] D. Novko, M. Blanco-Rey, J. I. Juaristi, and M. Alducin, Phys. Rev. B **92**, 201411 (2015).
[22] S. P. Rittmeyer, J. Meyer, J. I. Juaristi, and K. Reuter, Phys. Rev. Lett. **115**, 046102 (2015).
[23] B. Jiang, M. Alducin, and H. Guo, J. Phys. Chem. Lett. **7**, 327 (2016).
[24] D. Novko, M. Blanco-Rey, M. Alducin, and J. I. Juaristi, Phys. Rev. B **93**, 245435 (2016).
[25] L. Martin-Gondre, M. Alducin, G. A. Bocan, R. Díez Muiño, and J. I. Juaristi, Phys. Rev. Lett. **108**, 096101 (2012); **108**, 139901(E) (2012).
[26] I. Goikoetxea, J. I. Juaristi, M. Alducin, and R. D. Muiño, J. Phys. Condens. Matter **21**, 264007 (2009).
[27] G. Füchsel, S. Schimka, and P. Saalfrank, J. Phys. Chem. A **117**, 8761 (2013).
[28] G. Wahnström, Chem. Phys. Lett. **163**, 401 (1989).
[29] R. D. Diehl and R. McGrath, J. Phys. Condens. Matter **9**, 951 (1997).
[30] C. Huang, G. Fratesi, D. A. MacLaren, W. Luo, G. P. Brivio, and W. Allison, Phys. Rev. B **82**, 081413 (2010).
[31] A. Arnau, P. Echenique, and R. Ritchie, Nucl. Instrum. Methods Phys. Res., Sect. B **33**, 138 (1988).
[32] H. Winter, C. Auth, A. Mertens, A. Kirste, and M. J. Steiner, Europhys. Lett. **41**, 437 (1998).
[33] A. Jardine, H. Hedgeland, G. Alexandrowicz, W. Allison, and J. Ellis, Prog. Surf. Sci. **84**, 323 (2009).
[34] A. P. Jardine, J. Ellis, and W. Allison, J. Chem. Phys. **120**, 8724 (2004).
[35] A. P. Jardine, G. Alexandrowicz, H. Hedgeland, W. Allison, and J. Ellis, Phys. Chem. Chem. Phys. **11**, 3355 (2009).
[36] We define a full monolayer such that $\Theta = 1\text{ML}$ corresponds to one Na atom per Cu(111) surface atom in the first layer.
[37] C. T. Chudley and R. J. Elliott, Proc. Phys. Soc. **77**, 353 (1961).
[38] P. D. Gennes, Physica **25**, 825 (1959).
[39] G. Alexandrowicz, A. P. Jardine, P. Fouquet, S. Dworski, W. Allison, and J. Ellis, Phys. Rev. Lett. **93**, 156103 (2004).
[40] See Supplemental Material at http://link.aps.org/supplemental/10.1103/PhysRevLett.117.196001, which includes Refs. [41–57], for a description of computational and experimental details.

[41] SAES Getters, Alkali metal dispensers, https://www.saesgetters.com/products/alkali-metals-dispensers.

[42] D. Tang, D. McIlroy, X. Shi, C. Su, and D. Heskett, Surf. Sci. Lett. **255**, L497 (1991).

[43] A. Carlsson, S.-A. Lindgren, C. Svensson, and L. Walldén, Phys. Rev. B **50**, 8926 (1994).

[44] S. D. Borisova, G. G. Rusina, S. V. Eremeev, G. Benedek, P. M. Echenique, I. Y. Sklyadneva, and E. V. Chulkov, Phys. Rev. B **74**, 165412 (2006).

[45] G. Witte, J. Phys. Condens. Matter **16**, S2937 (2004).

[46] D. Vanderbilt, Phys. Rev. B **41**, 7892 (1990).

[47] H. J. Monkhorst and J. D. Pack, Phys. Rev. B **13**, 5188 (1976).

[48] A. P. Graham, J. Toennies, and G. Benedek, Surf. Sci. **556**, L143 (2004).

[49] H. Lüth, *Solid Surfaces, Interfaces and Thin Films*, 5th ed., Graduate Texts in Physics (Springer, Berlin, 2014).

[50] M. Diamant, S. Rahav, R. Ferrando, and G. Alexandrowicz, J. Phys. Condens. Matter **27**, 125008 (2015).

[51] G. Bussi and M. Parrinello, Phys. Rev. E **75**, 056707 (2007).

[52] G. Bussi, D. Donadio, and M. Parrinello, J. Chem. Phys. **126**, 014101 (2007).

[53] T. L. Ferrell and R. H. Ritchie, Phys. Rev. B **16**, 115 (1977).

[54] M. J. Puska and R. M. Nieminen, Phys. Rev. B **27**, 6121 (1983).

[55] F. Hirshfeld, Theor. Chim. Acta **44**, 129 (1977).

[56] J. Ellis and A. Graham, Surf. Sci. **377–379**, 833 (1997).

[57] L. Van Hove, Phys. Rev. **95**, 249 (1954).

[58] B. A. J. Lechner, H. Hedgeland, A. P. Jardine, W. Allison, B. J. Hinch, and J. Ellis, Phys. Chem. Chem. Phys. **17**, 21819 (2015).

[59] S. J. Clark, M. D. Segall, C. J. Pickard, P. J. Hasnip, M. I. J. Probert, K. Refson, and M. C. Payne, Z. Kristallogr. **220**, 567 (2005).

[60] J. P. Perdew, K. Burke, and M. Ernzerhof, Phys. Rev. Lett. **77**, 3865 (1996); **78**, 1396 (1997).

[61] W. Kohn and K.-H. Lau, Solid State Commun. **18**, 553 (1976).

[62] N. Fischer, S. Schuppler, T. Fauster, and W. Steinmann, Surf. Sci. **314**, 89 (1994).

[63] J. Topping, Proc. R. Soc. A **114**, 67 (1927).

[64] J. Ellis, A. P. Graham, F. Hofmann, and J. P. Toennies, Phys. Rev. B **63**, 195408 (2001).

[65] T. Ala-Nissila, R. Ferrando, and S. C. Ying, Adv. Phys. **51**, 949 (2002).

[66] R. Martínez-Casado, A. Sanz, J. Vega, G. Rojas-Lorenzo, and S. Miret-Artés, Chem. Phys. **370**, 180 (2010).

[67] M. Askerka, R. J. Maurer, V. S. Batista, and J. C. Tully, Phys. Rev. Lett. **116**, 217601 (2016).

[68] M. Timmer and P. Kratzer, Phys. Rev. B **79**, 165407 (2009).

Energy Dissipation during Diffusion at Metal Surfaces: Disentangling the Role of Phonons vs. Electron-Hole Pairs

Simon P. Rittmeyer,[1, *] David J. Ward,[2] Patrick Gütlein,[1] John Ellis,[2] William Allison,[2] and Karsten Reuter[1]

[1]*Chair for Theoretical Chemistry and Catalysis Research Center,*
Technische Universität München, Lichtenbergstr. 4, 85747 Garching, Germany
[2]*Cavendish Laboratory, University of Cambridge, Madingley Road, Cambridge, CB3 0HE, United Kingdom*

S1. EXPERIMENTAL DETAILS

A. Sample Preparation and Characterization

A mechanically polished single crystal Cu(111) sample (Surface Prep. Lab., NL) used in the study is mounted on a sample manipulator, allowing translational, polar and azimuthal rotations as well as temperature control. The manipulator is fitted into a scattering chamber for the spectrometer which is evacuated to 2×10^{-11} mbar base pressure post baking. Preparation of the surface consists of repeated cycles of argon ion sputtering ($I_{emiss} \approx 6\,\mu A/cm^2$, 800 V Ar^+ ions, $T_s = 300\,K$ for 30 mins) followed by surface annealing ($T_s = 800\,K$, 30 secs). The surface quality is monitored through measurement of helium reflectivity. A high quality surface was confirmed regularly by exceptionally strong helium reflectivity ($> 34\%$ measured at $T_s = 300\,K$). A typical incident energy of 8 meV was used for the experiments with the beam energy recorded at regular intervals.

The clean Cu(111) crystal was aligned to the $[11\bar{2}]$ surface azimuth, by optimizing the pattern of helium scattered from high purity carbon monoxide adsorbed to monolayer (ML) saturation. The temperature of the sample is monitored using a type-K [1] thermocouple spot welded onto a sample mount constructed from tantalum. Temperature control is achieved with cryogenic sample cooling using liquid nitrogen ($T_s > 120\,K$), balanced against radiative heating from a coiled tungsten filament.

Alkali metals are dosed onto the Cu(111) sample from dispensers supplied by SAES Getters[2], which provide a convenient method for introducing high purity films in vacuum. In order to deliver alkali vapor efficiently, the front edge of the dispenser and the surface must be brought into close proximity. For the current work an apparatus has been constructed consisting of a linear vacuum below with a dosing insert onto which the dispenser is fixed with a titanium flag in front connected to an external rotary vacuum feed-through. When the flag is closed the sample is shielded from the dispenser. Opening and closing the flag allows a precise initiation and termination of dosing irrespective of the dispenser pre-loading conditions. Before starting to dose with a new dispenser it is degassed to remove adsorbed gases from the casing and support mountings.

---

* Corresponding author: simon.rittmeyer@tum.de
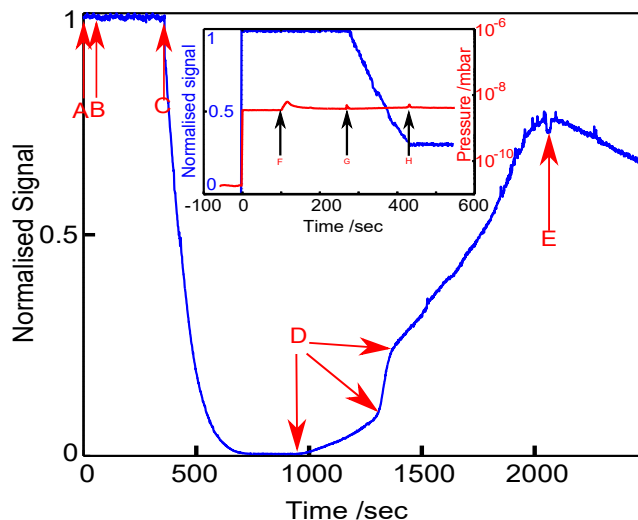
FIG. S1. Na on Cu(111) dosing curve. The gate valve between the scattering chamber and dosing arm is opened at "A" ($t = 0\,s$), the dispenser current is enabled at "B" ($t = 50\,s$), but no loss of specular reflectivity is observed until the flag is opened at "C" ($t = 350\,s$). In the period from "C" onwards sodium is deposited on the surface, demonstrated by an initial decrease in helium reflectivity as the surface entropy increases and then an increase as the surface stabilizes, "D", approaching the complete monolayer, highlighted at "E". At the points indicated by "D" different compressed surface structures are formed. The inset shows helium reflectivity and chamber pressure, in blue and red respectively. In this instance the dose is stopped by closing the dosing flag at "H", where the specular signal is $I_0/3$. The points "F" and "G" indicate the times when the dispensing current is enabled and the flag opened, respectively

Figure S1 shows an uptake curve taken to a coverage greater than monolayer saturation. The period marked "A" through "C" demonstrates that there is no change in specular reflectivity between opening the dosing arm chamber and opening the flag. Sodium is deposited from a clean surface at "C" to monolayer saturation at "E" and beyond. In order to work at a specific coverage the dosage may be stopped virtually instantaneously by closing the flag, as demonstrated in the inset of Fig. S1, where the sample is dosed to a specular attenuation of $I_0/3$.

From the uptake curve (see Fig. S1) and assuming a unity sticking co-efficient, as in the coverage dependent LEED and TPD studies conducted by Tang *et al.* [3], and photo emission spectra in Ref. 4, the coverage can be linearly interpolated from the region "C" through "E" on Fig. S1. The dynamics mea-

FIG. S2. ^{3}He diffraction scan for Na on Cu(111), along the [11$\bar{2}$] substrate direction, at coverage of $\Theta = 0.025$ ML. The signal is normalized to one at the peak of the diffraction ring. The total scattering angle and beam energy are fixed at 44.4° and 8 meV respectively, while the angle of incidence is varied in order to obtain the diffraction pat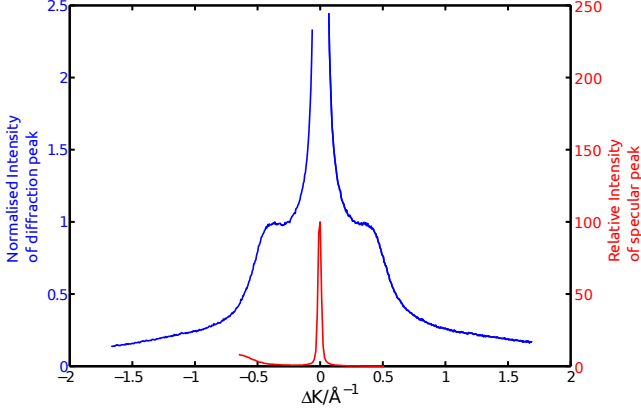tern. The central peak, shown as a red line, is the specular reflected beam and the weak diffraction features are apparent in the expanded curve (blue line). The diffraction features do not vary significantly with azimuthal sample orientation, indicating an absence of azimuthal ordering.

FIG. S3. A typical Na/Cu(111) ISF measured on the [11$\bar{2}$] surface direction and presented for a momentum transfer $\Delta K = 0.08\,\text{Å}^{-1}$ at a coverage of $\Theta = 0.025$ ML and temperature 155 K. The blue line shown is of the form $A_1 \exp(-\alpha t) + A_2$ where A_1, A_2 and α are determined using a nonlinear least squares fit. The line is in excellent agreement with the data for $t_{SE} > 5$ ps.

surements were collected at a coverage corresponding to an attenuation such that $I = I_0/3$, as shown in the inset of Fig. S1, which translates to a coverage of 0.045% of the atoms at saturation coverage. The periodicity of the structure at monolayer coverage is (3×3) but with 4 adatoms per unit cell [3, 5]. So the saturation coverage, defined with respect to the number of substrate atoms in the top most layer is 4/9. Using the known monolayer structure and uptake curve the coverage with respect to the number of substrate atoms in the current study is thus $\Theta = 0.025$ ML.

The coverage calibration can be cross-checked using the location of diffraction features. An angular intensity scan taken at the same coverage is presented in Fig. S2, which shows a strong, sharp specular signal at $\Delta K = 0\,\text{Å}^{-1}$ together with broader, weaker diffraction-peaks. The observed features correspond to isotropic diffraction rings that result from the quasi-hexagonal distribution of sodium atoms with well defined nearest-neighbor distance but no long-range orientation order. The radius of the inner ring, K_{ring}, is related to the average nearest-neighbour distance r by $K_{ring} = 4\pi/\sqrt{3}r$ [6]. The data gives $\Theta = r^2/a^2 = 0.025$ ML which is in excellent agreement with the coverage calculated using the uptake curve.

B. Measurement and Analysis of the ISF

During measurements care is taken to avoid contamination. The variation of helium-3 reflectivity of the clean copper surface over a period over 5 hours; longer than the maximum measurement session of 3 hours shows no significant variation. ISFs are measured non-sequentially in momentum transfer or

temperature, and spectra recorded at the the beginning of each measurement session are repeated at the end with no variation noted.

Figure S3 shows a typical ISF with experimental data shown as red circles. The blue line represents a model of the form $A_1 \exp(-\alpha t) + A_2$, with the free parameters A_1, A_2 and α, optimized using a nonlinear least squares method implemented using the Matlab^{TM} curve fitting toolbox. The model does not represent the data at small times, $t_{SE} < 10$ ps, which are therefore excluded, using an iterative routine to find the optimum exclusion limit. We quantify the quality of the fit using the adjusted coefficient of determination R^2_{adj}. If we define the data as a series $y^n_{i=1}$ and the fit as $f^n_{i=1}$, then R^2_{adj} is defined as

$$R^2_{adj} = 1 - \frac{(n-1)\sum\limits_{i=1}^{n}(y_i - f_i)^2}{(n-m)\sum\limits_{i=1}^{n}(y_i - \bar{y})^2} , \tag{S1}$$

where m is the number of degrees of freedom in the model and $\bar{y}$ is the arithmetic mean of the data.

Figure S4 shows the quality of the fit measured using R^2_{adj}, and the decay rate α for the blue line shown in figure S3, as a function of the cut off time, starting with the slowest 5 data points and incrementing towards $t = 0$ ps. At large cut-off times, the quality of the fit is limited by the lack of data. Therefore the R^2_{adj} value starts small, and the value of α varies over a relatively large range. As the number of data points increases, α stabilizes around 0.05 ps and R^2_{adj} increases, indicating that the model represents the data. At times less than 12 ps there is a slight reduction in R^2_{adj}, which is attributable to the incomplete removal of the inelastic scattering signal in this case. At

FIG. S4. Sensitivity of the time cut off, when optimizing an exponential model $A_1 \exp(-\alpha t)$ to experimental data (see Fig. S3). Blue circles show the adjusted coefficient of determination R^2_{adj}, and red crosses the value of the obtained decay rate α as a function of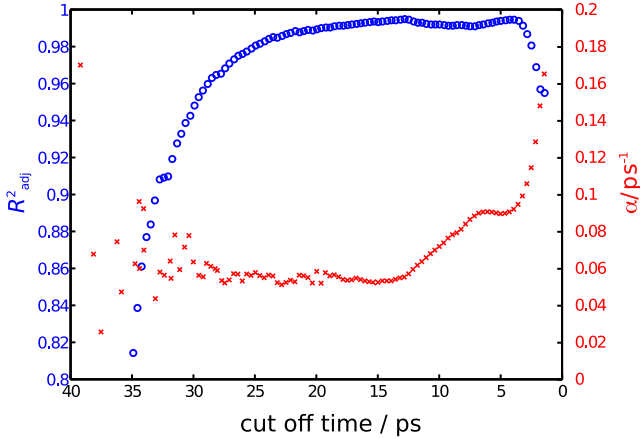 the cut-off time. It is clear that at large cut off time the fit to the exponential is weak, and as at small times the influence of the clearly defined faster decay distorts the result. The starting point of the current work is 18 ps, yielding a value for α of $0.055 \pm 0.005 \, \text{ps}^{-1}$.

times less then 5 ps R^2_{adj} decreases rapidly as the quantity of data not described by the exponential model increases, which is consistent with the clear fast decay process in figure S3. A cut off limit for the dataset is found to be 18 ps, yielding a value for α of $0.055 \pm 0.005 \, \text{ps}^{-1}$. The same method is applied to analyse the diffusion signal in the rest of the dataset.

The features presented and described in figure S3 are typical for the whole dataset, and can be summarised as a rapidly decaying contribution at times less than 5 ps, followed by a slower decay process. There is a strong inelastic component present in some spectra which is not treated in the current work and does not affect the results presented. It is clear that there is a significant deviation from the exponential fit at small times, typically below 5 ps, which is considered in future work.

S2. COMPUTATIONAL DETAILS

A. DFT Calculations and Interpolation of the Interaction Potential

We generate a two-dimensional adsorbate-substrate interaction potential using density-functional theory (DFT) within the generalized gradient approximation (GGA) in terms of the PBE functional [7] as implemented in the plane-wave pseudopotential code CASTEP [8]. In detail, we model the Na on Cu(111) system in a (3×3) surface unit cell, where the metal substrate is represented by 5-layer slabs separated by a 20 Å vacuum layer in z-direction between the periodic images. We further employ a plane wave cut-off energy of 400 eV, ultrasoft pseudopotentials [9] and an $(8 \times 8 \times 1)$ Monkhorst-Pack [10] **k**-point grid. For all calculations presented we rely on the frozen surface approximation: We evaluate the optimal

clean-surface configuration only once (where the lowermost two layers are constrained to the truncated bulk positions) and subsequently keep all substrate degrees of freedom fixed. To calculate the interaction energies, we then place the Na atom at a defined (x, y) position in the surface unit cell and fully relax its z-coordinate using the BFGS algorithm with a residual force tolerance of $0.05 \, \text{eV/Å}$. All computational parameters have been carefully tested to yield interaction energies that are converged to within $< 5 \, \text{meV}$.

To obtain a continuous analytical description of energies and forces, we use the calculated Na interaction energies at the four high-symmetry sites of the Cu(111) surface (top, bridge, fcc and hcp) and expand these in a truncated Fourier series

$$
V(\mathbf{R}) = \sum_{i,n} A_n \cos\left(n\mathbf{g}_i \cdot \mathbf{R}\right)
$$
$$
+ \sum_{i,m} B_m \sin\left(m\mathbf{g}_i \cdot \mathbf{R}\right) + C \quad , \tag{S2}
$$

Here, we use two cosine, one sine component (that in principle allows to distinguish between non-degenerate hcp and fcc hollow sites) and a constant offset, such that all parameters are uniquely determined by the four input energies shown in Tab. S1. We further use a redundant set of reciprocal lattice vectors

$$
\mathbf{g}_i = \frac{4\pi}{\sqrt{3}a_{\text{Cu(111)}}} \begin{pmatrix} \cos(\varphi_i) \\ \sin(\varphi_i) \end{pmatrix}; \quad \varphi_i \in \left[0, \frac{\phi}{3}, \frac{2\pi}{3}\right] ,
\tag{S3}
$$

where the optimized Cu(111) surface lattice constant is $a_{\text{Cu(111)}} = 2.55 \, \text{Å}$ within our computational setup. Our so-gained analytic interaction potential exhibits an RMSD value of $< 2 \, \text{meV}$ as compared to a test set of 231 explicitly calculated DFT relative interaction energies at (x, y) Na-positions covering the entire irreducible wedge of the primitive surface unit cell (see Fig. S5).

B. Pairwise Interaction Potential

On top of the *ab initio*-based adsorbate-substrate interaction potential we add pairwise repulsive dipole-dipole interactions in our molecular dynamics (MD) simulations. The same pair potentials have been shown to yield convincing results in previous studies of Na on Cu(100) [11]. Other interactions, for

TABLE S1. Relative DFT interaction energies of Na on Cu(111). The hcp and fcc hollow sites are energetically degenerate. These four energies are the input values for the Fourier expansion of the analytic interaction potential in Eq. (S2).

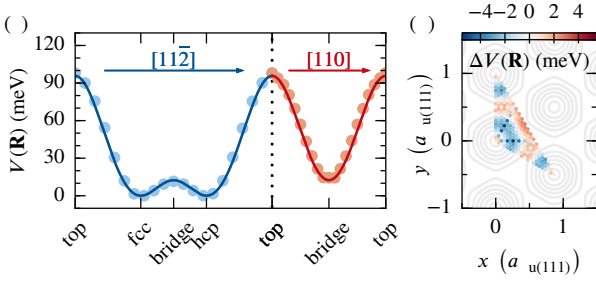| site	relative interaction energy (meV)
top	96
bridge	12
hcp	0
fcc	0

FIG. S5. **(a)** Interpolated Na-Cu(111) interaction potential along two high symmetry lines along the Cu(111) surface (drawn lines) as compared to respective DFT data points from the test set. **(b)** Deviations $\Delta V(\mathbf{R}) = V(\mathbf{R}) - V_{\mathrm{DFT}}(\mathbf{R})$ of the interpolation function from the entire test set of 231 data points in the irreducible wedge of the surface unit cell. The top position is located at $(0,0)$. We obtain an RMSD value of 1.9 meV for the entire test set.

example those mediated by surface-states [12], are oscillatory in nature and are significantly weaker so we do not include them here. According to Kohn and Lau [13], the interaction potential of two dipoles with dipole moments μ_i and μ_j on a metal surface is given by

$$V_{ij}^{\mathrm{KL}}(\mathbf{r}) = 2\mu_i\mu_j \frac{\mathbf{r}}{r^4}, \tag{S4}$$

where $\mathbf{r}$ is the distance vector between the dipoles. The additional factor of 2 as compared to the classical dipolar interaction energy in vacuum accounts for image charge effects.

The respective dipole moment of the adsorbed Na atoms is coverage-dependent; the closer the packing is the smaller the dipole moments. An analytical model to include the underlying dipole-induced surface depolarization effects has been proposed by Topping [14]. Treating the adsorbate layer within a plate capacitor-model, the work function change of the substrate as induced by the adsorbates is given by [15],

$$\Delta\phi(\Theta) = -\frac{n_0\Theta\mu_0}{\varepsilon_0 \left[1 + 9\alpha \left(n_0\Theta\right)^{3/2}\right]} \quad, \tag{S5}$$

where α is the adsorbate polarizability and μ_0 the adsorbate dipole moment in the zero-coverage limit. The adsorbate density per unit surface area at full coverage $\Theta = 1$ is n_0. We define the coverage Θ as number of adsorbates per surface substrate atom. Hence, for a hexagonal (111) surface $n_0 = 2/\sqrt{3}a^2$, where a is the surface lattice constant. The remaining free parameters α and μ_0 are obtained through fitting experimental work function change-measurements for Na on Cu(111) by Fischer *et al.* [16] in the low-coverage region to Eq. (S5) (see Fig. S6). We obtain $\alpha = 46.6,\ \mathring{\mathrm{A}}^3$ and $\mu_0 = 7.8$ D. This finally results in the effective dipole moment

$$\mu_{\mathrm{eff}}(\Theta) = \frac{\mu_0}{1 + 9\alpha \left(n_0\Theta\right)^{3/2}} \quad. \tag{S6}$$

In our simulations, we truncate the resulting pairwise forces
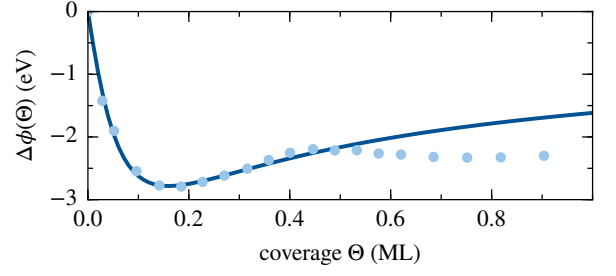
FIG. S6. Fit (dark drawn line) of the work function change with coverage within the Topping model (cf. Eq. (S5)) to experimental measurements (light circles) by Fischer *et al.* [16]. Only values $\Theta < 0.25$ ML enter the fitting procedure. Note that the coverage definition in this work differs from that in the original work in Ref. 16.

$$\mathbf{F}_{ij}^{\mathrm{KL}} = -\nabla V_{ij}^{\mathrm{KL}}(\mathbf{r}) = 6\frac{\mu_{\mathrm{eff}}^2(\Theta)}{r_{ij}^5}\mathbf{r}_{ij} \tag{S7}$$

at a cut-off distance of 20 Å.

C.   Langevin Equation and Numerical Propagation

As routinely applied in the context of analyzing ^{3}He-SE measurements [17–19], we simulate the actual adsorbate motion using Langevin dynamics that incorporate both the dynamical interaction with substrate phonons as well as with *eh*-pairs equivalently as coupling to an implicit heat bath. Within the Markov approximation the adsorbate dynamics is then determined by

$$m\frac{\mathrm{d}^2\mathbf{R}}{\mathrm{d}t^2} = -\nabla V_{\mathrm{int}}(\mathbf{R}) - \eta\frac{\mathrm{d}\mathbf{R}}{\mathrm{d}t} + \mathcal{F}(t). \tag{S8}$$

Here, $\mathbf{R}$ denotes the combined adsorbate coordinates vector, m is the adsorbate mass and $V_{\mathrm{int}}(\mathbf{R})$ is the total interaction potential that includes the Na-Cu(111) interactions V as well as all pairwise repulsive interactions V^{KL}. The fluctuating forces $\mathcal{F}(t)$ are modeled as Gaussian white noise with zero mean and a variance that is related to the friction coefficient η and the temperature T by the fluctuation dissipation theorem such that $\langle\mathcal{F}(t)\mathcal{F}(t')\rangle = 2\eta k_{\mathrm{B}}T\delta(t - t')$.

The actual time-propagation of Eq. (S8) is done using the modified velocity Verlet algorithm proposed by Bussi and Parinello [20]. The latter allows to conveniently control the error due to the time discretization of the stochastic Langevin equation by monitoring drifts in the effective energy [20, 21]. With the chosen time step of $\Delta t = 5$ fs we find the latter to be stable to within 0.1 meV per degree of freedom over 2×10^8 steps.

D.   Electronic Friction

We address the electronically non-adiabatic contributions to the apparent friction coefficient relying on the local density

FIG. S7. **(a)** Interpolated Na electronic friction coefficient within the LDFA-AIM model along two high symmetry lines along the Cu(111) surface (drawn lines). Individual input values are shown as filled circles. Note that the majority of deviations is found around the top-site, which is only very rarely visited at the simulated temperatures. **(b)**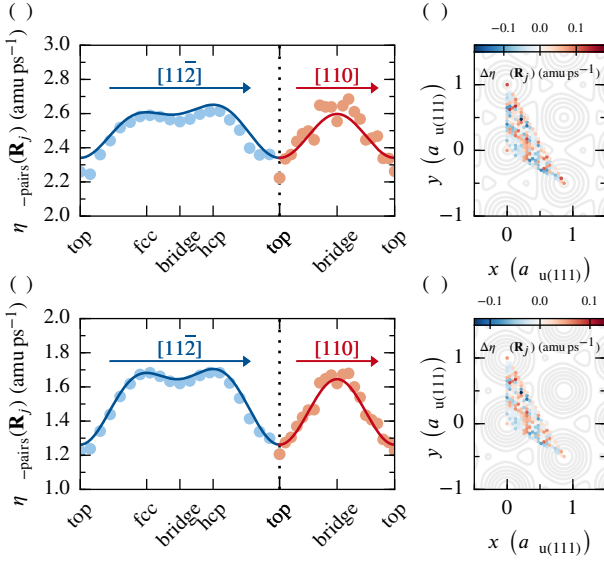 Deviations $\Delta\eta_{eh}(\mathbf{R}_j) = \eta_{eh\text{-pairs}}(\mathbf{R}_j) - \eta_{eh\text{-pairs}}^{\mathrm{DFT}}(\mathbf{R}_j)$ of the interpolation function from the entire input set of 231 data points in the irreducible wedge of the surface unit cell. **(c)** and **(d)** same as **(a)** and **(b)** but for the LDFA-IAA model.

friction approximation (LDFA) [22, 23]. Within the LDFA, atomic electronic friction coefficients $\eta_{eh-\mathrm{pairs},j}$ are individually evaluated from a reference system of a radially symmetric impurity embedded in a free electron gas of a given position-dependent embedding density $\rho_{\mathrm{emb},j}$

$$\eta_{eh-\mathrm{pairs},j}\left(\mathbf{R}_j\right) = \rho_{\mathrm{emb},j}\left(\mathbf{R}_j\right) k_F \sigma_{\mathrm{tr}} , \qquad (S9)$$

where σ_{tr} is the transport cross section that is evaluated from the phase shifts of the respective Kohn-Sham orbitals at the Fermi momentum k_F [24–27]. Regarding the density of the host free-electron gas in Eq. (S9) we compare a recently proposed atoms-in-molecules (AIM) embedding scheme [28] based on a Hirshfeld decomposition [29] of the self-consistent system electronic density with the independent-atom approximation (IAA) relying on clean-surface embedding densities [22]. For our analysis we achieve a continuous representation of the electronic friction coefficient $\eta_{eh-\mathrm{pairs},j}(\mathbf{R}_j)$ similar to the adsorbate-substrate interaction potential (see Eq. (S2)). A comparison of the arc-lengths of the actual three dimensional minimum energy paths and their respective two dimensional projections for all relevant single jumps yields deviations of $< 0.5\%$ in all cases. We are thus confident to not neglect any relevant information about the non-adiabatic energy dissipation that comes along with the reduction of the dimensionality of the dynamics.

The respective electronic friction coefficient is highly sensitive to the actual height of the adsorbate due to the exponential decay of the metal electron density above the surface. However, the actual adsorbate height we obtain from our geometry optimizations is determined by minimizing the Hellmann-Feynman forces projected on the adsorbate's z-coordinate. Residual numerical uncertainties that do not affect the latter may still have a small impact on the electronic friction coefficient. This explains the fluctuations of the data points shown in Fig. S7. In order to be less susceptible, we therefore do not only use the electronic friction coefficients at the four high-symmetry sites for the parametrization of the Fourier series, but rather fit a 3 component Fourier expansion (one sine and cosine component, respectively, and a constant contribution) to all 231 data points of our test set from the interaction potential validation using a least-square algorithm. Doing so we obtain a smooth interpolation function with an RMSD value of 0.06 amu ps^{-1} and 0.04 amu ps^{-1} for AIM and IAA, respectively.

E. Evaluation of the Intermediate Scattering Function

To make the connection between our simulations and the experimental ^{3}He-SE measurements we follow a procedure promoted by Ellis and coworkers [11, 18, 30] that avoids the numerically demanding evaluation of the van Hove pair correlation function $G(\mathbf{R}, t)$ for the interacting system [31]. Instead, we rather rely on the kinematic scattering approximation, i.e., we disregard multiple scattering events and consequently evaluate the coherent intermediate amplitudes

$$A_n(\Delta\mathbf{K}, t) = \sum_{j}^{N\mathrm{atoms}} \exp\left[-i\Delta\mathbf{K} \cdot \mathbf{R}_{n,j}(t)\right] \qquad (S10)$$

at each MD time step directly as a superposition of contributions from the trajectories $\mathbf{R}_{n,j}(t)$ generated for an ensemble of N_{atoms} adatoms in a single run n [32]. The dynamical structure factor

$$S_n(\Delta\mathbf{K}, \omega) = \left|\int_{-\infty}^{\infty} A_n(\Delta\mathbf{K}, t) \exp\left(-i\omega t\right) \mathrm{d}t\right|^2 \qquad (S11)$$

is then averaged over several runs and a subsequent inverse Fourier transform finally yields the intermediate scattering function (ISF) [33]

$$I(\Delta\mathbf{K}, t) = \frac{1}{N_{\mathrm{runs}}} \int_{-\infty}^{\infty} \sum_{n}^{N_{\mathrm{runs}}} S_n(\Delta\mathbf{K}, \omega) \exp\left(i\omega t\right) \mathrm{d}\omega. \qquad (S12)$$

Based on this procedure, we subsequently treat both our experimental measurements as well as the simulated (normalized) ISFs on an equal footing by fitting an exponential decay to the latter using the procedure described in Sec. S1 B. Here, special care has to be taken to run trajectories long enough, i.e., well beyond the decay of the ISF to ensure an adequate estimate of the respective decay rate $\alpha(\Delta\mathbf{K})$ that is free of any boundary effects imposed by the numerical Fourier transforms.
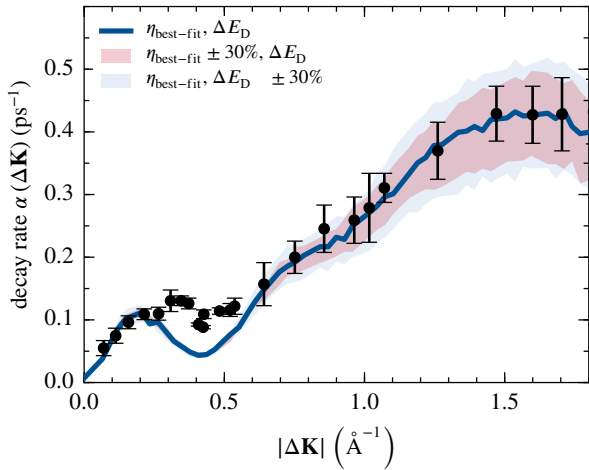
FIG. S8. Experimentally measured decay rates $\alpha(\Delta\mathbf{K})$ along the $[11\bar{2}]$ surface direction as opposed to those extracted from simulations with a best-fit friction coefficient of $\eta = 10$ amu ps^{-1} (solid blue line). The red corridor indicates the range of respective decay rates in simulations with η varied by $\pm30\%$, whereas the blue corridor indicates simulations where the hollow-bridge diffusion barrier as obtained from DFT calculations has been changed by $\pm30\%$.

F. Sensitivity Analysis

Our estimate for the total friction coefficient η naturally depends on the quality of the underlying interaction potential. Even though the latter is evaluated on an *ab initio* basis, there are numerical and conceptual approximations inherently included. In order to assess this dependence, we varied the relevant hollow-bridge diffusion barrier in our simulations by up to $\pm30\%$, which should more than account for values obtained with different sets of pseudo potentials or exchange-correlation functionals. The hollow-top amplitude (see Tab. S1) was left unchanged. Fortunately, given the best-fit friction coefficient, the variations of our so-calculated decay rates (see Fig. S8) are very consistent with the corridor we obtain by varying the friction coefficient as outlined in the main text, and which we already consider as our uncertainty anyway.

[1] Type-K thermocouple: chromel (90% nickel and 10% chromium) alumel (95% nickel, 2% manganese, 2% aluminium and 1% silicon).
[2] SAES Getters, "Alkali metal dispensers," https://www.saesgetters.com/products/alkali-metals-dispensers (2000), accessed: 2016-08-08.
[3] D. Tang, D. McIlroy, X. Shi, C. Su, and D. Heskett, Surf. Sci. Lett. **255**, L497 (1991).
[4] A. Carlsson, S.-A. Lindgren, C. Svensson, and L. Walldén, Phys. Rev. B **50**, 8926 (1994).
[5] S. D. Borisova, G. G. Rusina, S. V. Eremeev, G. Benedek, P. M. Echenique, I. Y. Sklyadneva, and E. V. Chulkov, Phys. Rev. B **74**, 165412 (2006).
[6] G. Witte, J. Phys. Condens. Matter **16**, S2937 (2004).
[7] J. P. Perdew, K. Burke, and M. Ernzerhof, Phys. Rev. Lett. **77**, 3865 (1996); **78**, 1396 (1997).
[8] S. J. Clark, M. D. Segall, C. J. Pickard, P. J. Hasnip, M. I. J. Probert, K. Refson, and M. C. Payne, Z. Kristallogr. **220**, 567 (2005).
[9] D. Vanderbilt, Phys. Rev. B **41**, 7892 (1990).
[10] H. J. Monkhorst and J. D. Pack, Phys. Rev. B **13**, 5188 (1976).
[11] J. Ellis, A. P. Graham, F. Hofmann, and J. P. Toennies, Phys. Rev. B **63**, 195408 (2001).
[12] A. P. Graham, J. Toennies, and G. Benedek, Surf. Sci. **556**, L143 (2004).
[13] W. Kohn and K.-H. Lau, Solid State Commun. **18**, 553 (1976).
[14] J. Topping, Proc. R. Soc. London A **114**, 67 (1927).
[15] H. Lüth, *Solid Surfaces, Interfaces and Thin Films*, 5th ed., Graduate Texts in Physics (Springer, Berlin, 2014).
[16] N. Fischer, S. Schuppler, T. Fauster, and W. Steinmann, Surf. Sci. **314**, 89 (1994).
[17] A. P. Jardine, J. Ellis, and W. Allison, J. Chem. Phys. **120**, 8724 (2004).
[18] A. P. Jardine, G. Alexandrowicz, H. Hedgeland, W. Allison, and J. Ellis, Phys. Chem. Chem. Phys. **11**, 3355 (2009).
[19] M. Diamant, S. Rahav, R. Ferrando, and G. Alexandrowicz, J. Phys. Condens. Matter **27**, 125008 (2015).
[20] G. Bussi and M. Parrinello, Phys. Rev. E **75**, 056707 (2007).
[21] G. Bussi, D. Donadio, and M. Parrinello, J. Chem. Phys. **126**, 014101 (2007).
[22] J. I. Juaristi, M. Alducin, R. Díez Muiño, H. F. Busnengo, and A. Salin, Phys. Rev. Lett. **100**, 116102 (2008).
[23] Y. Li and G. Wahnström, Phys. Rev. Lett. **68**, 3444 (1992).
[24] T. L. Ferrell and R. H. Ritchie, Phys. Rev. B **16**, 115 (1977).
[25] P. Echenique, R. Nieminen, and R. Ritchie, Solid State Commun. **37**, 779 (1981).
[26] P. M. Echenique, R. M. Nieminen, J. C. Ashley, and R. H. Ritchie, Phys. Rev. A **33**, 897 (1986).
[27] M. J. Puska and R. M. Nieminen, Phys. Rev. B **27**, 6121 (1983).
[28] S. P. Rittmeyer, J. Meyer, J. I. Juaristi, and K. Reuter, Phys. Rev. Lett. **115**, 046102 (2015).
[29] F. Hirshfeld, Theor. Chim. Acta **44**, 129 (1977).
[30] J. Ellis and A. Graham, Surf. Sci. **377–379**, 833 (1997).
[31] L. Van Hove, Phys. Rev. **95**, 249 (1954).
[32] For simulations relying on super cells under periodic boundary conditions, it is crucial to avoid spurious phase contributions to the intermediate amplitudes by choosing $\Delta\mathbf{K}$ vectors that match the reciprocal lattice of the respective super cell.
[33] Following the reasoning in Ref. 30 we approximate the form factor $F(\Delta\mathbf{K}, \omega)$, usually a very slowly varying function of $\Delta\mathbf{K}$ and ω, to be unity over the entire variable range.

Energy Dissipation at Metal Surfaces

S.P. Rittmeyer, V.J. Bukas, and K. Reuter
Adv. Phys. X, *accepted* (2017).
DOI: http://dx.doi.org/10.1080/23746149.2017.1381574

Energy Dissipation at Metal Surfaces

Simon P. Rittmeyer,* Vanessa J. Bukas,† and Karsten Reuter

Chair for Theoretical Chemistry and Catalysis Research Center,

Technische Universität München, Lichtenbergstr. 4, 85747 Garching, Germany

Abstract

Conversion of energy at the gas-solid interface lies at the heart of many industrial applications such as heterogeneous catalysis. Dissipation of parts of this energy into the substrate bulk drives the thermalization of surface species, but also constitutes a potentially unwanted loss channel. At present, little is known about the underlying microscopic dissipation mechanisms and their (relative) efficiency. At metal surfaces, prominent such mechanisms are the generation of substrate phonons and the electronically non-adiabatic excitation of electron-hole pairs. In recent years, dedicated surface science experiments at defined single-crystal surfaces and predictive-quality first-principles simulations have increasingly been used to analyze these dissipation mechanisms in prototypical surface dynamical processes such as gas-phase scattering and adsorption, diffusion, vibration and surface reactions. In this topical review we provide an overview of modeling approaches to incorporate dissipation into corresponding dynamical simulations starting from coarse-grained effective theories to increasingly sophisticated methods. We illustrate these at the level of individual elementary processes through applications found in the literature, while specifically highlighting the persisting difficulty of gauging their performance based on experimentally accessible observables.

---

* Corresponding author: simon.rittmeyer@tum.de

† Present address: SUNCAT Center for Interface Science and Catalysis, Department of Chemical Engineering, Stanford University, Stanford, California 94305, United States

I. Introduction: Concepts & Open Questions

In chemical reactions at solid surfaces, different forms of energy are converted into one another. Chemical energy is released or consumed by breaking and making individual chemical bonds of adsorbed species or intermediates formed in the course of the reaction. Along the way, parts of this chemical energy are converted (transiently) into kinetic or vibrational energy of these surface species. Energy exchange can also occur with substrate degrees of freedom (DOF), which (ultimately) will lead to a thermalization of adsorbates prevailing for sufficiently long at the surface. Net energy flow out of the adsorbate/surface fringe is thereby denoted as dissipation. Apart from (vibrationally excited) desorbing species, energy dissipation proceeds prominently into the substrate bulk. Largely, this occurs through the excitation of lattice vibrations, so-called substrate phonons [1, 2]. At metal surfaces, however, the non-adiabatic excitation of electron-hole (*eh*) pairs provides another competing energy dissipation channel. The continuous distribution of electronic states across the Fermi level allows in principle to even excite lowest-energy *eh*-pairs—an argument that has often been used to suspect a high relevance of this channel at metal surfaces [3–7].

However, the real role and relative importance of both dissipation channels and how this varies across systems are presently largely unclear [3, 8]. In fact, on this microscopic level we still know very little about these mechanisms of energy dissipation in general. This is rather intriguing, considering that chemical reactions at metal surfaces drive important applications and technologies like heterogeneous catalysis or surface growth. In the established microkinetic theories used in these fields [9–11] one, for instance, generally assumes that any reaction heat released in an exothermic reaction step is quasi-instantaneously dissipated away to ensure an immediate thermalization of the surface species. This motivates a Markovian view of an overall surface chemical reaction as a sequence of *independent* elementary steps such as adsorption, diffusion, reaction and desorption as depicted in Fig. 1. Even though unanimously applied today [12], the general validity of this Markovian picture is less clear from the microscopic perspective of the phononic and *eh*-pair dissipation mechanisms. In a typical exothermic surface reaction like dissociative oxygen adsorption at a transition metal surface heats of the order of a few electron volts (eV) are released. Considering that, e.g., the energy scale of phonons is meV, one may start to wonder how instantaneous the phononic energy uptake and concomitant thermalization of surface species really is. [Fig. 1 near here]

Additionally fueled by sustainability considerations concerning waste heat recovery or general

2

heat management in heterogeneous catalysis, this has motivated fundamental research to arrive at a better microscopic understanding of energy dissipation at metal surfaces. Experimentally, the key approach are dedicated surface science experiments that study individual elementary processes at well-defined single-crystal surfaces in ultra-high vacuum [13, 14]. The question of energy dissipation is thereby a sub-topic in the broader context of long-researched gas-surface dynamics (GSD). A central problem here is that key observables accessible in GSD experiments are often ensemble averages (*vide infra*). At present it is largely unclear in how much these observables are actually sensitive to details of the microscopic energy dissipation mechanisms. In fact, an unambiguous interpretation of the measured data is typically impossible without detailed modeling efforts. The dramatic increase in computer and algorithmic power has in this respect led to a strong surge of corresponding, in particular first-principles based theoretical work in recent years. This work has its own limitations though. It centrally still struggles with the necessity to simultaneously provide a reliable account of the surface electronic structure (and ensuing energetics) and adequately follow or sample the on-going surface dynamics. At the electronic structure level, the difficult task is to procure a description of localized orbitals of surface species on the one hand and the highly delo-calized metallic band structure on the other [15, 16]. Considering dynamical simulations, issues arise in turn from the extensive ensemble averaging required to compute key experimental observ-ables, and from excessive system sizes when aiming to explicitly resolve the energy transfer to the multitude of electronic and phononic DOF of an extended metal substrate.

These challenges can presently only be met by numerically efficient, effective theories. They typically rely on density-functional theory (DFT) with semi-local exchange-correlation functionals [16–20] and still often have to resort to bath-type treatments of the substrate DOF. Open questions these theories try to address at the level of an individual elementary process (cf., Fig. 1) include the relevance of each dissipation channel under specific conditions, whether these channels interact and influence each other or simply provide additive contributions, and how this picture will change from one system to another. Since all theories potentially able to consistently address these ques-tions in practice are by nature approximate, validation by comparison to experiment is obviously vital. As such, another important aspect is also how experimentally accessible quantities in differ-ent types of GSD experiments at single crystal surfaces can be calculated. This not only from the perspective of reproducing these quantities accurately, but also to understand to which extent the details of the underlying energy dissipation mechanisms actually matter for the target properties of

interest. In this topical review we survey the state-of-the-art of corresponding theories and their application in practice. For this we focus in subsequent sections on work done to elucidate the role of energy dissipation in adsorption processes (Section II), in vibrational motion (Section III) and in surface diffusion (Section IV). Emphasis is placed on concepts and in how much the impressive amount of work carried out in particular over the last years allows already to derive some general insights and ruling principles. An extensive list of references guides the interested reader to the methodological and technical details. The scope of this work is instead to introduce this lively field, it accomplishments and challenges to a broader audience.

II.   Inelastic Scattering & Adsorption

Energy dissipation in adsorption processes is suitably studied in molecular beam experiments that expose an initially clean single-crystal surface to a beam of gas-phase species of defined initial kinetic energy and impinging from a defined initial angle. Detailed information about energy dissipation can then, e.g., be derived from an analysis of the translational and quantum state resolved vibrational and rotational energy distributions of inelastically scattered molecules [14, 21]. For the ensemble of gas-phase molecules in a molecular beam, another central experimentally accessible kinetic quantity is the (initial) sticking coefficient, i.e., the fraction of molecules that has lost sufficient energy to remain adsorbed at the surface [22]. The latter is usually a function of several variables such as beam incidence energy and angle, substrate temperature and specifically prepared rotational and vibrational quantum state of the impinging molecules [23]. Sticking coefficients are thus beam-ensemble averages over the binary measure of whether an individual molecule adsorbs on a surface or not. So-gained information thus naturally convolutes effects of energy dissipation from several successive elementary processes that occur, e.g., during a dissociative adsorption process, such as the actual dissociation event, vibrational motion in a potential trapped precursor state, and subsequent diffusion of the reaction products (cf., Fig. 1). As such sticking coefficients are a prime example of GSD observables for which it is clear from the start that they will at best provide only very indirect insight into the detailed energy dissipation mechanisms. A substantial amount of first-principles modeling has nevertheless been devoted to compute these quantities. On the one hand, this is because high-accuracy references from experiment are available for a wide range of systems. On the other hand, sticking coefficients are fundamental kinetic quantities describing ad-

4

sorption processes in microkinetic models. As such, it is most intriguing and relevant to understand which aspects of microscopic energy dissipation propagate through to this more coarse-grained, technological level.

A   *Gas-Surface Dynamics within the Frozen Surface Approximation*

Addressing sticking coefficients from a modeling perspective poses a significant challenge to theory. While impinging on the surface, the adsorbing species sample a wide range of configurations far away from the (ultimate) equilibrated adsorption geometry. This requires to accurately describe the potential energy surface (PES) representing the adsorbate-surface interaction over corresponding wide regions. Even for simplest diatomic adsorbates just accounting for the molecular DOF (the position of the center of the molecule above the surface, its bond length and angular orientation) leads already to a six-dimensional PES that needs to be computed and represented. Explicitly treating at least all these molecular DOF has thereby been established as a complete necessity by numerous studies which have specifically outlined the dangers of a reduced dimensionality treatment and shown how (intuition-based) simplifications over the adsorbate coordinates can yield dramatically wrong results with respect to extracted dynamical properties [2, 24–31]. A proper description of the beam-ensemble requires on top of this extensive statistical sampling of typically several tens of thousands of impinging molecular trajectories starting from varying initial conditions. A key concern thus foremost lies in procuring a numerically efficient, yet sufficiently accurate description of the aforementioned adsorbate-surface interaction potential.

The twofold nature of this challenge has promoted a likewise two-step, 'divide-and-conquer'-like strategy [25, 32–34]: First, a continuous PES function is constructed by interpolating or fitting to a large set of *ab initio* data points that sample the adsorbate DOF over a rigid, or so-called 'frozen' surface (FS) (depicted in blue in Fig. 2). The evaluation of energies and forces on this continuous PES function then comes at a practically negligible computational cost which allows for extensive molecular dynamics (MD) simulations in a second step. While computationally tractable, at this FS level the inherent neglect of substrate mobility obviously precludes any (phononic) energy exchange with the lattice. Focusing for the time being also exclusively on the adiabatic Born-Oppenheimer PES, there is thus no energy dissipation mechanism explicitly considered in the model. Sticking must correspondingly be concluded by some *ad hoc* criterion, typically assuming a molecule to

5

stick after its trajectory has prevailed for a sufficiently long time close to the surface.

Generally one would expect this crude approximation to work the better, the weaker the adsorbate couples to the lattice vibrations. Due to the large mass mismatch, this is best fulfilled for lightest H_2 molecular adsorbates at transition metal surfaces, which for many reasons has been a prototypical GSD system [35] that has received significant attention over the years anyway [24–28, 35–37]. It is thus not altogether surprising that already FS simulations based on DFT-derived, six-dimensional PESs have been found to largely reproduce experimental H_2 sticking curves [8, 37–39]. For heavier and more strongly chemisorbing adsorbates, however, energy exchange with the lattice is expected to play an increasingly important role and requires that some (at least approximate) account of substrate mobility is included in the theory.

B *Effective Models for Phononic Energy Dissipation*

Opening the phononic dissipation channel generally implies an exploding dimensionality for the problem at hand. Explicitly considering the motion of substrate atoms was hitherto largely prohibitive within the divide-and-conquer ansatz due to the increasing difficulty that is associated with each added DOF when constructing a continuous PES representation [34]. This situation has just started to change as advanced, high-dimensional interpolation schemes such as the Behler-Parinello atomistic neural network approach [40–42] become increasingly applicable in the context of GSD [43, 44]. As already conceivable from the simple Baule limit [2, 14], however, energy transferred to the lattice in each direct adsorbate-surface collision is still small for light diatomic adsorbates. On this level, one can then tentatively consider the interaction with surface phonons to be more of a small perturbation to the FS-dynamics such that an explicit full-dimensional description of the lattice motion may not be altogether necessary.

This motivates energy sink models that incorporate an effective treatment of surface mobility [45–51]. Such approaches generally target to reduce the phononic fine structure of the substrate into computationally convenient augmentations of the static-surface interaction in order to include some (approximate) account of energy exchange with the lattice. Motivated by an Einstein-like picture for the phononic system, the surface oscillator (SO) model [45, 46] mimics a rigidly moving substrate by a single harmonic oscillator of assigned frequency and mass parameters. As shown in Fig. 2, coupling to the adsorbate is then straightforwardly described through a space-rigid shift in

the FS expression for the PES. Extending on the latter as further depicted in Fig. 2, the generalized Langevin oscillator (GLO) additionally incorporates the approximate effect of a bulk thermal bath by coupling the SO reaction zone to an additional so-called 'ghost' oscillator [45, 47–51]. Energy dissipation and thermal fluctuations are consequently accounted for by subjecting the latter to frictional and random forces, respectively, rigorously satisfying the fluctuation-dissipation theorem in the numerical solution of the resulting generalized Langevin equation. While thus incorporating only a very limited number of additional DOF, these models still allow to lift the FS-approximation by introducing the concept of a surface temperature with concomitant thermal motion [1, 46]—even if it is just described in a coarse-grained way. [Fig. 2 near here]

One of the main practical advantages of the SO/GLO approaches is their convenient application to any pre-existing adsorbate-surface PES that has already been derived on the level of the FS approximation. This also includes, of course, the continuous PES representations obtained from DFT within the aforementioned divide-and-conquer framework. In a first such application to H_2 scattering from Pd(111) [52], Busnengo and coworkers successfully used the SO model to reveal a channel of dynamic surface trapping that could explain the otherwise puzzling temperature dependence which was observed experimentally in the rotational excitation of scattered molecules [53]. A similar result was reached only shortly afterwards also by Wang and coworkers for D_2 scattering off Cu(111), but on the basis of quantum-mechanical wave-packet calculations [54]. Opening also the GLO bulk dissipation channel as an outlet for the accumulating heat could further predict the low-temperature stabilization of a molecularly chemisorbed H_2 species at Pd(110) [55]. While thus revealing important mechanistic details of the adsorption process, the inclusion of SO/GLO dissipation nevertheless provided only marginal corrections to averaged sticking probabilities for the light H_2 adsorbate [56] (consistent with the previously mentioned good agreement with experiment already at the FS level). A much more dramatic effect was instead demonstrated for the heavier O_2 molecule, during its highly exothermic adsorption at Pd(100) [57]. Here, even a qualitative change in the shape of the calculated sticking curve was reported in comparison to the corresponding FS results, yielding thus a considerably improved agreement to experimental data [58].

Despite these and many more successes (cf., for example Refs. 59–63), it is nevertheless always prudent to bear in mind the inherent limitations that come with the underlying SO/GLO approximations. Recognizing foremost situations where these are bound to fail are cases where energy uptake cannot be reliably described on the level of only a single phonon excitation. Based mainly

on energetic considerations, the frequency of the single SO oscillation is often taken to correspond to the surface (low-frequency, acoustic) Rayleigh modes, as these are generally assumed to be predominantly excited upon first impact with the surface (cf., for example Refs. 64–67 and references therein). The validity extent of this assumption, however, remains to its larger part unknown and could represent a highly dangerous over-simplification [68, 69], in particular when going beyond prototypical studies of lightest adsorbates [70–73]. Even within a dominant one-phonon picture though, the SO model can only go as far as to provide a mechanical coupling of adsorbate-surface momentum exchange, i.e., accounting thus for energy loss to the substrate through lattice recoil and a back transfer to the adsorbate with surface temperature. Thereby considered 'stiff' lattice shifts will thus inherently fail to capture concomitant changes in the FS-PES that are induced by thermal displacements of the metal atoms from their equilibrium positions. This additional effect of vibrational surface motion can play an important role in the adsorption dynamics, as demonstrated prominently for (direct) CH_4 dissociation at several metal surfaces [74]. Here, DFT calculations specifically showed significant lowering of the activation barrier as a metal atom is puckered out of the surface at the transition state [75, 76]. Effectively accounting for both of the aforementioned effects through two (independent) DFT-derived adsorbate-surface coupling parameters [77], the quantum dynamics simulations of Jackson and coworkers thus arrived at a semi-quantitative agreement to experimental sticking curves (also reproducing the observed mode specificity and bond selectivity) that could not otherwise be achieved on the SO level alone [78]. In conclusion, we note that this so-called barrier height modulation arising from thermal fluctuations of the lattice is expected to depend strongly on both the specific system and surface temperature under investigation, so that its overall relevance remains altogether *a priori* unclear in the context of other gas-surface reactions, as will be further discussed in the following.

C *Explicitly Resolving Surface Motion*

Direct *ab initio* molecular dynamics (AIMD) simulations stand fundamentally free of the aforementioned limitations discussed in the context of effective energy sink models. In this method the forces needed to propagate the equations of motion are full-dimensional Hellmann-Feynman forces computed from DFT 'on-the-fly' at each MD time step, so that no fitting or interpolation of the PES is required. Metal atoms are thereby treated explicitly within a fully mobile substrate and no *a pri-*

ori assumptions have to be made with respect to the heat bath Hamiltonian. This further naturally circumvents the extensive PES pre-evaluation required within the divide-and-conquer ansatz, but in turn comes at a tremendous increase in computational cost for each individual trajectory. With the advent of supercomputers and continuous developments towards improved algorithms for electronic structure calculations, this challenge is being steadily overcome and it is now increasingly possible to compute a meaningful number of AIMD trajectories for many systems that could not even be addressed in static calculations a few years ago [79].

The combined dynamical picture of both adsorbate-surface coupling effects discussed previously (i.e., mechanical coupling of momentum exchange and barrier height modulation due to thermal fluctuations), should in principle be completely accounted for within AIMD simulations. Indeed, for the aforementioned CH_4 dissociation (where both effects are known to be important [74]) Kroes and coworkers predicted satisfying, semi-quantitative agreement to experimental reaction probabilities [80]. In the meantime, similar results have also been reached for H_2[37, 81, 82], N_2[83, 84], O_2[85], and CO_2[86] adsorbates, overall showing AIMD simulations to provide a reasonable account of surface temperature effects. With reaction probabilities as the target observable, the effective advantage of the detailed AIMD account of adsorbate-surface energy transfer—over corresponding, numerically more attractive SO/GLO models—ultimately depends on the importance of thermal fluctuations (assuming of course the validity of the single-phonon approximation). As such, a simple GLO model has for example been shown to perform on an equal level as AIMD regarding calculated sticking probabilities for the dissociative N_2 adsorption on W(110) [87], while being entirely inappropriate for other systems such as, e.g., the aforementioned CH_4 on various transition metals [74]. Unfortunately, however, such performance is extremely difficult to predict *a priori*, especially in view of the fact that both lattice coupling effects will induce qualitatively similar changes to the overall experimental sticking function with surface temperature.

At this point, however, it must be emphasized that the microscopic description of phononic dissipation as provided by present-day AIMD simulations is still far from perfect—a fact which stems (foremost) from practical, rather than conceptual, considerations. As the involved computational cost is largely determined by the substrate size, state-of-the-art AIMD studies are limited in practice to supercell setups involving slab models consisting of typically only a few surface lattice constants and layers [79]. By construction, such models fail to provide the desired (high) resolution when representing the underlying phononic fine structure. For example the description of surface modes—

9

which are assumed to be crucial for the initial energy uptake at the interface [72]—will unavoidably suffer from the limited slab thickness that must be adopted in computationally tractable DFT supercells. Most importantly, the imposed periodic boundaries (which are essential to describing the underlying metallic band structure) will restrict any phonon propagation within the finite extent of the latter, thereby leading to an unphysical confinement of the released chemical energy. Largely exothermic reactions in particular are thus increasingly prone to significant overheating of the metal substrate—an effect which severely compromises the description of the ensuing equilibration process and may even critically modify the actual adsorbate dynamics, as will be discussed in more detail in Section IV B.

An explicit treatment of substrate mobility within a (suitably) sizable heat bath thus continues to pose a big challenge to contemporary AIMD simulations and thereby derived accounts of phononic dissipation. This situation is aggravated by the extensive statistical sampling that is hereby required not only for describing the beam-ensemble, but also the thermal distribution of metal atoms at finite surface temperatures. In this respect, using existing AIMD configuration sampling as the basis for parameterizing the aforementioned upcoming high-dimensional neural network-based interpolation schemes [40–42] represents a promising alternative for the future that will allow for routinely evaluating several orders of magnitude more trajectories as compared to further explicit AIMD simulations [43, 44]. In the meantime, while entirely neglected so far, the channel of non-adiabatic energy dissipation adds yet another facet of complexity to GSD and toward which attention is directly turned in the following.

D *Exciting Electron-Hole Pairs: Non-Adiabatic Effects*

Energy dissipation arising from non-adiabatic effects, i.e., the dynamical coupling of the adsorbate nuclear motion to excitations in the metallic continuum of electronic states at the Fermi level, still holds a rather suspect role in gas-surface scattering/adsorption processes [3–7]. One of the most controversial showcases in this respect is the highly exothermic oxygen dissociation at Al(111) that proceeds through an O_2 triplet-singlet spin transition as the molecule approaches the surface [8, 72]. Here, extremely low initial sticking coefficients measured for small O_2 incidence energies are strongly indicative of activated adsorption—a process which goes entirely amiss within the essentially barrierless (adiabatic) PES that is evaluated on the level of the DFT generalized gra-

dient approximation [88]. It remains, however, altogether unclear whether this actually indicates a hindered triplet-singlet transition due to spin selection rules that would gives rise to corresponding dynamical barriers. Alternatively, this omission could instead be rooted in shortcomings of the employed semi-local exchange-correlation functionals [72, 89, 90]. Another prominent example vouching for pronounced non-adiabatic effects is the energy loss associated with vibrationally excited NO scattering from Au(111) [7, 91, 92]. The non-adiabatic relevance is strongly suggested here by multi-quantum relaxation of the vibrating molecule that is clearly observable on the metal, but completely absent on an insulating LiF surface [92].

Going beyond the Born-Oppenheimer approximation in order to account for such non-adiabatic effects requires in principle the full propagation of a combined, high-dimensional nuclear-electron wave function that would naturally also include the multitude of potential electronic excitations. Such an endeavor, however, is computationally out of reach in the context of GSD for at least decades still to come. Including electronically non-adiabatic effects in computational simulations thus inevitably requires further approximations and simplifications leading to an effective treatment, such as applying a mixed quantum-classical description of the system in terms of a meanfield Ehrenfest [93, 94] or surface hopping framework [95–99]. The latter has, for instance, been successfully invoked to explain the aforementioned NO vibrational de-excitation on Au(111) through an electron-transfer mechanism [98, 100, 101]. Further coarse-graining the electron dynamics can be achieved on the basis of time-dependent perturbation theory [102–104]. Counting among the disadvantages of all these methods is that they either remain computationally very intense, or require extensive parametrization, or impose specific symmetry constraints on the simulated trajectories such that a general applicability to routinely performed gas-surface calculations is lost.

Presently the only viable solution for large-scale gas-surface simulations thus lies in entirely replacing the electronic degrees of freedom within the concept of electronic friction [105–107]. As formally shown by Tully and Head-Gordon [107]—and recently more rigorously also by Dou and Subotnik [108–110]—the idea behind this approach is to start with a mixed quantum-classical description of the dynamical (electron-nuclear) system. Following a suitable Miller-Meyer action-angle transformation, the explicit electronic degrees of freedom are subjected to a generalized Langevin replacement that is valid within the weak-coupling approximation and results in a generalized Langevin equation for the nuclear degrees of freedom. This, however, is not the form of electronic friction theory that is used in practical MD simulations today. Hence, in a second step

the explicit time-dependence of the friction kernel (collectively condensing the dynamics of the electronic degrees of freedom) is removed by invoking a Markov approximation in the electronic subspace implying (infinitely) short electronic coherence times [104]. Thus assuming memoryless *eh*-pairs that immediately 'forget' about the past yields ultimately a Langevin equation for the nuclear dynamics that combines all non-adiabatic effects in a single electronic friction coefficient. Altogether, the electronic friction approach thus allows to augment the Born-Oppenheimer ground-state dynamics with a dissipative friction force and a temperature-dependent fluctuating force, as manifested through the fluctuation-dissipation theorem. This combination of conceptual simplicity and numerical efficiency, along with the possibility of application to dynamics on a potentially pre-calculated Born-Oppenheimer PES has overall served to the great popularity of this method.

While the idea of including frictional energy losses into nuclear dynamics dates back to more than 30 years ago [105, 111–115] it was not until much more recently that Juaristi and coworkers adopted this concept for routine DFT-based applications within the divide-and-conquer framework [116]. The key ingredient hereupon relied on is an approximate construction of the required molecular friction tensor from independent contributions of individual atoms. As depicted in Fig. 3, these are estimated from a simple jellium-based embedding model [111, 112, 117–119] to finally yield isotropic atomic friction coefficients as a function of an embedding electronic density. Within this so-called local density friction approximation (LDFA) [106, 116], the latter is taken as the local electron density of the clean metal surface at the position of the (individual) adsorbate atoms. This simplification consequently allows for a straightforward interpolation of the friction coefficients into a convenient analytical function of the electronic density only. This distinguishes the LDFA from more refined orbital-dependent friction (ODF) methodology [107, 115, 120, 121] whose numerical involvement [121–123] (until only very recently [124]) has hindered application to high-dimensional models though [125–130]. [Fig. 3 near here]

The inherent assumption of independent atoms within the original LDFA approach, however, triggered a controversial discussion [116, 131, 132], mostly because it ignores the adsorbate's molecular character and thus lacks, for instance, the steep increase of friction coefficients at dissociative transition states predicted from ODF [127, 128]. In this regard, it has recently been suggested to introduce molecular information through suitably Hirshfeld-partitioned [133] full system densities to map to the LDFA model system [134] rather than relying on clean metal densities (*vide infra*). Moreover, one may pragmatically argue that the immanently low velocities in such transition

12

state regions effectively suppress the contribution of the velocity-scaled friction term within the actual dynamics and thus wash out potential inaccuracies [116]—at least when focusing on reaction probabilities [124].

Retaining the LDFA within the independent atom approximation (IAA) and its unique numerical efficiency, many divide-and-conquer studies have been revisited over the past years to augment the existing FS-based MD simulations with electronic friction. Alducin and coworkers specifically investigated the dissociative adsorption of several small molecules such as H_2 [116], N_2 [116, 135], H_2O [136] and CH_4 [137] on various metal surfaces. The overall conclusion drawn from these studies is that the non-adiabatic energy dissipation channel produces only small effects on calculated sticking probabilities. Alone a full dimensional account of the adsorbate PES was in fact found to alleviate certain discrepancies with respect to experiment that had previously been erroneously assigned to non-adiabatic effects through a low-dimensional ODF-description. Prominent such examples are N_2 adsorption on Ru(0001) [127] and the vibrational de-excitation of H_2 scattering from Cu(111) [37, 38, 128, 138].

Similar to what has already been discussed in the context of phononic dissipation, however, the overall insensitivity reported for averaged sticking coefficients does not necessarily extend to mechanistic details of the underlying adsorption/scattering process. Conclusions along these lines have, e.g., already been independently reached for the dissociative H_2 adsorption on Ru(0001)[139] and Ag(111)[124]. Here, the authors specifically noted minor non-adiabatic energy losses that may be unimportant to reaction probabilities, yet significantly influence other experimentally accessible observables such as the energy distribution of backscattered molecules. As a concluding remark, it must be emphasized though that the popular electronic friction approach may even be altogether inappropriate for generally gauging the relevance of this dissipative channel. This is due to its inability to describe strong non-adiabatic coupling, as has, e.g., been most prominently shown for the multi-quantum vibrational transitions occurring during NO scattering on Au(111) [140]. Notwithstanding, at present electronic friction is the best shot we have at all to address non-adiabatic energy dissipation in high-dimensional surface simulations.

13

E Combining Phonons and Electron-Hole Pair Excitations

Combining the two dissipation channels in dynamical simulations promises illuminating insight into the relevant importance of each channel, at least on the specific level of the theory employed. Unfortunately, such applications have hitherto been rather scarce. In the late 1990s Tully and coworkers were the first to combine the electronic friction approach with an explicit description of lattice degrees of freedom for the scattering of CO from Cu(100)[141]. In this early study, however, the authors relied on a semi-empirical potential for describing the adsorbate-metal interaction and no supporting experimental data were available at the time. A dominating role of the phononic dissipation channel was reported that outperformed the non-adiabatic energy losses by up to a factor of ten (depending on the CO incidence energies). Similar findings were also reported much more recently for the scattering of nitrogen atoms and molecules using a combined electronic friction/GLO model applied to DFT-derived continuous PES models [59, 60, 142, 143]. Here, phononic effects were found superior over the non-adiabatic counterpart on essentially every measure that was considered. This said, most qualitative aspects of the dynamics could admittedly already be reached on the level of a purely adiabatic FS model when accounting for all adsorbate DOF.

Quite in contrast, for somewhat lighter (atomic) adsorbates, an outstanding importance of *eh*-pair excitations has been reported. Evaluating frictional non-adiabatic energy losses non-self consistently from AIMD trajectories, Kroes and coworkers predicted that the latter exceeds phononic energy losses by factor of 2.5 and 6 for H atom scattering off Cu(111) and Au(111), respectively [144]. This picture was later substantiated by Wodtke and coworkers who reported a pronounced disagreement between experimentally measured energy-loss spectra for backscattered H atoms from Au(111) and adiabatic simulations on a carefully parametrized full-dimensional PES based on effective medium theory including all surface degrees of freedom [145–147]. Adding LDFA-electronic friction forces, however, resulted in a spot-on agreement with experimental measurements. Altogether it nevertheless remains doubtful whether these findings actually reflect an absolutely increased relevance of non-adiabatic energy losses. The increased relative relevance compared to phononic channel could also merely arise from a suppression of efficient phononic dissipation for these lightest adsorbates.

14

III.   Trapped at the Surface: Gauging the Tools for Vibrational Damping

Vibrations of molecular adsorbates that are 'trapped' at the metal surface can, in principle, decay via coupling to substrate phonons, and/or through the electronically non-adiabatic excitation of *eh*-pairs [3]. In addition, vibrational energy may flow to other internal molecular modes, adsorbate-surface vibrations, and even (sufficiently close) neighboring species. In disentangling the contributing role of numerous such mechanisms, it is useful to consider corresponding coupling strengths in terms of smaller or larger mismatch in timescale. High-frequency adsorbate vibrations are, for example, expected to be predominantly relaxed through *eh*-pair excitations, simply due to their large frequency mismatch with all other vibrations present [148, 149]. Advocated by Persson and Persson already more than thirty years ago [115, 150–155], this notion was further substantiated by Tully and coworkers by investigating the C-O stretching mode of CO on Cu(100) [156]. In their study, agreement to the experimentally measured vibrational lifetime of about 2 ps [157] could only be achieved by including dissipative non-adiabatic effects in terms of electronic friction, which lowered the corresponding adiabatic prediction by a whopping six orders of magnitude. More recently, Saalfrank and coworkers reported similar findings for the FT_z-mode (frustrated translation perpendicular to the surface) of adsorbed hydrogen atoms on Pb using explicit high-level AIMD plus electronic friction (AIMD+EF) simulations [158].

Vibrational damping of high-frequency adsorbate modes thus provides the idealized 'isolated' setting for gauging the accuracy of non-adiabatic theories in GSD. The process is (at least, largely) dominated by a single dissipation channel and atoms are confined to the vicinity of their energy minima, thereby eliminating the need for exploring vast PES regions as required for modeling gas-phase impingement. Most importantly, vibrational lifetimes provide a direct measure for the rate of energy flow and are accurately accessible as benchmark observables from real-time experimental measurements using e.g. pump-probe spectroscopy [149].

Based on this foundation, a plethora of computational studies focused on reproducing experimentally measured vibrational lifetimes for small molecular adsorbates on metal surfaces using different underlying models for the electronic friction coefficients [120, 121, 134, 159–162]. In detail, Persson and coworkers [162] as well as Tully and coworkers [120, 121, 159–161] evaluated elements of the ODF friction tensor along certain normal modes for CO [120, 121, 159–162], CN [121, 161, 162] and NO [121, 161] on various coinage and transition metals. Given the numerical challenges in-

volved in adequately sampling the underlying metallic band structure and evaluating the required matrix elements to arrive at ODF friction coefficients [121, 122, 161], the reported values emerging from various implementations and numerical setups show considerable spread. Notwithstanding, in particular for highest-frequency (and thus anticipated to be 'most non-adiabatic') adsorbate stretch modes, calculated vibrational lifetimes were generally found to agree with experiment to within the same order of magnitude. The computed non-adiabatic decay rates further illustrated a pronounced mode-specificity that, at least so far, eludes any clear, system-transferable trend [120, 121, 159, 161]. Unfortunately, an unambiguous experimental verification of this prediction remains unattainable, in particular for low-frequency modes, as the latter are more likely to couple to surface phonons and thus again open Pandora's box of competing dissipation mechanisms.

Confined therefore to investigating only high-frequency adsorbate stretch modes, a more recent benchmark study [134] focused on assessing the performance of the popular LDFA approach [106, 112, 116, 118]. As mentioned before, electronic structure information here only enters on the level of an atomic embedding density. Given this simplicity, it is rather surprising to note that dynamically evaluated vibrational lifetimes obtained with LDFA-based friction coefficients were found to perform on an equal level as previous ODF-based studies for several experimentally well-characterized systems [134]. A recent study suggested this good performance of the LDFA to arise from finite electronic coherence times, which wash out details of the electronic band structure that are in any case neglected in the LDFA [104]. Further work is, however, required to better assess the full validity and performance of the LDFA. As a pragmatic bottom line, at least for the time being it seems that both the very simple LDFA approach as well as the computationally more demanding ODF model account reasonably well for the non-adiabatic energy losses of high-frequency stretch modes of molecular adsorbates on metal surfaces. Yet, as appealing as it may be to interpret this performance as a justification to rely on these models also for other surface dynamical processes, a respective generalization has to be taken with considerable caution. Benchmarking against vibrational lifetimes avoids delicate situations encountered in simulating, e.g., adsorption processes such as a steep increase of friction coefficients at dissociative transition states [116, 124, 127, 128, 131, 132] or singularities in the latter at spin transitions [125, 126, 163]. However, these are situations, that anyhow question the limits and validity of the electronic friction approach in general, not only the LDFA [107–110, 163].

IV. Surface Diffusion

Similar to the vibrational motion of adsorbed species, on-surface diffusion is largely controlled by the rate of energy exchange with the underlying substrate [164, 165]. However, here no striking argument (such as the frequency mismatch detailed in the previous section) can be invoked in order to safely disregard either one of the available microscopic dissipation channels. Quite on the contrary. Good reasons can be brought forward to argue in favor of both channels: Long adsorbate-surface contact times and the concomitant high embedding densities are suggestive of non-adiabatic coupling within an electronic friction-based description, while the relatively long time scales that are characteristic of diffusive motion should intuitively favor a more efficient phononic dissipation channel.

A   Thermal Diffusion

For a long time the classical notion was that once thermalized with the surface, energy exchange during diffusion of surface species happens predominantly through phononic coupling [164]. This picture was also nurtured from a pioneering study by Tully and coworkers who showed that electronic friction forces do not significantly influence the equilibrium diffusive motion of CO on Cu(100) [141]. Notwithstanding, even the authors themselves remarked at the time that the absence of a notable influence on the diffusion rate in this study neither necessarily implies a non-existent coupling to *eh*-pairs nor any generality of their findings. Instead, their description of the phononic bath through harmonic oscillators may have just provided an energy sink effective enough to inhibit correlated multi-jump diffusive motion, such that additional non-adiabatic damping effects could be masked when focusing only on diffusion rates. This is in line with findings by Wahnström. These suggested a dominant role of *eh*-pair excitations over very inefficient phononic couplings for the diffusion of H on Ni(100) that is indeed found to proceed via correlated jumps [166].

Similar to the situation for adsorption processes, more sensitive observables than mere diffusion rates thus seem to be necessary to develop further insight into the role of the dissipative channels. Along this line of thinking, Rittmeyer and coworkers recently analyzed Helium-3 spin echo (^{3}He-SE) measurements [167], which provide time-resolved access to the surface (auto-)correlation function. With the corresponding decay rates very sensitive to the adsorbate-substrate coupling and the

underlying diffusion mechanism [168–170], the authors evaluated the non-adiabatic contribution to these rates within the LDFA approach. Intriguingly, a high degree of non-adiabaticity suggested a more pronounced role of *eh*-pair excitations than anticipated by the classical 'textbook notion', at least for this system.

B 'Hot' Diffusion

The prevalent notion of thermal diffusion presupposes the adsorbate's continuous equilibration with the surface—regardless of the detailed origin of the coupling—and correspondingly predicts substrate temperature as the ruling factor. This is contrasted by the concept of hyperthermal transient mobility which can arise from the intrinsic exothermicity of an immediately preceding elementary step like (dissociative) adsorption. Non-instantaneous thermalization of the released chemical energy drives the ensuing 'hot' adsorbate diffusion that is then governed by dissipation to the underlying surface, rather than the substrate's overall temperature. This transient mobility thus intricately couples the elementary reaction steps of adsorption and diffusion—an implication hitherto not considered in the present-day Markovian microkinetic formulations in surface catalysis [9, 10]. Concepts embracing such processes are nevertheless becoming increasingly established over the past decades [171]. Ensuing for example the (exothermic) dissociative oxygen adsorption, so-called 'hot' adatom motion has been persistently reported by scanning tunneling microscopy (STM) experiments for several metal surfaces [172–178]. Working at temperatures that are sufficiently low to suppress thermal diffusion, corresponding STM studies infer hyperthermal diffusion from recorded larger or smaller separation distances between adatom pairs after equilibration—an indirect procedure that has in fact caused quite some controversy [179–181].

From a modeling perspective, the accuracy of energy sink models in describing such hyperthermal motion is challenged head on as the entire process hinges on the rate of dissipation to the substrate. Such a sensitive dependence was already demonstrated in the aforementioned seminal work of Tully and coworkers for hyperthermal CO migration on Cu(100) [141]. Including electronic friction in classical MD simulations was found to significantly quench the molecules' on-surface transient mobility—an effect which did not extend to the case of equilibrium diffusion. On the other hand, Wahnström and co-workers estimated the *eh*-pair dissipation mechanism to be relatively unimportant for the hyperthermal adatom motion following the dissociative O_2 adsorption at

Al(111) [166, 182]. Even when focusing solely on phononic damping within a Langevin framework, however, corresponding simulations showed no evidence of a high transient mobility that could reconcile the exceptionally large O–O separation distances derived from STM experiments [172]. Lateral displacements were instead found to be primarily limited by the high PES corrugation and concomitant rapid randomization of the adatom motion, while adsorbate-phonon coupling was overall reported to be weak. At this point, however, it is worth noting that the semi-empirical potentials used in this work to describe the O-Al interaction could not be extended to modeling the actual (preceding) O_2 dissociation event, thereby prohibiting a realistic sampling of the employed initial conditions. Unless there is a problem in the STM interpretation [179, 180], this obvious limitation represents an equally likely cause for the discrepancy to experiment as the approximate treatment of adsorbate-surface energy transfer.

Overcoming this limitation, a pioneering study of Groß employed AIMD to consistently model H_2 dissociation and the subsequent adatom thermalization at Pd(100) [19]. Based on substrates of about 100-200 metal atoms, this predicted 'hot' H adatoms that transiently diffuse to an average separation distance of three to four surface lattice constants. Adding an LDFA-based electronic friction to this description, Blanco-Rey and coworkers later on arrived at halved H–H separations only [183]. The authors consequently advocated a dominating role for the electronic dissipation channel arguing an efficiency of about five times larger than provided by the phonon bath [183]. Subsequent work in this direction [184, 185] specifically highlighted the increasing contribution of *eh*-pair excitations during the later stages of the relaxation process (i.e., for long adsorbate-surface contact times), even if non-adiabatic effects can be neglected during the preceding dissociation event [103, 116, 127, 139, 186]. At this point, however, it has to be noted that in present-day combined AIMD+EF simulations, the effective 0 K-Langevin description of the non-adiabatic bath provides an infinite energy sink, thus conflicting with an explicitly described, energy conserving lattice motion.

As already mentioned in Section II, even self-standing AIMD (and AIMD+EF) simulations remain challenged in providing an altogether satisfactory reference for phononic dissipation. Computationally tractable slab models compromise the description of the phonon band structure and limit their propagation to a finite volume of few substrate atoms in each direction. This gains particular relevance in the present context of hyperthermal diffusion by considering that a (preceding) exothermic surface reaction may easily release several electronvolts of energy. Unphysical phonon

19

reflections at the periodic boundaries of the employed supercell may thereby quickly lead to severe substrate 'overheating', while falsifying the ps-scale equilibration of the actual adsorbate dynamics [187].

In solving this problem, the recent development of the QM/MM embedding approach for metals (originally coined, and hence referred to, as 'QM/Me') [187] represents a big step forward. Here, a DFT-based treatment of the immediate reaction zone (i.e., typically around the adsorbate impingement site) is complemented by an extended substrate that is described on the level of a many-body classical interatomic potential. The latter are generally sufficiently accurate in providing a realistic, material-specific representation of lattice deformations (cf., for example, Refs. 188 and 189), while their numerical efficiency allows for capturing all associated long-range elastic effects. Within a multi-scale modeling philosophy, QM/Me thus augments standard AIMD with a fully quantitative account of phononic dissipation as heat flows from the embedding region and into the macroscopic metal bath, as schematically illustrated in Fig. 4. [Fig. 4 near here]

In a first application to oxygen dissociation over Pd(100), QM/Me showed phonons dissipating the vast majority of the released chemical energy into the bulk, i.e., outside of the QM-cell, already within ca. 1.5 ps after the initial O_2 bond breaking [187]. The observed ps-scale rate of heat transfer to the substrate nevertheless clearly demonstrated that this process is not instantaneous on the timescale of the actual adsorbate dynamics. Furthermore, the predicted equilibrium O–O separation distance of four surface lattice constants could not be reproduced within 'pure' AIMD simulations, thus underscoring the importance of an extended and explicit description of the surface degrees of freedom for microscopic details. Analyzing the role of surface symmetry, a subsequent QM/Me study compared this result for different Pd facets to reveal a striking difference in the transient lifetime of the hyperthermal O state [73, 181]. More specifically, a much slower equilibration was found on Pd(111) that would seemingly contradict the shorter O–O end distances previously reported from STM measurements [176]. Relying on the atomic resolution of the QM/Me heat bath allowed for rationalizing this finding through a mode-specific analysis of corresponding phonon excitations: This identified the dominant dissipation channels as qualitatively different groups of localized surface modes that do not necessarily involve a predominant Rayleigh excitation, as principally assumed for energy sinks in model bath Hamiltonians (cf., for example, Refs. 66, 67, 190, and 191 and references therein). Instead, the complex adsorbate-phonon dynamics give rise to a sensitive dependence on details of the phononic fine structure that may lie on either the high- and/or low-frequency end of

the spectrum. This can ultimately lead to intrinsically different rates of dissipation to the bulk that would otherwise go entirely unnoticed from the perspective of experimentally accessible product end distances.

V.   Summary and Conclusions

In the present review we set out to provide a comprehensive overview on modeling efforts for describing the conversion of energy at the gas-solid interface. Focusing on technologically relevant metal surfaces, we consistently address energy dissipation through the (competing) excitation of substrate phonons and *eh*-pairs at the level of individual elementary processes. Principal questions of focus concern the appropriate tools for modeling each of these microscopic dissipation channels, their effective role in driving the dynamics, and how this is ultimately reflected in (experimental) target observables of interest. Throughout the review, we report on numerous studies aimed at answering these questions, but note that we do not even come close to a full reference list for this highly active field. While thus demonstrating the considerable progress that has been made over the past few decades, we specifically highlight the persisting difficulty of gauging the performance of the various theoretical tools that have been proposed or, *vice versa*, the level of detail that is required to be accounted for. While each of the discussed methods comes with its own limitations and challenges, this problem stems mainly from the largely inconclusive picture drawn on the basis of different experimental, targeted quantities and across different systems.

This is, for example, clearly demonstrated for the processes of inelastic scattering/adsorption reviewed in Section II. Here, the importance and ubiquity of reaction probabilities (i.e., sticking coefficients) as measured from molecular beam experiments have typically provided a key measure to compare against. Attempts to reproduce such sticking data from theory has shown that dissipation from phonons can require in some cases an explicit treatment of substrate motion, while satisfactory agreement is often already achieved on the level of effective energy sink models, or even a complete neglect of energy exchange with the lattice. While some prediction of the phononic relevance can be made based on the adsorbate-substrate mass mismatch, this does not always appear to be accurate [82, 86, 192]. This uncertainty adds yet another facet of complexity when considering also the contributing role of the non-adiabatic dissipation channel, whose relevance remains to date similarly obscure and inconclusive. It must be noted, however, that our judgment here is

likely further clouded by the limited DFT accuracy, particularly manifested in the calculation of encountered energy barriers [37, 38]. As reaction probabilities very sensitively depend on the latter, it could even be that effective dissipation models are simply "compensating" for incorrect barrier heights. Experimental sticking coefficients thus overall represent a rather inappropriate measure for gauging the accuracy of dissipation models: They convolute many different effects along the trajectory course of impinging gas-phase species, while their stochastic nature prevents a sensitive response to microscopic details of the dynamics which may even "wash out" all signatures of phononic and/or non-adiabatic dissipation. Alternative experimental measures such as the, potentially state-resolved, energy distribution of backscattered molecules thus appear as more promising benchmark references [124].

Also in this respect, the vibrational damping studies addressed in Section III are of great value. Here, only a limited phase-space region of the PES is encountered during the dynamics, the non-adiabatic dissipation channel provides a clearly dominating contribution and, most importantly, detailed, dissipation-specific experimental support is made available from pump-probe measurements. Thereby derived vibrational lifetimes have thus provided an extremely sensitive measure to non-adiabatic effects and have largely served as benchmark observables in establishing the performance of the numerically efficient electronic friction approach. Notwithstanding, the extent to which this trust can be transferred also to other elementary processes remains mostly unclear, especially when accommodating the adsorbate's description at a (reaction) transition state during the making/breaking of chemical bonds. One crucial requirement in this regard is the validity of the underlying physical picture that implies only weak non-adiabatic coupling. Despite its limitations, however, electronic friction presently remains the only tractable method in terms of computational resources needed for extended systems and times scales also relevant to phononic motion. As such, already this assessment as extracted from studies of vibrational damping, even if not necessarily universal, is of great importance.

Generally establishing such trust is very important also for simulating surface diffusion as discussed in Section IV. Here, long adsorbate-surface contact times call for all the more accuracy in describing energy exchange with an atom-resolved substrate. Microscopic details are, in principle, hereby expected to gain increasing importance for phonon effects (showing, e.g., a pronounced dependence on surface symmetry [73, 181]) and *eh*-pair exciations [185] alike. However, the relevance of the two dissipation channels is again here far from obvious. Unfortunately, only very few

22

first-principles diffusion studies have so far simultaneously included both of these contributions, while existing indications support a more pronounced role for non-adiabatic couplings than hitherto anticipated [164]. In this respect, further comparisons against high-quality, atomically resolved experimental data such as, e.g., provided from STM-derived adsorbate end-distances or ^{3}He-SE signatures will undoubtedly play a key role in systematic future studies. Largely removing uncertainties with respect to the phononic heat bath, the QM/Me embedding scheme (described in Section IV B) now represents a promising way forward. Coupling to the efficient electronic friction approach will specifically allow for a statistically meaningful number of trajectories that can better assess the performance of the latter and quantitatively disentangle the contribution of non-adiabatic effects in the presence of a realistic mobile substrate. We further envision corresponding QM/Me+EF studies to establish mechanistic trends for yet more complex systems beyond diatomic adsorbates, while elucidating the potential implications of "hot" chemistry to many important dynamical processes such as the self-assembly of surface nanostructures, the first steps of oxide nucleation and epitaxial growth, or adsorbate-induced surface reconstructions.

[1] J.C. Tully, Annu. Rev. Phys. Chem. 31 (1980), pp. 319 – 343.

[2] A. Groß, *Theoretical Surface Science: A Microscopic Perspective*, 2nd ed., Springer, Berlin, 2009 Jul.

[3] J.C. Tully, Annu. Rev. Phys. Chem. 51 (2000), pp. 153–178.

[4] A.M. Wodtke, J.C. Tully, and D.J. Auerbach, Int. Rev. Phys. Chem. 23 (2004), pp. 513–539.

[5] E. Hasselbrink, Curr. Opin. Solid St. M. 10 (2006), pp. 192 – 204.

[6] I. Rahinov, R. Cooper, D. Matsiev, C. Bartels, D.J. Auerbach, and A.M. Wodtke, Phys. Chem. Chem. Phys. 13 (2011), pp. 12680–12692.

[7] A.M. Wodtke, Chem. Soc. Rev. 45 (2016), pp. 3641–3657.

[8] K. Golibrzuch, N. Bartels, D.J. Auerbach, and A.M. Wodtke, Annu. Rev. Phys. Chem. 66 (2015), pp. 399–425.

[9] I. Chorkendorff and J.W. Niemantsverdriet, *Kinetics of reactions on surfaces*, in *Concepts of Modern Catalysis and Kinetics*, chap. 7, Wiley-VCH Verlag GmbH & Co. KGaA, 2005, pp. 267–299.

[10] K. Reuter, *First-principles kinetic monte carlo simulations for heterogeneous catalysis: Concepts, status and frontiers*, in *Modeling and Simulation of Heterogeneous Catalytic Reactions: From the Molecular Process to the Technical System*, O. Deutschman, ed., Wiley VCH, Weinheim, 2011, pp. 77–111.

[11] K. Reuter, Catal. Lett. 146 (2016), pp. 541–563.

[12] M.K. Sabbe, M.F. Reyniers, and K. Reuter, Catal. Sci. Technol. 2 (2012), pp. 2010–2024.

[13] K.W. Kolasinski, *Surface Science: Foundations of Catalysis and Nanoscience*, 3rd ed., John Wiley & Sons, Hoboken, New Jersey, USA, 2012.

[14] A.C. Luntz, *Dynamics of gas-surface interactions*, in *Surface and Interface Science*, chap. 47, Wiley-VCH Verlag GmbH & Co. KGaA, 2016, pp. 1255–1314.

[15] A.J. Cohen, P. Mori-Sánchez, and W. Yang, Science 321 (2008), pp. 792–794.

[16] J.K. Nørskov, F. Abild-Pedersen, F. Studt, and T. Bligaard, Proc. Natl. Acad. Sci. USA 108 (2011), pp. 937–943.

[17] A. Groß, Surf. Sci. 500 (2002), pp. 347–367.

[18] M. Scheffler and C. Stampfl, *Theory of adsorption on metal substrates*, in *Electronic Structure*, K. Horn and M. Scheffler, eds., Handbook of Surface Science, Vol. 2, chap. 5, North-Holland, 2000, pp. 285 – 356.

[19] A. Groß, Phys. Rev. Lett. 103 (2009), p. 246101.

[20] J.K. Nørskov, T. Bligaard, J. Rossmeisl, and C.H. Christensen, Nature Chem. 1 (2009), pp. 37–46.

[21] C.T. Rettner, D.J. Auerbach, J.C. Tully, and A.W. Kleyn, J. Phys. Chem. 100 (1996), pp. 13021–13033.

[22] L. Vattuone, G. Bracco, M. Smerieri, L. Savio, and M. Rocca, *Supersonic molecular beams studies of surfaces*, in *Dynamics of Gas-Surface Interactions: Atomic-level Understanding of Scattering Processes at Surfaces*, R. Díez Muiño and H.F. Busnengo, eds., chap. 1, Springer Berlin Heidelberg, Berlin, Heidelberg, 2013, pp. 1–23.

[23] H. Chadwick and R.D. Beck, Chem. Soc. Rev. 45 (2016), pp. 3576–3594.

[24] A. Groß and M. Scheffler, Prog. Surf. Sci. 53 (1996), pp. 187–196.

[25] A. Groß and M. Scheffler, Phys. Rev. B 57 (1998), pp. 2493–2506.

[26] A. Groß, Surf. Sci. Rep. 32 (1998), pp. 291–340.

[27] D.A. McCormack, G. Kroes, R.A. Olsen, J.A. Groeneveld, J.N.P. van Stralen, E.J. Baerends, and R.C. Mowrey, Faraday Discuss. 117 (2000), pp. 109–132.

[28] G.J. Kroes, A. Groß, E.J. Baerends, M. Scheffler, and D.A. McCormack, Acc. Chem. Res. 35 (2002), pp. 193–200.

[29] C. Díaz, J.K. Vincent, G.P. Krishnamohan, R.A. Olsen, G.J. Kroes, K. Honkala, and J.K. Nørskov, Phys. Rev. Lett. 96 (2006), p. 096102.

[30] B. Jiang and H. Guo, J. Chem. Phys. 144 (2016), p. 091101.

[31] X. Shen, Z. Zhang, and D.H. Zhang, J. Chem. Phys. 144 (2016), p. 101101.

[32] J. Behler, S. Lorenz, and K. Reuter, J. Chem. Phys. 127 (2007), p. 014705.

[33] H.F. Busnengo, A. Salin, and W. Dong, J. Chem. Phys. 112 (2000), pp. 7641–7651.

[34] V.J. Bukas, J. Meyer, M. Alducin, and K. Reuter, Z. Phys. Chem. 227 (2013), pp. 1523–1542.

[35] A. Groß, Surf. Sci. 606 (2012), pp. 690 – 691.

[36] A. Groß, Appl. Phys. A 67 (1998), pp. 627–635.

[37] G.J. Kroes and C. Díaz, Chem. Soc. Rev. 45 (2016), p. 3658.

[38] G.J. Kroes, Science 321 (2008), p. 794.

[39] C. Díaz, E. Pijper, R.A. Olsen, H.F. Busnengo, D.J. Auerbach, and G.J. Kroes, Science 326 (2009), p. 832.

[40] J. Behler and M. Parrinello, Phys. Rev. Lett. 98 (2007), p. 146401.

[41] J. Behler, J. Chem. Phys. 134 (2011), p. 074106.

[42] J. Behler, J. Chem. Phys. 145 (2016), p. 170901.

[43] B. Kolb, X. Luo, X. Zhou, B. Jiang, and H. Guo, J. Phys. Chem. Lett. 8 (2017), pp. 666–672.

[44] K. Shakouri, J. Behler, J. Meyer, and G.J. Kroes, J. Phys. Chem. Lett. 8 (2017), pp. 2131–2136.

[45] M. Hand and J. Harris, J. Chem. Phys. 92 (1990), pp. 7610–7617.

[46] A. Luntz and J. Harris, Surf. Sci. 258 (1991), pp. 397 – 426.

[47] S.A. Adelman and J.D. Doll, J. Chem. Phys. 64 (1976), pp. 2375–2388.

[48] M. Shugard, J.C. Tully, and A. Nitzan, J. Chem. Phys. 66 (1977), pp. 2534–2544.

[49] J.C. Tully, J. Chem. Phys. 73 (1980), pp. 1975–1985.

[50] J.C. Polanyi and R.J. Wolf, J. Chem. Phys. 82 (1985), pp. 1555–1566.

[51] M. Dohle and P. Saalfrank, Surf. Sci. 373 (1997), pp. 95–108.

[52] H.F. Busnengo, W. Dong, P. Sautet, and A. Salin, Phys. Rev. Lett. 87 (2001), p. 127601.

[53] E. Watts and G.O. Sitz, J. Chem. Phys. 111 (1999), pp. 9791–9796.

[54] Z.S. Wang, G.R. Darling, and S. Holloway, Phys. Rev. Lett. 87 (2001), p. 226102.

[55] H.F. Busnengo, W. Dong, and A. Salin, Phys. Rev. Lett. 93 (2004), p. 236103.

[56] H.F. Busnengo, M.A. Di Césare, W. Dong, and A. Salin, Phys. Rev. B 72 (2005), p. 125411.

[57] V.J. Bukas, S. Mitra, J. Meyer, and K. Reuter, J. Chem. Phys. 143 (2015), 034705.

[58] A. den Dunnen, S. Wiegman, L. Jacobse, and L.B.F. Juurlink, J. Chem. Phys. 142 (2015), 214708.

[59] L. Martin-Gondre, M. Alducin, G.A. Bocan, R. Díez Muiño, and J.I. Juaristi, Phys. Rev. Lett. 108 (2012), p. 096101.

[60] L. Martin-Gondre, M. Alducin, G.A. Bocan, R. Díez Muiño, and J.I. Juaristi, Phys. Rev. Lett. 108 (2012), p. 139901(E).

[61] M. Blanco-Rey, E. Díaz, G.A. Bocan, R. Díez Muiño, M. Alducin, and J.I. Juaristi, J. Phys. Chem. Lett. 4 (2013), pp. 3704–3709.

[62] R. Pétuya, P.A. Plötz, C. Crespos, and P. Larregaray, J. Phys. Chem. C 118 (2014), pp. 21904–21910.

[63] I. Goikoetxea, J. Meyer, J.I. Juaristi, M. Alducin, and K. Reuter, Phys. Rev. Lett. 112 (2014), p. 156101.

[64] J.P. Toennies, J. Phys. Condens. Matter 5 (1993), p. A25.

[65] M.D. Stiles and J.W. Wilkins, Phys. Rev. Lett. 54 (1985), pp. 595–598.

[66] M.D. Stiles, J.W. Wilkins, and M. Persson, Phys. Rev. B 34 (1986), pp. 4490–4510.

[67] B. Jackson, Comput. Phys. Commun. 80 (1994), pp. 119 – 144.

[68] M. Dohle, P. Saalfrank, and T. Uzer, Surf. Sci. 409 (1998), pp. 37 – 45.

[69] M. Dohle, P. Saalfrank, and T. Uzer, J. Chem. Phys. 108 (1998), pp. 4226–4236.

[70] D.J. Auerbach, Phys. Scripta 1983 (1983), p. 122.

[71] A.S. Sanz and S. Miret-Artés, Phys. Rep. 451 (2007), pp. 37 – 154.

[72] C. Carbogno, A. Groß, J. Meyer, and K. Reuter, *Dynamics of gas-surface interactions: Atomic-level understanding of scattering processes at surfaces*, in *Dynamics of Gas-Surface Interactions: Atomic-level Understanding of Scattering Processes at Surfaces*, R. Díez Muiño and F.H. Busnengo, eds., chap. 16, Springer Berlin Heidelberg, Berlin, Heidelberg, 2013, pp. 389–419.

[73] V.J. Bukas and K. Reuter, J. Chem. Phys. 146 (2017), p. 014702.

[74] A.C. Luntz and R.D. Beck, J. Vac. Sci. Technol. A 35 (2017), p. 05C201.

[75] A.K. Tiwari, S. Nave, and B. Jackson, Phys. Rev. Lett. 103 (2009), p. 253201.

[76] A.K. Tiwari, S. Nave, and B. Jackson, J. Chem. Phys. 132 (2010), p. 134702.

[77] B. Jackson, *The effects of lattice motion on gas-surface reactions*, in *Dynamics of Gas-Surface Interactions: Atomic-level Understanding of Scattering Processes at Surfaces*, R. Díez Muiño and H.F. Busnengo, eds., chap. 9, Springer Berlin Heidelberg, Berlin, Heidelberg, 2013, pp. 213–237.

[78] B. Jackson and S. Nave, J. Chem. Phys. 138 (2013), p. 174705.

[79] A. Groß, *Dynamics of reactions at surfaces*, in *Modeling and Simulation of Heterogeneous Catalytic Reactions*, chap. 2, Wiley-VCH Verlag GmbH & Co. KGaA, 2011, pp. 39–70.

[80] F. Nattino, H. Ueta, H. Chadwick, M.E. van Reijzen, R.D. Beck, B. Jackson, M.C. van Hemert, and G.J. Kroes, J. Phys. Chem. Lett. 5 (2014), pp. 1294–1299.

[81] F. Nattino, C. Díaz, B. Jackson, and G.J. Kroes, Phys. Rev. Lett. 108 (2012), p. 236104.

[82] G. Füchsel, M. del Cueto, C. Díaz, and G.J. Kroes, J. Phys. Chem. C 120 (2016), pp. 25760–25779.

[83] F. Nattino, F. Costanzo, and G.J. Kroes, J. Chem. Phys. 142 (2015), p. 104702.

[84] F. Nattino, D. Migliorini, M. Bonfanti, and G.J. Kroes, J. Chem. Phys. 144 (2016), p. 044702.

[85] A. Groß, Catal. Today 260 (2016), pp. 60–65.

[86] X. Zhou, B. Kolb, X. Luo, H. Guo, and B. Jiang, J. Phys. Chem. C 121 (2017), pp. 5594–5602.

[87] F. Nattino, O. Galparsoro, F. Costanzo, R. Díez Muiño, M. Alducin, and G.J. Kroes, J. Chem. Phys. 144 (2016), p. 244708.

[88] J. Behler, B. Delley, S. Lorenz, K. Reuter, and M. Scheffler, Phys. Rev. Lett. 94 (2005), p. 036104.

[89] C. Carbogno, J. Behler, A. Groß, and K. Reuter, Phys. Rev. Lett. 101 (2008), p. 096104.

[90] F. Libisch, C. Huang, P. Liao, M. Pavone, and E.A. Carter, Phys. Rev. Lett. 109 (2012), p. 198303.

[91] Y. Huang, A.M. Wodtke, H. Hou, C.T. Rettner, and D.J. Auerbach, Phys. Rev. Lett. 84 (2000), pp. 2985–2988.

[92] Y. Huang, C.T. Rettner, D.J. Auerbach, and A.M. Wodtke, Science 290 (2000), p. 111.

[93] M. Lindenblatt and E. Pehlke, Phys. Rev. Lett. 97 (2006), p. 216101.

[94] M. Grotemeyer and E. Pehlke, Phys. Rev. Lett. 112 (2014), p. 043201.

[95] J.C. Tully, Int. J. Quantum Chem. 40 (1991), pp. 299–309.

[96] J.C. Tully, Faraday Discuss. 110 (1998), pp. 407–419.

[97] M.D. Hack and D.G. Truhlar, J. Phys. Chem. A 104 (2000), pp. 7917–7926.

[98] N.A. Shenvi, S. Roy, and J.C. Tully, J. Chem. Phys. 130 (2009), 174107.

[99] W. Dou and J.E. Subotnik, J. Chem. Theo. Comp. 13 (2017), pp. 2430–2439.

[100] N.A. Shenvi, S. Roy, and J.C. Tully, Science 326 (2009), pp. 829–832.

[101] S. Roy, N.A. Shenvi, and J.C. Tully, J. Chem. Phys. 130 (2009), 174716.

[102] M. Timmer and P. Kratzer, Phys. Rev. B 79 (2009), p. 165407.

[103] J. Meyer and K. Reuter, New J. Phys. 13 (2011), p. 085010.

[104] S. Rittmeyer, J. Meyer, and K. Reuter, submitted to Phys. Rev. Lett. (2017).

[105] E.G. d'Agliano, P. Kumar, W. Schaich, and H. Suhl, Phys. Rev. B 11 (1975), pp. 2122–2143.

[106] Y. Li and G. Wahnström, Phys. Rev. Lett. 68 (1992), pp. 3444–3447.

[107] M. Head-Gordon and J.C. Tully, J. Chem. Phys. 103 (1995), pp. 10137–10145.

[108] W. Dou, A. Nitzan, and J.E. Subotnik, J. Chem. Phys. 143 (2015), p. 054103.

[109] W. Dou and J.E. Subotnik, J. Chem. Phys. 146 (2017), p. 092304.

[110] W. Dou and J.E. Subotnik, pre-print (2017), arXiv:1703.04717.

[111] T.L. Ferrell and R.H. Ritchie, Phys. Rev. B 16 (1977), pp. 115–123.

[112] P. Echenique, R. Nieminen, and R. Ritchie, Solid State Commun. 37 (1981), pp. 779 – 781.

[113] P. Sigmund, Phys. Rev. A 26 (1982), pp. 2497–2517.

[114] K. Schönhammer and O. Gunnarsson, *Energy dissipation at metal surfaces: The electron hole-pair mechanism*, in *Many-Body Phenomena at Surfaces*, D. Langreth and H. Suhl, eds., Academic Press, 1984, pp. 421 – 451.

[115] B. Hellsing and M. Persson, Phys. Scr. 29 (1984), p. 360.

[116] J.I. Juaristi, M. Alducin, R. Díez Muiño, H.F. Busnengo, and A. Salin, Phys. Rev. Lett. 100 (2008), p. 116102.

[117] M.J. Puska and R.M. Nieminen, Phys. Rev. B 27 (1983), pp. 6121–6128.

[118] P.M. Echenique, R.M. Nieminen, J.C. Ashley, and R.H. Ritchie, Phys. Rev. A 33 (1986), pp. 897–904.

[119] P. Echenique and M. Uranga, *Density functional theory of stopping power*, in *Interaction of Charged Particles with Solids and Surfaces*, A. Gras-Marti, H.M. Urbassek, N.R. Arista, and F. Flores, eds., Nato ASI Series, Vol. 271, Plenum Press, New York, 1991, pp. 39–71.

[120] M. Askerka, R.J. Maurer, V.S. Batista, and J.C. Tully, Phys. Rev. Lett. 116 (2016), p. 217601.

[121] R.J. Maurer, M. Askerka, V.S. Batista, and J.C. Tully, Phys. Rev. B 94 (2016), p. 115432.

[122] J. Trail, M. Graham, and D. Bird, Comp. Phys. Comm. 137 (2001), pp. 163 – 173.

[123] N. Lorente and M. Persson, Faraday Discuss. 117 (2000), pp. 277–290.

[124] R.J. Maurer, B. Jiang, H. Guo, and J.C. Tully, Phys. Rev. Lett. 118 (2017), p. 256001.

[125] J.R. Trail, M.C. Graham, D.M. Bird, M. Persson, and S. Holloway, Phys. Rev. Lett. 88 (2002), p. 166802.

[126] J.R. Trail, D.M. Bird, M. Persson, and S. Holloway, J. Chem. Phys. 119 (2003), pp. 4539–4549.

[127] A.C. Luntz and M. Persson, J. Chem. Phys. 123 (2005), 074704.

[128] A.C. Luntz, M. Persson, S. Wagner, C. Frischkorn, and M. Wolf, J. Chem. Phys. 124 (2006), p. 244702.

[129] A.C. Luntz, M. Persson, and G.O. Sitz, J. Chem. Phys. 124 (2006), 091101.

[130] G. Füchsel, T. Klamroth, S. Monturet, and P. Saalfrank, Phys. Chem. Chem. Phys. 13 (2011), pp. 8659–8670.

[131] A.C. Luntz, I. Makkonen, M. Persson, S. Holloway, D.M. Bird, and M.S. Mizielinski, Phys. Rev. Lett. 102 (2009), p. 109601.

[132] J.I. Juaristi, M. Alducin, R. Díez Muiño, H.F. Busnengo, and A. Salin, Phys. Rev. Lett. 102 (2009), p. 109602.

[133] F. Hirshfeld, Theor. Chim. Acta 44 (1977), pp. 129–138.

[134] S.P. Rittmeyer, J. Meyer, J.I. Juaristi, and K. Reuter, Phys. Rev. Lett. 115 (2015), p. 046102.

[135] I. Goikoetxea, J.I. Juaristi, M. Alducin, and R. Díez Muiño, J. Phys. Condens. Matter 21 (2009), p. 264007.

[136] B. Jiang, M. Alducin, and H. Guo, J. Phys. Chem. Lett. 7 (2016), pp. 327–331.

[137] X. Luo, B. Jiang, J.I. Juaristi, M. Alducin, and H. Guo, J. Chem. Phys. 145 (2016), 044704.

[138] A.S. Muzas, J.I. Juaristi, M. Alducin, R. Díez Muiño, G.J. Kroes, and C. Díaz, J. Chem. Phys. 137 (2012), 064707.

[139] G. Füchsel, S. Schimka, and P. Saalfrank, J. Phys. Chem. A 117 (2013), pp. 8761–8769.

[140] R. Cooper, C. Bartels, A. Kandratsenka, I. Rahinov, N. Shenvi, K. Golibrzuch, Z. Li, D.J. Auerbach, J.C. Tully, and A.M. Wodtke, Angew. Chem. Int. Ed. 51 (2012), pp. 4954–4958.

[141] J.T. Kindt, J.C. Tully, M. Head-Gordon, and M.A. Gomez, J. Chem. Phys. 109 (1998), pp. 3629–3636.

[142] L. Martin-Gondre, G. Bocan, M. Alducin, J. Juaristi, and R. Díez Muiño, Comput. Theor. Chem. 990 (2012), pp. 126–131.

[143] L. Martin-Gondre, G.A. Bocan, M. Blanco-Rey, M. Alducin, J.I. Juaristi, and R. Díez Muiño, J. Phys. Chem. C 117 (2013), pp. 9779–9790.

[144] G.J. Kroes, M. Pavanello, M. Blanco-Rey, M. Alducin, and D.J. Auerbach, J. Chem. Phys. 141 (2014), p. 054705.

[145] S.M. Janke, M. Pavanello, G.J. Kroes, D. Auerbach, A.M. Wodtke, and A. Kandratsenka, Z. Phys. Chem. 227 (2013), pp. 1467–1490.

[146] O. Bünermann, H. Jiang, Y. Dorenkamp, A. Kandratsenka, S.M. Janke, D.J. Auerbach, and A.M. Wodtke, Science 350 (2015), pp. 1346–1349.

[147] S.M. Janke, D.J. Auerbach, A.M. Wodtke, and A. Kandratsenka, J. Chem. Phys. 143 (2015), 124708.

[148] P. Saalfrank, Chem. Rev. 106 (2006), pp. 4116–4159.

[149] H. Arnolds, Prog. Surf. Sci. 86 (2011), pp. 1 – 40.

[150] B.N.J. Persson, J. Phys. C: Solid State Phys. 11 (1978), p. 4251.

[151] B. Persson and M. Persson, Surf. Sci. 97 (1980), pp. 609 – 624.

[152] B. Persson and M. Persson, Solid State Commun. 36 (1980), pp. 175 – 179.

[153] M. Persson and B. Hellsing, Phys. Rev. Lett. 49 (1982), pp. 662–665.

[154] B. Hellsing, M. Persson, and B. Lundqvist, Surf. Sci. 126 (1983), pp. 147 – 153.

[155] B.N.J. Persson, J. Phys. C: Solid State Phys. 17 (1984), p. 4741.

[156] J.C. Tully, M. Gomez, and M. Head-Gordon, J. Vac. Sci. Technol. A 11 (1993), pp. 1914–1920.

[157] M. Morin, N.J. Levinos, and A.L. Harris, J. Chem. Phys. 96 (1992), pp. 3950–3956.

[158] P. Saalfrank, J.I. Juaristi, M. Alducin, M. Blanco-Rey, and R. Díez Muiño, J. Chem. Phys. 141 (2014), 234702.

[159] M. Head-Gordon and J.C. Tully, J. Chem. Phys. 96 (1992), pp. 3939–3949.

[160] M. Head-Gordon and J.C. Tully, Phys. Rev. B 46 (1992), pp. 1853–1856.

[161] V. Krishna and J.C. Tully, J. Chem. Phys. 125 (2006), p. 054706.

[162] M. Forsblom and M. Persson, J. Chem. Phys. 127 (2007), p. 154303.

[163] M.S. Mizielinski, D.M. Bird, M. Persson, and S. Holloway, J. Chem. Phys. 122 (2005), 084710.

[164] J. Barth, Surf. Sci. Rep. 40 (2000), pp. 75 – 149.

[165] T. Ala-Nissila, R. Ferrando, and S.C. Ying, Adv. Phys. 51 (2002), pp. 949–1078.

[166] G. Wahnström, A.B. Lee, and J. Strömquist, J. Chem. Phys. 105 (1996), pp. 326–336.

[167] S.P. Rittmeyer, D.J. Ward, P. Gütlein, J. Ellis, W. Allison, and K. Reuter, Phys. Rev. Lett. 117 (2016), p. 196001.

[168] A. Jardine, H. Hedgeland, G. Alexandrowicz, W. Allison, and J. Ellis, Prog. Surf. Sci. 84 (2009), pp.

323 – 379.

[169] A.P. Jardine, J. Ellis, and W. Allison, J. Chem. Phys. 120 (2004), pp. 8724–8733.

[170] A.P. Jardine, G. Alexandrowicz, H. Hedgeland, W. Allison, and J. Ellis, Phys. Chem. Chem. Phys. 11 (2009), pp. 3355–3374.

[171] A. Carley, P. Davies, and M. Roberts, Catal. Lett. 80 (2002), pp. 25–34.

[172] H. Brune, J. Wintterlin, R.J. Behm, and G. Ertl, Phys. Rev. Lett. 68 (1992), pp. 624–626.

[173] J. Wintterlin, R. Schuster, and G. Ertl, Phys. Rev. Lett. 77 (1996), pp. 123–126.

[174] B.G. Briner, M. Doering, H.P. Rust, and A.M. Bradshaw, Phys. Rev. Lett. 78 (1997), pp. 1516–1519.

[175] S. Schintke, S. Messerli, K. Morgenstern, J. Nieminen, and W.D. Schneider, J. Chem. Phys. 114 (2001), pp. 4206–4209.

[176] M. Rose, A. Borg, J. Dunphy, T. Mitsui, D. Ogletree, and M. Salmeron, Surf. Sci. 561 (2004), pp. 69 – 78.

[177] M.F. Hsieh, D.S. Lin, H. Gawronski, and K. Morgenstern, J. Chem. Phys. 131 (2009), 174709.

[178] C. Sprodowski, M. Mehlhorn, and K. Morgenstern, J. Phys.-Condens. Mat. 22 (2010), p. 264005.

[179] M. Schmid, G. Leonardelli, R. Tscheließnig, A. Biedermann, and P. Varga, Surf. Sci. 478 (2001), pp. L355 – L362.

[180] A.J. Komrowski, J.Z. Sexton, A.C. Kummel, M. Binetti, O. Weiße, and E. Hasselbrink, Phys. Rev. Lett. 87 (2001), p. 246103.

[181] V.J. Bukas and K. Reuter, Phys. Rev. Lett. 117 (2016), p. 146101.

[182] C. Engdahl and G. Wahnström, Surf. Sci. 312 (1994), pp. 429–440.

[183] M. Blanco-Rey, J.I. Juaristi, R. Díez Muiño, H.F. Busnengo, G.J. Kroes, and M. Alducin, Phys. Rev. Lett. 112 (2014), p. 103203.

[184] D. Novko, M. Blanco-Rey, J.I. Juaristi, and M. Alducin, Phys. Rev. B 92 (2015), p. 201411.

[185] D. Novko, M. Blanco-Rey, J. Juaristi, and M. Alducin, Nucl. Instrum. Meth. B 382 (2016), pp. –.

[186] P. Nieto, E. Pijper, D. Barredo, G. Laurent, R.A. Olsen, E.J. Baerends, G.J. Kroes, and D. Farías, Science 312 (2006), pp. 86–89.

[187] J. Meyer and K. Reuter, Angew. Chem. Int. Ed. 53 (2014), pp. 4721–4724.

[188] M.S. Daw and M.I. Baskes, Phys. Rev. B 29 (1984), pp. 6443–6453.

[189] M.I. Baskes, Phys. Rev. B 46 (1992), pp. 2727–2742.

[190] B. Jackson, Comput. Phys. Commun. 63 (1991), pp. 154 – 170.

[191] B. Jackson, J. Chem. Phys. 108 (1998), pp. 1131–1139.

[192] B. Kolb and H. Guo, J. Chem. Phys. 145 (2016), p. 011102.
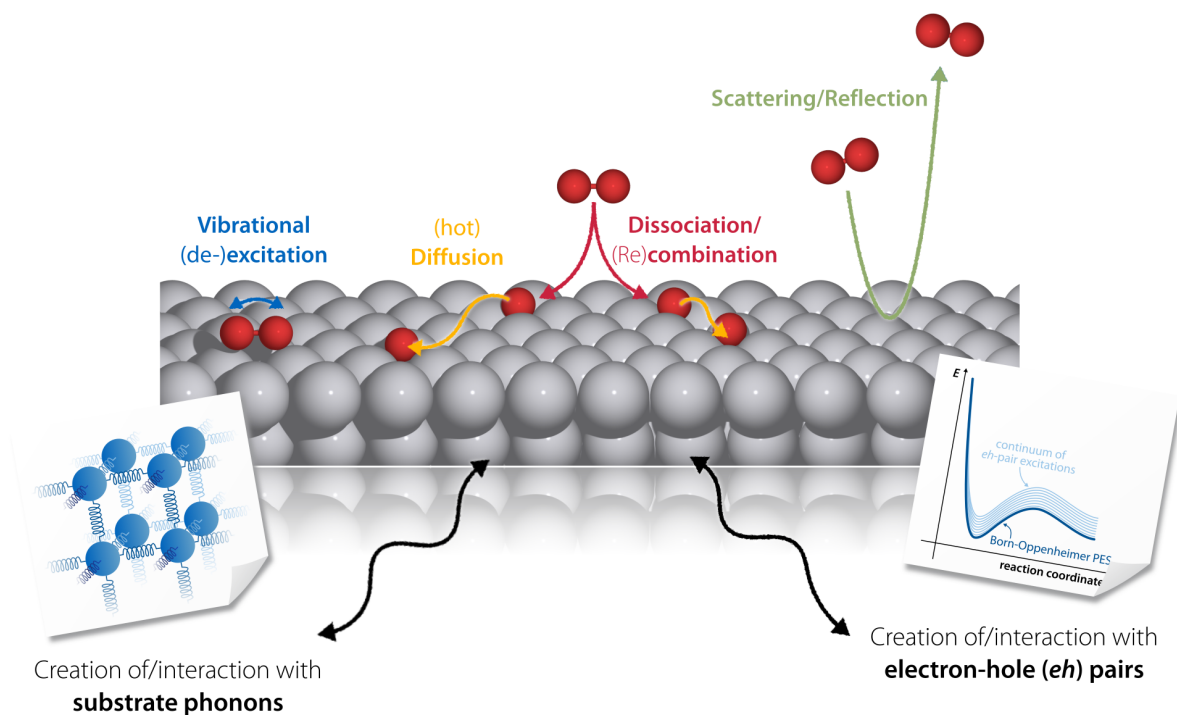
Figure 1. Various elementary processes in the context of gas-surface dynamics. An impinging molecule may, for instance, be directly reflected from the metal substrate, nevertheless exchanging energy and momentum with the surface. It may, however, as well dissociate on the surface—potentially through a vibrational precursor state—with the excess kinetic energy leading to hyperthermal motion of the fragments, so-called 'hot diffusion'. In all of these processes, energy exchange with the metal occurring either through the excitation of lattice vibrations (phonons) or non-adiabatic electron-hole (*eh*)-pairs may significantly influence the resulting dynamics.
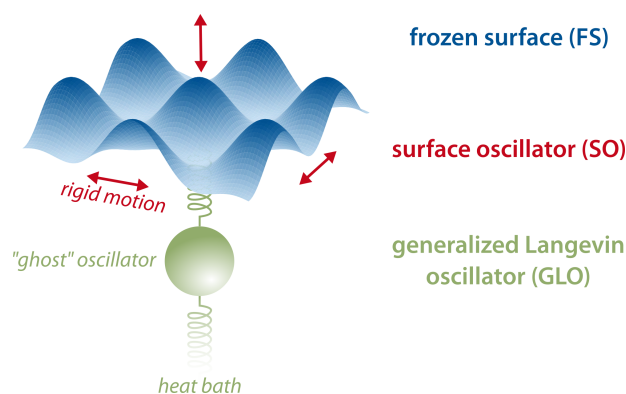
Figure 2. Hierarchical approaches to enrich simulations on a frozen surface (FS) potential energy surface (PES) with an account of lattice motion. The surface oscillator (SO) model first introduces a 3D harmonic oscillator corresponding to a rigid shift of the entire PES in all spatial directions, thus allowing for adsorbate-surface energy transfer following a simple collision model. Building on this, the generalized Langevin oscillator (GLO) adds a further ghost oscillator linearly coupled to the SO, which in turn is further coupled to a heat bath within an effective generalized Langevin description. This allows to also include energy dissipation from the SO to the bulk.
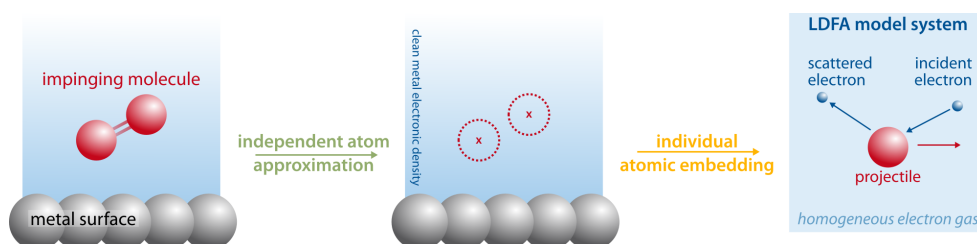
Figure 3. Construction of electronic friction coefficients within the local density friction approximation (LDFA)[116]. The interacting molecule-surface system is first approximated through independent atoms being embedded in the electron density of the clean metal surface. The local electronic density at the atomic positions is then used to independently map to an isotropic atomic embedding model system of a spherically symmetric impurity in jellium. Finally, electronic friction coefficients are evaluated from the scattering phase shifts of the Kohn-Sham states at the Fermi-momentum for this model [111, 112, 117–119]. This ultimately yields, for each element, an electronic friction coefficient as a function of the embedding density and can thus be conveniently evaluated and tabulated prior to dynamical simulations. It has later been suggested to introduce molecular information by constructing the embedding density via a suitable Hirshfeld-partitioning [133] of the full system electronic density [134].

34
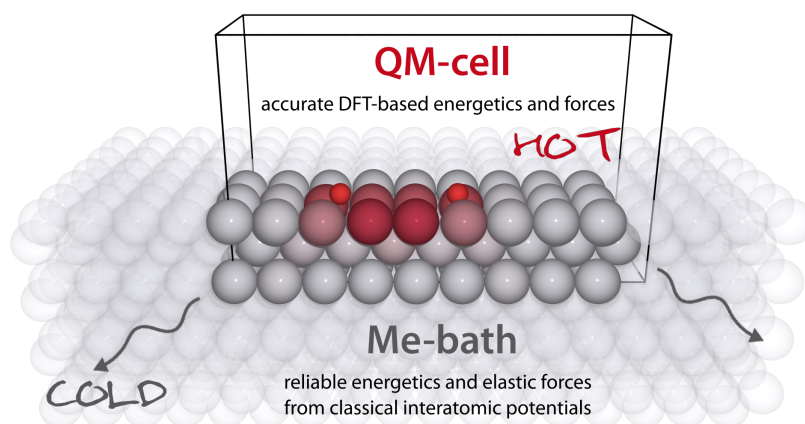
Figure 4. Schematic illustration of the QM/Me embedding approach, applied here to the dissociative O_2 adsorption over Pd(100) [181]. A quantum-mechanical (QM) description of the immediate reaction zone is based on periodic DFT calculations to yield an accurate description of the short range, adsorbate-induced chemical interactions. This QM-cell is embedded into an extended metal (Me) substrate that is treated at the level of a numerically efficient classical interatomic potential to provide the elastic contribution to the forces due to deformation of the lattice. Released chemical energy is thus dissipated out of the "hot" reaction zone and into a "cold" macroscopic heat bath, while atoms in the embedding cell are color-coded according to kinetic energy.

Nonadiabatic Vibrational Damping of Molecular Adsorbates: Insights into Electronic Friction and the Role of Electronic Coherence

S.P. Rittmeyer, J. Meyer, and K. Reuter

Nonadiabatic Vibrational Damping of Molecular Adsorbates: Insights into Electronic Friction and the Role of Electronic Coherence

Simon P. Rittmeyer,[1,*] Jörg Meyer,[2] and Karsten Reuter[1]

[1]*Chair for Theoretical Chemistry and Catalysis Research Center, Technische Universität München,
Lichtenbergstraße 4, 85747 Garching, Germany*
[2]*Leiden Institute of Chemistry, Gorlaeus Laboratories, Leiden University, P.O. Box 9502, 2300 RA Leiden, The Netherlands*
(Received 13 April 2017; published 27 October 2017)

We present a perturbation approach rooted in time-dependent density-functional theory to calculate electron-hole (*e-h*) pair excitation spectra during the nonadiabatic vibrational damping of adsorbates on metal surfaces. Our analysis for the benchmark systems CO on Cu(100) and Pt(111) elucidates the surprisingly strong influence of rather short electronic coherence times. We demonstrate how in the limit of short electronic coherence times, as implicitly assumed in prevalent quantum nuclear theories for the vibrational lifetimes as well as electronic friction, band structure effects are washed out. Our results suggest that more accurate lifetime or chemicurrentlike experimental measurements could characterize the electronic coherence.

The tortuous ways in which kinetic and chemical energy is transferred between adsorbates and substrate atoms fundamentally govern the dynamics of surface chemical reactions, for instance, in the context of heterogeneous catalysis or advanced deposition techniques. For metal substrates, the two main energy dissipation mechanisms in this regard are the adsorbate interaction with lattice vibrations, i.e., substrate phonons, and the excitation of electron-hole (*e-h*) pairs. The latter are attributable to the nonadiabatic coupling of nuclear motion to the substrate electronic degrees of freedom (d.o.f.) and seem to be substantial in order to rationalize an increasing number of experimental findings [1,2]. Important steps towards an accurate, yet efficient first-principles-based modeling of the energy uptake into phononic d.o.f. have recently been taken [3–10]. In contrast, the explicit description of *e-h* pair excitations and corresponding nonadiabatic couplings directly from first principles still poses a formidable challenge.

In this regard, electronic friction theory (EFT) [11,12] has become a popular workhorse to effectively capture the effects of such nonadiabatic energy loss on the adsorbate dynamics in a computationally convenient way [13–19]. Inspired by vibrational lifetimes obtained via response theory [20] or Fermi's golden rule in the nuclear system [21], a Langevin equation for the nuclei emerges from a semiclassical picture implying complete electronic decoherence in terms of the Markov approximation [12]. This approach thus avoids an explicit propagation of the electron dynamics and concomitant ultrafast time scales by coarse-graining the effects into electronic friction forces linear in nuclear velocities. This enables an efficient combination even with density-functional theory (DFT) based *ab initio* molecular dynamics (AIMD) simulations on high-dimensional potential energy surfaces as required for surface dynamical studies [15,22,23].

Independent of the particular recipe employed to obtain the electronic friction coefficients [12,14,17,20,24,25], however, the downside of the coarse-graining of the electron dynamics is that it precludes a more fundamental understanding of the underlying *e-h* pair excitations. For instance, recent such calculations for nonadiabatic vibrational lifetimes of several small molecules [17,25,26] still do not elucidate the seemingly nonsystematic trends for different adsorbate-substrate combinations [26–28].

Going beyond the EFT approach is conceptually challenging, in particular, without sacrificing a predictive-quality description of the metallic band structure at least on the DFT level. In principle, mixed quantum-classical dynamics in terms of Ehrenfest dynamics can provide access to *e-h* pair excitation spectra [29,30]. Notwithstanding, in the context of surface dynamical studies at extended metal surfaces, this approach struggles with exceeding computational costs. In this Letter, we therefore pursue a perturbation approach rooted in time-dependent DFT (TDDFT) that provides a computationally more appealing access to explicit *e-h* pair excitation spectra. Aiming to scrutinize the confusing and inconclusive picture obtained from EFT as well as from experimental measurements, we revisit the vibrational damping of the CO stretch mode on Cu(100) and Pt(111). These represent two established benchmark systems for which accurate experimental lifetimes are available [31,32] and energy loss into phononic d.o.f. is commonly considered to be negligible [33–35]. In contrast to previous EFT-based work [25], the nonadiabatic energy loss derived from our calculated *e-h* pair excitation spectra differs significantly for both systems when the electronic coherence is longer than five vibrational periods (≈ 80 fs). In this case, as intuitively expected from the much higher density of states (DOS) in the vicinity of the Fermi level, we find a notably

higher nonadiabatic energy dissipation rate for CO on Pt (111). In the limit of short electronic coherence times, i.e., approaching the Markov limit for the electronic d.o.f. as relied upon in EFT, however, the detailed dependence on the metallic band structure is washed out.

Since the CO stretch mode is far above the substrate phonon continuum, the vibrational lifetime on a metal surface ($\hbar\omega_{\text{vib}} \approx 260$ meV) is commonly assumed to be one of few experimentally accessible observables that is governed by nonadiabatic energy dissipation [34,35]. For both benchmark systems CO on Cu(100) and Pt(111), experimental reference lifetimes are around 2 ps [31,32]. Even though these lifetimes could be nicely reproduced by EFT using different models for the friction coefficient [17,25–28], the missing correlation of the vibrational lifetime with the underlying metal band structure remains an unresolved mystery [26–28]. As a transition metal with an only partially filled d band, platinum shows a significantly higher metallic DOS in the energetically relevant region close to the Fermi level as compared to a coinage metal such as copper [36]. Intuitively, it should thus allow for more e-h pair excitations [37]. However, neither this nor the different adsorbate-induced DOS on both substrates seems to result in notable variations of the nonadiabatic vibrational lifetimes [28].

There have been several attempts to deduce a more detailed understanding of the e-h pair excitations behind frictional energy losses [24,40,41] by connecting the latter to a forced oscillator model (FOM) [42]. In essence, the FOM describes electronic excitations in the substrate through a collection of independent harmonic oscillators driven by an external force of identical functional form but different strength [41]. It may thus be seen as a simple illustration of the ideas also underlying EFT [41]. Excitation spectra predicted by the FOM for the vibrational damping dynamics of CO on Cu(100) and Pt(111) are shown in Fig. 1 below. Specifically, the hole excitation spectrum $P_{\text{ex},h}(\epsilon_i)$ denotes the probability that created e-h pair excitations involve the formation of a hole in the occupied energy level ϵ_i, whereas the electron excitation spectrum $P_{\text{ex},e}(\epsilon_j)$ shows this probability as a function of the unoccupied level ϵ_j that is filled with an electron. The symmetric sigmoidlike spectra stepped at the stretch vibrational frequency look exactly the same for both systems, as one would expect from their similar vibrational frequencies and friction coefficients. This functional form of the spectra is, in fact, a direct consequence of the motion pattern underlying the nuclear dynamics. It is essentially independent of the precise recipe used to obtain the electronic friction coefficients (cf. Supplemental Material [43]), and it does not exhibit any correlation with the underlying metallic band structure [24].

To scrutinize this picture, we follow a perturbation approach to explicitly describe adsorbate-induced e-h pair excitations in the metallic substrate. Originally developed for molecular scattering [55,56], we here present its straightforward extension to periodic motion. According
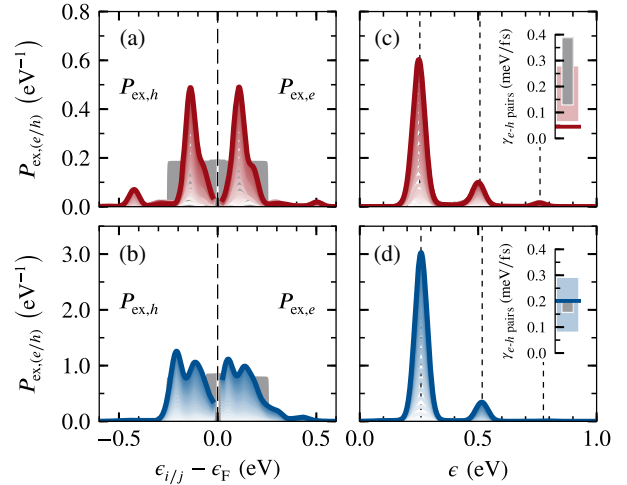
FIG. 1. Excitation spectra for the nonadiabatic coupling of the stretch mode of CO on Cu(100) (upper panels, red) and Pt(111) (lower panels, blue) to the metallic continuum assuming infinite electronic coherence. The corresponding long-time limit is achieved by integrating Eq. (3) over increasing times. The resulting spectral growth is indicated by lines of decreasing brightness, with the final bold line corresponding to an integration over $t_n = 20T \approx 320$ fs. Left panels (a) and (b) show electron and hole excitation spectra ($P_{\text{ex},e}$ and $P_{\text{ex},h}$) and additionally contain spectra calculated from the FOM (gray-shaded areas). Note that for direct comparability the FOM spectra are scaled to equal area with the respective explicitly evaluated spectra from perturbation theory. Right panels (c) and (d) show e-h pair excitation spectra with peaks at multiples of the CO vibrational stretch frequency (dotted vertical lines). The insets depict the corresponding nonadiabatic energy loss rates as compared to the experiment (gray-shaded area indicating the reported error bars) [31,32] and to the range of values obtained from EFT (red- or blue-shaded range) [25].

to the Runge-Gross theorem [57], mapping to an effective single-particle picture described by $\hat{h}(t) = \hat{h}_0 + \hat{v}_{\text{pert}}(t)$ is possible. Here, $\hat{h}_0$ is the unperturbed static Hamiltonian corresponding to the adsorbed molecule in its equilibrium geometry, and $\hat{v}_{\text{pert}}(t)$ describes the periodic time-dependent electronic perturbation potential exerted by the nuclear vibrational motion. The key idea to arrive at a computationally tractable scheme that avoids an explicit time-dependent evaluation of the perturbation potential is to approximate the latter through a series of snapshots along the periodic molecular trajectory $\boldsymbol{Q}(t)$ around the equilibrium geometry $\boldsymbol{Q}_0$ such that

$$\hat{h}(t) \approx \hat{h}_0 + \underbrace{\hat{v}_{\text{eff}}(\boldsymbol{Q}(t)) - \hat{v}_{\text{eff}}(\boldsymbol{Q}_0)}_{=\hat{v}_{\text{pert}}(\boldsymbol{Q}(t))}, \qquad (1)$$

where $\hat{v}_{\text{eff}}(\boldsymbol{Q})$ is the effective Kohn-Sham (KS) single-particle potential at the respective snapshots. Each of these snapshots can in turn be treated within the framework of time-independent DFT, as the dynamic information has entirely been shifted into the time dependence of $\boldsymbol{Q}(t)$. For

the Hamiltonian defined in Eq. (1), first-order time-dependent perturbation theory then leads to the *e-h* pair excitation spectrum at time $t_n = nT$, i.e., the probability to generate *e-h* pair excitations of energy ϵ after n molecular oscillations with period T, as

$$P_{\text{ex}}(\epsilon; t_n) = \sum_{i,j} \left| \frac{\lambda_{ij}(t_n)}{\epsilon_j - \epsilon_i} \right|^2 \delta(\epsilon - \epsilon_{ji}). \quad (2)$$

Here, $\epsilon_{ji} = \epsilon_j - \epsilon_i$ is the energy difference between KS states i and j of the unperturbed system with eigenenergies ϵ_i and ϵ_j, while $\lambda_{ij}(t_n)$ is the corresponding transition matrix element. Separate hole $P_{\text{ex},h}(\epsilon_i; t_n)$ and electron $P_{\text{ex},e}(\epsilon_j; t_n)$ spectra are obtained by equations analogous to Eq. (2), in which the energy of the initial and final state relative to the Fermi level rather than the energy difference ϵ_{ji} is considered [55,56]. Integration by parts allows us to calculate the matrix elements in Eq. (2) for an $i \rightarrow j$ transition according to

$$\lambda_{ij}(t_n) = \int_0^{t_n} \langle j | \nabla_{\boldsymbol{Q}} \hat{v}_{\text{pert}}(\boldsymbol{Q}(t)) | i \rangle \cdot \dot{\boldsymbol{Q}}(t) e^{i(\epsilon_{ji}/\hbar)t} dt. \quad (3)$$

The integral limits are chosen such that the integration spans integer multiples of a vibrational period and the boundary terms conveniently vanish [56]. Further details on our evaluation of Eq. (3) within the framework of semilocal DFT at the generalized-gradient level [58,59] are presented in Supplemental Material [43]. Finally, the actual nonadiabatic energy loss is consistently evaluated as an energy-weighted integral over the *e-h* pair spectrum [55,56] such that we can approximate the energy dissipation rate as

$$\gamma_{e\text{-}h\,\text{pairs}} = \frac{1}{t_n} \int_0^{\infty} \epsilon P_{\text{ex}}(\epsilon; t_n) d\epsilon. \quad (4)$$

We first note the striking similarity between Eq. (3) and the matrix elements required in the context of an orbital-dependent formulation of the electronic friction tensor [orbital-dependent friction (ODF)] [12,17,20,26,40]. This is not surprising as—in contrast to the popular purely embedding density-based local density friction approximation (LDFA) [14,60–62]—ODF is also based on a time-dependent perturbation treatment of the *e-h* pair excitations. Alike [26,63], we consider only inter-**k** and thus intraband transitions here in order to mimic the coherent vibrational excitation in experiments. However, the subtle difference is that our approach targets effects of the nonadiabatic coupling on the electronic rather than the nuclear d.o.f., allowing us to explicitly evaluate excitation spectra and to follow the coherent time evolution of the electronic excitations for varying propagation times (cf. Supplemental Material [43]). In contrast, ODF does not explicitly describe electronic excitations as a function either of energy or of time but condenses the matrix elements at the Fermi level into a friction coefficient which then acts as an effective energy

sink for the nuclear motion. This implies a constant coupling in the region energetically relevant to the *e-h* pair excitations [12]. Unlike what is assumed in EFT-equivalent lifetime theory [21,26], our perturbation operator further deviates from a purely harmonic perturbation due to the consideration of spatially varying transition matrix elements $\lambda_{ij}(t)$. Correspondingly, the *e-h* pair excitation spectra calculated using an unperturbed trajectory for the long-time limit, which is in practice already reached after $t_n = 5T = 80$ fs for both systems, also exhibit higher-frequency components; cf. Fig. 1. Such overtones that correspond to excitations of multiple quanta of the molecular stretch frequency arise in the present formalism as a consequence of the simultaneous consideration of infinite electronic coherence and a perturbation that constantly drives *e-h* pair excitations without being affected by the latter.

Integrating the *e-h* pair excitation spectra via Eq. (4) allows us to compare the resulting nonadiabatic energy dissipation rate to the one predicted by EFT, both within the LDFA and ODF (cf. Supplemental Material for further details [43]). First of all, we note that in both theories these rates are very small—less than 1.5% of the vibrational quantum is dissipated per vibrational period—suggesting that first-order perturbation theory should be valid. As further apparent from Fig. 1, our results for CO on Pt(111) fall within the corresponding range spanned by EFT. In contrast, a lower rate is obtained for CO on Cu(100). Consequently, a significantly different nonadiabatic energy dissipation arises for the two systems, exactly as one would have expected on the basis of their metallic band structure. This difference results irrespective of the higher-frequency overtones and is robust, even if the latter are excluded from the integration. The underlying electron and hole excitation spectra shown in Fig. 1 rationalizes this varying agreement between the two theories for both metals. On Pt(111), the most dominant spectral contributions evenly originate from excitations within 250 meV around the Fermi level. Overall, this yields a spectral shape that largely resembles the sigmoid shape of the friction-inspired FOM and—without being imposed—justifies the constant-coupling approximation underlying EFT, which assumes an equal excitation probability of states in the vicinity of the Fermi level and yields the decoherent (Markov) limit [12]. In contrast, on Cu(100), the vibrational motion of the CO molecule specifically triggers excitations from and to a very narrow region of initial and final states. The corresponding spectra thus exhibit prominent peaks at about ± 130 meV but only comparably little contributions directly around the Fermi level as expected within the FOM and EFT. As such, the electron and hole excitation spectra for the two substrates as obtained in the perturbation approach directly reflect their very different band structure: an abundance of available *e-h* pairs resulting in a broad range of excitations on the transition metal as opposed to a distinct coupling between a limited number of states on the coinage metal.

Simultaneously, the occurrence and location of the pronounced excitation peaks for CO on Cu(100) rationalize, for instance, the very large broadening used to obtain ODF tensor elements for this system [17,26,64].

Within the long-time limit, the present theory thus sketches an intuitive picture of the e-h pair excitations governing the vibrational damping. On the other hand, the predicted difference in nonadiabatic energy dissipation rates for the two systems is not reflected in the measured lifetimes; cf. Fig. 1. This calls to scrutinize key assumptions entering the perturbation approach in this long-time limit. Notably, these first concern a perturbation operator that is unaffected by the excitations it triggers which allows us to cast the respective time evolution into an unperturbed trajectory in the nuclear subspace. Second, addressing the electronic subspace, we have so far assumed the persistence of electronic phase coherences as induced through the perturbation for infinite times. We can estimate the consequences of the prior approximation by considering an exponential damping of the (nuclear) vibrational amplitude due to the ongoing energy dissipation. Adding a corresponding exponential damping factor in Eq. (3) simply yields long-time spectra that are convoluted with a Lorentzian of width proportional to the damping but at an otherwise unchanged spectral weight. As such, this approximation unlikely affects the relative dissipation rate of the two systems.

In contrast, the assumption of infinite electronic coherence allows only e-h pair excitations that are resonant with the vibrational perturbation to accumulate appreciable transition probabilities. Shorter coherence times will consequently have an immediate impact on the spectral shape. In the present perturbation approach, we can easily assess this by integrating Eq. (3) over one vibrational period ($T \approx 16$ fs) only, thus assuming that all phase information is reset after this characteristic period of time. The spectra calculated for such pseudo-Markovian systems are shown in Fig. 2. Interestingly, even though a continuum of off-resonant e-h pair excitations is possible now for both systems, this has little effect on the electron and hole excitation spectra, as well as on the energy dissipation rate in the case of Pt(111). This is consistent with the constant-coupling approximation being much better fulfilled for this system even in the long-time limit. In contrast, both $P_{\text{ex},h}(\epsilon_i)$ and $P_{\text{ex},e}(\epsilon_j)$ are strongly modulated in the case of Cu(100) and now resemble much more the sigmoidlike shape of the FOM. Consistently, the energy dissipation rate rises and becomes more compatible with EFT-based results. In consequence, the relative difference in the energy dissipation rate of the two systems decreases and gets closer to the experimental findings.

As such, shorter electronic coherence times could indeed be one reason why the largely different metallic band structure of the two systems does not markedly show up in the vibrational lifetimes. The concomitant possibility to generate off-resonant excitations provides so many individual excitation channels that the detailed density of initial and final states
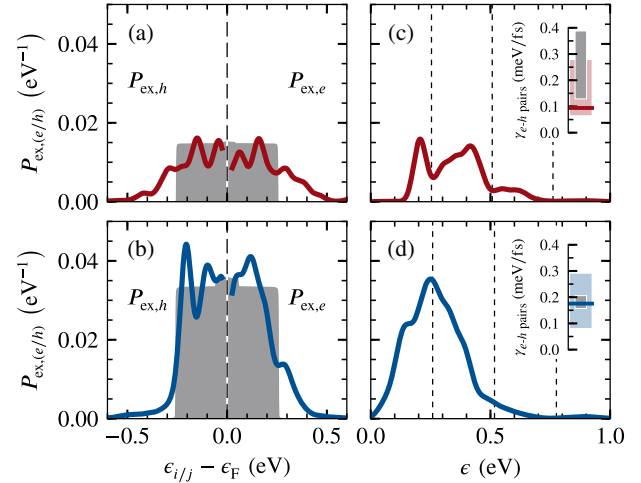
FIG. 2. The same as Fig. 1 but for integration over one vibrational period only to mimic the effect of a finite electronic phase coherence. Please note that, opposed to the energy dissipation rates in the insets, the actual spectra are not normalized with respect to the integration time and thus show significantly lower excitation probabilities as compared to Fig. 1.

averages out. Incidentally, this then justifies the constant-coupling approximation fundamentally relied on in EFT [12] and could rationalize the good agreement of the vibrational lifetimes obtained with this approach. Notwithstanding, even in the present limit of a finite electronic coherence time over one vibrational period only, the energy dissipation rate on Pt(111) remains about double as large as the one on Cu(100). Especially due to the large error bars for the measured vibrational lifetime of CO on Cu(100) [31], it is unclear if this small difference is compatible with the experimental data. New high-precision measurements would thus be most valuable in this respect. Likewise, our calculated spectra suggest that chemicurrentlike measurements as pioneered by Nienhaus *et al.* [66] could allow us to distinguish the two limits for the electronic coherence times. Should such measurements disconfirm the present theoretical prediction, we speculate that other hitherto disregarded dissipation channels have a notable contribution to the measured lifetimes, thus questioning the notion of purely nonadiabatic vibrational energy losses. Likely candidates to this end are small but non-negligible couplings to other adsorbate vibrational modes or the substrate phononic system.

In conclusion, we have extended a numerically efficient TDDFT-based perturbation approach to evaluate explicit e-h pair excitation spectra for the vibrational damping of high-frequency adsorbate modes—a phenomenon that stimulated the popular EFT approach and is still of crucial importance for its justification. This framework allows us to study the detailed effect of different models for the perturbation operator on the electronic subsystem and thus to explicitly test assumptions about the electronic dynamics entering the EFT formalism directly at its roots. Our analysis

shows an unexpectedly large influence of electronic coherence which allows us to rationalize the hitherto enigmatic similarity of measured vibrational lifetimes of CO on Pt(111) and Cu(100). In the limit of infinite electronic coherence, specific state-to-state coupling dominates a smaller nonadiabatic energy dissipation for CO on Cu(100), as one would intuitively expect from the coinage metal band structure. It requires a finite electronic coherence time to open up off-resonant e-h pair excitation channels that raise the dissipation rate to similar levels as found for CO on Pt(111). The resulting multitude of excitation channels washes out the differences in the underlying transition and coinage metal band structure and leads to unstructured electron and hole excitation spectra. Such a spectral shape can, in principle, be measured experimentally and thus constitutes a direct access to most fundamental electronic coherence times. Moreover, the resulting constant coupling is implicitly assumed in EFT, which might explain the good performance of this effective theory in reproducing the experimental lifetimes. Intriguingly, a small relative difference in dissipation rates between the two benchmark systems remains even in the limit of short electronic coherence times. Most accurately determined by new high-precision experiments, this difference is thus a sensitive measure of contributions of hitherto disregarded dissipation mechanisms like vibrational mode coupling or residual coupling to phononic d.o.f. and thus allows us to ultimately shed light into fundamental questions such as the actual degree of nonadiabaticity of the vibrational energy decay.

---

[*]Corresponding author.
simon.rittmeyer@tum.de

[1] J. C. Tully, J. Chem. Phys. **137**, 22A301 (2012).

[2] A. M. Wodtke, Chem. Soc. Rev. **45**, 3641 (2016).

[3] A. Groß, Phys. Rev. Lett. **103**, 246101 (2009).

[4] J. Meyer, Ph.D. thesis, Freie Universität Berlin, 2012.

[5] J. Meyer and K. Reuter, Angew. Chem., Int. Ed. **53**, 4721 (2014).

[6] F. Nattino, D. Migliorini, G.-J. Kroes, E. Dombrowski, E. A. High, D. R. Killelea, and A. L. Utz, J. Phys. Chem. Lett. **7**, 2402 (2016).

[7] V. J. Bukas and K. Reuter, Phys. Rev. Lett. **117**, 146101 (2016).

[8] V. J. Bukas and K. Reuter, J. Chem. Phys. **146**, 014702 (2017).

[9] B. Kolb, X. Luo, X. Zhou, B. Jiang, and H. Guo, J. Phys. Chem. Lett. **8**, 666 (2017).

[10] K. Shakouri, J. Behler, J. Meyer, and G.-J. Kroes, J. Phys. Chem. Lett. **8**, 2131 (2017).

[11] E. G. d'Agliano, P. Kumar, W. Schaich, and H. Suhl, Phys. Rev. B **11**, 2122 (1975).

[12] M. Head-Gordon and J. C. Tully, J. Chem. Phys. **103**, 10137 (1995).

[13] A. C. Luntz, M. Persson, S. Wagner, C. Frischkorn, and M. Wolf, J. Chem. Phys. **124**, 244702 (2006).

[14] J. I. Juaristi, M. Alducin, R. Díez Muiño, H. F. Busnengo, and A. Salin, Phys. Rev. Lett. **100**, 116102 (2008).

[15] M. Blanco-Rey, J. I. Juaristi, R. Díez Muiño, H. F. Busnengo, G. J. Kroes, and M. Alducin, Phys. Rev. Lett. **112**, 103203 (2014).

[16] O. Bünermann, H. Jiang, Y. Dorenkamp, A. Kandratsenka, S. M. Janke, D. J. Auerbach, and A. M. Wodtke, Science **350**, 1346 (2015).

[17] M. Askerka, R. J. Maurer, V. S. Batista, and J. C. Tully, Phys. Rev. Lett. **116**, 217601 (2016); **119**, 069901 (2017).

[18] B. Jiang, M. Alducin, and H. Guo, J. Phys. Chem. Lett. **7**, 327 (2016).

[19] S. P. Rittmeyer, D. J. Ward, P. Gütlein, J. Ellis, W. Allison, and K. Reuter, Phys. Rev. Lett. **117**, 196001 (2016).

[20] B. Hellsing and M. Persson, Phys. Scr. **29**, 360 (1984).

[21] M. Head-Gordon and J. C. Tully, J. Chem. Phys. **96**, 3939 (1992).

[22] P. Saalfrank, J. I. Juaristi, M. Alducin, M. Blanco-Rey, and R. Díez Muiño, J. Chem. Phys. **141**, 234702 (2014).

[23] D. Novko, M. Blanco-Rey, M. Alducin, and J. I. Juaristi, Phys. Rev. B **93**, 245435 (2016).

[24] J. R. Trail, M. C. Graham, D. M. Bird, M. Persson, and S. Holloway, Phys. Rev. Lett. **88**, 166802 (2002).

[25] S. P. Rittmeyer, J. Meyer, J. I. Juaristi, and K. Reuter, Phys. Rev. Lett. **115**, 046102 (2015).

[26] R. J. Maurer, M. Askerka, V. S. Batista, and J. C. Tully, Phys. Rev. B **94**, 115432 (2016).

[27] V. Krishna and J. C. Tully, J. Chem. Phys. **125**, 054706 (2006).

[28] M. Forsblom and M. Persson, J. Chem. Phys. **127**, 154303 (2007).

[29] M. Lindenblatt and E. Pehlke, Phys. Rev. Lett. **97**, 216101 (2006).

[30] M. Grotemeyer and E. Pehlke, Phys. Rev. Lett. **112**, 043201 (2014).

[31] M. Morin, N. J. Levinos, and A. L. Harris, J. Chem. Phys. **96**, 3950 (1992).

[32] J. D. Beckerle, R. R. Cavanagh, M. P. Casassa, E. J. Heilweil, and J. C. Stephenson, J. Chem. Phys. **95**, 5403 (1991).

[33] J. C. Tully, M. Gomez, and M. Head-Gordon, J. Vac. Sci. Technol. A **11**, 1914 (1993).

[34] P. Saalfrank, Chem. Rev. **106**, 4116 (2006).

[35] H. Arnolds, Prog. Surf. Sci. **86**, 1 (2011).

[36] B. Hammer and J. Nørskov, Surf. Sci. **343**, 211 (1995).

[37] This holds for both ODF and LDFA (*vide infra*), since both rely on a summation over states at the Fermi level— intuitively suggesting a high DOS at the Fermi level to correlate with larger friction coefficients (i.e., more efficient e-h pair excitations). Although the LDFA friction coefficients are obtained from an atom-in-jellium model

[38,39] with background electron densities taken to represent the Cu(100) and Pt(111) surfaces, the effect is not disguised—but rather has very little effect on the vibrational damping [25].

[38] E. Zaremba, J. H. Rose, L. M. Sander, and H. B. Shore, J. Phys. F **7**, 1763 (1977).
[39] M. J. Puska and R. M. Nieminen, Phys. Rev. B **27**, 6121 (1983).
[40] J. R. Trail, D. M. Bird, M. Persson, and S. Holloway, J. Chem. Phys. **119**, 4539 (2003).
[41] A. C. Luntz, M. Persson, and G. O. Sitz, J. Chem. Phys. **124**, 091101 (2006).
[42] K. Schönhammer and O. Gunnarsson, in *Many-Body Phenomena at Surfaces*, edited by D. Langreth and H. Suhl (Academic, New York, 1984), pp. 421–451.
[43] See Supplemental Material at http://link.aps.org/supplemental/10.1103/PhysRevLett.119.176808 for more details of the electronic friction-based molecular dynamics simulations, the evaluation of spectra within the FOM, and computational details regarding the underlying DFT calculations. Supplemental Material additionally includes Refs. [44–54].
[44] G. Schatz and M. Ratner, *Quantum Mechanics in Chemistry*, 1st ed., Dover Books on Chemistry Series (Dover, Mineola, NY, 2002).
[45] D. Vanderbilt, Phys. Rev. B **41**, 7892 (1990).
[46] T. L. Ferrell and R. H. Ritchie, Phys. Rev. B **16**, 115 (1977).
[47] F. Hirshfeld, Theor. Chim. Acta **44**, 129 (1977).
[48] G. Bussi and M. Parrinello, Phys. Rev. E **75**, 056707 (2007).
[49] B. Leimkuhler and C. Matthews, Appl. Math. Res. Express **2013**, 34 (2013).
[50] D. A. Sivak, J. D. Chodera, and G. E. Crooks, J. Phys. Chem. B **118**, 6466 (2014).
[51] D. R. Hamann, Phys. Rev. B **88**, 085117 (2013).
[52] M. Schlipf and F. Gygi, Comput. Phys. Commun. **196**, 36 (2015).
[53] H. J. Monkhorst and J. D. Pack, Phys. Rev. B **13**, 5188 (1976).
[54] J. C. Tully, Faraday Discuss. **110**, 407 (1998).
[55] M. Timmer and P. Kratzer, Phys. Rev. B **79**, 165407 (2009).
[56] J. Meyer and K. Reuter, New J. Phys. **13**, 085010 (2011).
[57] E. Runge and E. K. U. Gross, Phys. Rev. Lett. **52**, 997 (1984).
[58] S. J. Clark, M. D. Segall, C. J. Pickard, P. J. Hasnip, M. I. J. Probert, K. Refson, and M. C. Payne, Z. Kristallogr. **220**, 567 (2005).
[59] J. P. Perdew, K. Burke, and M. Ernzerhof, Phys. Rev. Lett. **77**, 3865 (1996); **78**, 1396 (1997).
[60] P. Echenique, R. Nieminen, and R. Ritchie, Solid State Commun. **37**, 779 (1981).
[61] P. M. Echenique, R. M. Nieminen, J. C. Ashley, and R. H. Ritchie, Phys. Rev. A **33**, 897 (1986).
[62] Y. Li and G. Wahnström, Phys. Rev. Lett. **68**, 3444 (1992).
[63] N. Lorente and M. Persson, Faraday Discuss. **117**, 277 (2000).
[64] The results of Refs. [17,26] were recently criticized [65] because of this large broadening. Quite in contrast, the effective broadening within the numerical evaluation of our e-h pair spectra (width of nascent δ functions) is more than 40 times smaller (cf. Supplemental Material [43]).
[65] D. Novko, M. Alducin, M. Blanco-Rey, and J. I. Juaristi, Phys. Rev. B **94**, 224306 (2016).
[66] H. Nienhaus, H. S. Bergh, B. Gergen, A. Majumdar, W. H. Weinberg, and E. W. McFarland, Phys. Rev. Lett. **82**, 446 (1999).

Non-Adiabatic Vibrational Damping of Molecular Adsorbates:
Insights into Electronic Friction and the Role of Electronic Coherence

Simon P. Rittmeyer,[1, *] Jörg Meyer,[2] and Karsten Reuter[1]

[1]*Chair for Theoretical Chemistry and Catalysis Research Center,*
Technische Universität München, Lichtenbergstr. 4, 85747 Garching, Germany
[2]*Leiden Institute of Chemistry, Gorlaeus Laboratories,*
Leiden University, P.O. Box 9502, 2300 RA Leiden, The Netherlands

CONTENTS

I. FORCED OSCILLATOR MODEL

The forced oscillator model (FOM) is a straightforward way to connect frictional energy losses with substrate electron/hole excitations. In essence, one describes the electronic excitations in the substrate through a collection of independent harmonic oscillators that are all driven by an external force of identical functional form but different strength for all excitations [1–3]. The electron excitation spectrum is then given by

$$P_{\text{ex},e}(\omega) = \int_\omega^\infty \frac{1}{\omega} \underbrace{\left(\frac{1}{\hbar\omega} \left| \int_{-\infty}^\infty \sqrt{\eta} \cdot \dot{R}(t)\, e^{-i\omega t}\, dt \right|^2 \right)}_{P_s(\omega)} d\omega.$$

(1)

* Corresponding author: simon.rittmeyer@tum.de

Here, η is the electronic friction tensor and $\dot{R}(t)$ the system velocity vector. By construction the FOM assumes symmetry between electron and hole excitations [2].

As shown in section III C 1 and Ref. 4, the vibrational damping of adsorbate vibrations can be well captured in an effective one-dimensional description using a constant (averaged) friction coefficient. Within the picture of a constantly damped harmonic oscillator (D-HO) we can then already deduce the qualitative shape of the excitation spectrum predicted by the FOM. For a D-HO $\eta \cdot \dot{R}(t)$ is just an exponentially decaying harmonic oscillation, such that the single excitation probability $P_s(\omega)$ in Eq. (1) is an inverse frequency-weighted Lorentzian centered around the oscillation frequency ω_{vib} and a width related to the friction coefficient. From these considerations it follows that the actual spectrum $P_{\text{ex},e}(\omega)$ from Eq. (1) is very similar to a sigmoid function stepped at the vibrational frequency ω_{vib}. This functional form is the same for any friction coefficient, as long as the D-HO picture remains within the weakly damped regime (which in turn is related with the weak coupling approximation underlying the electronic friction approach [5]). The only qualitative effect an increased/decreased friction coefficient has is to widen/narrow this step. Due to the construction of the FOM, there will not be any resolved peak structure revealing different electronic transitions. The entire form of the spectrum is determined by the functional form of the velocity vector and thus the friction force, convoluted with a friction-related broadening function. Neither details of the metallic band structure nor excitations with probabilities that may deviate from the predicted Lorentzian distribution are accounted for. Coupling to other vibrational modes, either due to PES anharmonicity or the friction tensor, will only introduce further steps at the respective vibrational frequencies. Finally, note that within its conceptual simplicity, the FOM as described by Eq. (1) assumes infinitely long coherence of the excited electrons — which is the exact opposite of the Markov limit for which electronic friction coefficients have been obtained [1–3].

II. ANALYTIC LONG-TIME LIMIT FOR PERIODIC PERTURBATION OPERATORS

A. Harmonic Perturbation

The textbook example for a periodic perturbation as given by a vibrating molecule is that of a harmonic perturbation op-

erator

$$\hat{v}_{\text{pert}}(t) = \hat{v}_{\text{pert}} \, e^{\pm i\omega_{\text{vib}}t} . \tag{2}$$

Here, the transition probability from state i to j due to the perturbation starting at $t = 0$ is given as

$$P_{ij}(t) = \left| \frac{1}{i\hbar} \int_o^t \langle j|\hat{v}_{\text{pert}}|i\rangle \, e^{i(\omega_{ji}\pm\omega_{\text{vib}})t'} \, dt' \right|^2 . \tag{3}$$

where $\omega_{ji} = (\epsilon_j - \epsilon_i)/\hbar$. Equation (3) can be solved analytically such that

$$P_{ij}(t) = \frac{2\pi t}{\hbar^2} \left| \langle j|\hat{v}_{\text{pert}}|i\rangle \right|^2 \underbrace{\frac{\sin^2\left(\frac{(\omega_{ji}\pm\omega_{\text{vib}})t}{2}\right)}{2\pi t\left(\frac{\omega_{ji}\pm\omega_{\text{vib}}}{2}\right)^2}}_{\tilde{\delta}(\omega_{ji}\pm\omega_{\text{vib}})} . \tag{4}$$

The function $\tilde{\delta}_t(\omega_{ji} \pm \omega_{\text{vib}})$ is a modified sinc-function in frequency space that can be described as a nascent δ-function by considering the limit

$$\lim_{t\to\infty} \tilde{\delta}_t \left(\omega_{ji} \pm \omega_{\text{vib}}\right) \approx \delta(\omega_{ji} \pm \omega_{\text{vib}}). \tag{5}$$

In the long-time limit the transition probability thus grows linear in time with the respective rate

$$\lim_{t\to\infty} \left[\frac{P_{ij}(t)}{t}\right] = \frac{2\pi}{\hbar^2} \left| \langle j|\hat{v}_{\text{pert}}|i\rangle \right|^2 \delta\left(\omega_{ji} \pm \omega_{\text{vib}}\right) . \tag{6}$$

Equation (6) is essentially the state-to-state form of Fermi's golden rule [6]. In the long-time limit thus only resonant transitions $\omega_{ji} = \pm\omega_{\text{vib}}$ contribute to the rate. Matching these resonant transitions with a discretized representation of the metallic continuum is a numerical nightmare (*vide infra*). Before reaching this limit, also transitions with $\omega_{ji} \neq \omega_{\text{vib}}$ have non-vanishing probabilities as the sudden stop of the perturbation at a certain point in time basically creates all frequencies in the perturbation.

The overall excitation spectrum is then readily obtained by collecting all transitions with $\omega_{ji} > 0$ and sampling at ω

$$P_{\text{ex}}(\omega, t) = \sum_{i,j} P_{ij}(t) \, \delta\left(\omega - \omega_{ji}\right) . \tag{7}$$

Please note the difference between the δ-function used for describing (sampling) the spectrum, and the nascent δ-function from Eq. (3) effectively sampling the density of frequencies of the system. Moreover, please also note that the linear growth of $P_{ij}(t)$ with time in the long-time limit is also reflected directly in a linear growth of the dissipated energy, i.e. the energy formally absorbed by the quantum system.

B. Generic Periodic Perturbation

The perturbation potential we construct based on the snapshot-approximation by Timmer and Kratzer [7, 8] will in

general not only consist of the fundamental vibrational frequency, but it will rather be described by a (suitably truncated) Fourier series expansion

$$\hat{v}_{\text{pert}}(t) = \sum_{m \in \mathbb{Z}} \hat{v}_{\text{pert}}^{(m)} \, e^{i\omega_{\text{vib}}t} \tag{8}$$

In complete analogy to Eq. (3) the transition probability is then obtained via

$$P_{ij}(t) = \frac{2\pi t}{\hbar^2} \sum_{m \in \mathbb{Z}} \left| \langle j|\hat{v}_{\text{pert}}^{(m)}|i\rangle \right|^2 \tilde{\delta}(\omega_{ji} + m\omega_{\text{vib}}), \tag{9}$$

and will thus naturally contain higher-frequency overtones.

III. COMPUTATIONAL DETAILS

A. MD Simulations with Electronic Friction

Assuming a frozen surface, we numerically propagate the coordinates $\boldsymbol{R}_i$ of the N adsorbate atoms via the Langevin equation for the $T = 0\,\text{K}$ case

$$m_i \frac{d^2 R_{i\alpha}}{dt^2} = -\frac{\partial V_{\text{PES}}}{\partial R_{i\alpha}} - \sum_{j=1}^N \sum_{\beta=1}^3 \eta_{i\alpha j\beta} \frac{dR_{j\beta}}{dt} . \tag{10}$$

Here, small latin and greek subscripts denote atoms and Cartesian degrees of freedom, respectively. The electronic friction tensor is $\boldsymbol{\eta}$, m_i is the adsorbate atom mass and V_{PES} is the potential energy surface (PES).

1. Potential Energy Surfaces

For our simulations, we re-use the PESs constructed in Ref. 4, to which the reader is referred to for a complete description of the respective computational details. The electronic energy of the system is evaluated via density functional theory (DFT) using the CASTEP code [9] within the generalized gradient approximation (GGA) by Perdew, Burke and Ernzerhoff (PBE) [10] using ultrasoft pseudopotentials [11]. The considered systems are modeled as top-site adsorbed CO molecules within a $c(2 \times 2)$ and $(\sqrt{3} \times \sqrt{3})\text{R}30°$ surface unit-cell on Cu(100) and Pt(111), respectively. In both cases, the adsorption is C-terminated with the molecular axis oriented perpendicular to the surface. Due to symmetry reasons, the stretch mode and the frustrated molecular translation in z-direction (FT$_z$) do not mix with lateral (xy) coordinates and thus form a decoupled subset of coordinates. An analytic representation of the respective PES is thus conveniently obtained from a bivariate cubic spline interpolation of the electronic energy in this subspace. Based on this interpolation we find $\hbar\omega_{\text{vib}} = 258\,\text{meV}$ and $\hbar\omega_{\text{vib}} = 261\,\text{meV}$ for CO on Cu(100) and Pt(111), respectively, where ω_{vib} is the CO-stretch normalmode frequency.

2. Electronic Friction Tensor

In our study we compare the perturbative non-adiabatic energy losses to results from different approaches based on electronic friction theory. Within the local density friction approximation (LDFA) the electronic friction tensor from Eq. (10) is approximated via isotropic atomic friction coefficients and is thus diagonal in Cartesian coordinates

$$\eta_{i\alpha j\beta} = \eta_i^{\text{LDFA}} \left(\boldsymbol{R}_i \right) \delta_{ij} \delta_{\alpha\beta}. \tag{11}$$

The atomic friction coefficients η_i^{LDFA} are individually evaluated from a reference system of a radially symmetric impurity embedded in a free electron gas of a given embedding density $\rho_{\text{emb},j}$

$$\eta_i^{\text{LDFA}} \left(\boldsymbol{R}_i \right) = \rho_{\text{emb},i} \left(\boldsymbol{R}_i \right) k_F \sigma_{\text{tr}} , \tag{12}$$

where σ_{tr} is the transport cross section obtained from the phase shifts of the respective Kohn-Sham orbitals at the Fermi momentum k_F [12–15]. However, the choice of the host free electron gas-density in Eq. (12) is ambiguous. We thus compare an atoms-in-molecules (AIM) embedding approach [4] based on a Hirshfeld decomposition [16] of the self-consistent system electronic density with the independent-atom approximation (IAA) relying on clean-surface embedding densities [17].

For CO on Cu(100) we additionally compare LDFA-based results to simulations using an orbital dependent formulation (ODF) of the electronic friction tensor (see Ref. 18 and 19 and references therein). In detail, we use a corresponding two-dimensional sub-tensor of the full version published by Askerka *et al.* [18]. In contrast to the LDFA-based simulations, we do not consider any spatial dependence of the so-gained friction tensor in this case.

We further note that neither of both formalisms yields a diagonal friction tensor in normalmode space. The potential electronic friction-induced mode coupling effects beyond PES-related anharmonicity as discussed recently [18, 19] thus also exist within the LDFA. In fact, as shown in Fig. 1, the respective coupling elements are most pronounced for LDFA-IAA. However, from our dynamical simulations we find that these effects are vanishingly small compared to anharmonic mode coupling-effects due to the underlying PES.

3. Numerical Propagation

We propagate Eq. (10) numerically using the modified version of the velocity Verlet algorithm proposed by Bussi and Parinello [20]. The latter is essentially just a particular case of an entire family of integrators originating from a general splitting scheme of the time evolution operator [21, 22]. In the $T = 0\,\text{K}$ case, the stochastic contribution to the Langevin equation of motion vanishes and the required modification of the velocity Verlet algorithm reduces to embracing velocity damping terms

$$\dot{\boldsymbol{R}} \rightarrow \dot{\boldsymbol{R}} \cdot \exp \left(-\tilde{\eta} \frac{\Delta t}{2} \right) \tag{13}$$

FIG. 1. Electronic friction tensor for CO on Cu(100) in equilibrium configuration with the LDFA approach (IAA and AIM) compared to a subset of the ODF-based values published by Askerka *et al.* [18] (in ps^{-1}). The upper row shows the respective tensors in mass-weighted Cartesian coordinates, where the LDFA-based tensors are diagonal by construction. The lower row in contrast shows the respective tensors transformed to normalmode space. None of the shown tensors is diagonal in this basis.

where Δt is the respective discretized time step and $\tilde{\boldsymbol{\eta}}$ is the mass-weighted electronic friction tensor. When propagating in Cartesian coordinates, the evaluation of the exponential of the LDFA-based friction tensor is straightforward. For the ODF tensor, however, Eq. (13) is to be evaluated in the eigenbasis of $\tilde{\boldsymbol{\eta}}$. If $\boldsymbol{\Gamma} = \boldsymbol{U}^T \cdot \tilde{\boldsymbol{\eta}} \cdot \boldsymbol{U}$ is a diagonal matrix [23], then Eq. (13) is replaced by

$$\dot{\boldsymbol{q}} = \boldsymbol{U}^T \cdot \boldsymbol{M}^{1/2} \cdot \dot{\boldsymbol{R}} \tag{14a}$$

$$\dot{\boldsymbol{q}} \rightarrow \exp \left(-\boldsymbol{\Gamma} \frac{\Delta t}{2} \right) \cdot \dot{\boldsymbol{q}} \tag{14b}$$

$$\dot{\boldsymbol{R}} = \boldsymbol{M}^{-1/2} \cdot \boldsymbol{U} \cdot \dot{\boldsymbol{q}}, \tag{14c}$$

where $M_{ij}^{1/2} = \sqrt{m_i} \delta_{ij} \delta_{\alpha\beta}$.

4. Frictional Energy Loss Rates

In the Markov limit, the frictional force is linear in velocity and the dissipated energy over one vibrational period is given by two times Rayleigh's dissipation function

$$E_{\text{diss}} = \int_{\underline{\tau}}^{\overline{\tau}} \dot{\boldsymbol{R}}^T(t) \cdot \boldsymbol{\eta}(\boldsymbol{R}) \cdot \dot{\boldsymbol{R}}(t) \, \text{d}t, \tag{15}$$

where $\boldsymbol{\eta}(\boldsymbol{R})$ is the position-dependent friction tensor, and $\overline{\tau} - \underline{\tau} = T$. In principle, the energy loss rate is well-defined by the integrand in Eq. (15) at each point of the trajectory. Yet, to allow for a valid comparison of both approaches in the main manuscript, we average the frictional energy loss rates over

one vibrational period T to yield

$$\gamma_{eh\text{-pairs}} \approx \frac{1}{T} \int_{\underline{\tau}}^{\underline{\tau}+T} \dot{\boldsymbol{R}}^T(t) \cdot \boldsymbol{\eta}(\boldsymbol{R}) \cdot \dot{\boldsymbol{R}}(t) \, \mathrm{d}t. \qquad (16)$$

Due to the minute energy losses over one vibrational period Eq. (16) actually yields the mean energy loss rate for a virtually unperturbed trajectory (see section III C 1 for an in-depth discussion). We hence consider this to be a well justified quantity to be compared with our perturbative energy loss rates as obtained through Eq. (23).

B. Experimental Energy Loss Rates

To allow for a concise comparison with the different theoretical approaches, we deduce an energy dissipation rate from experimentally measured vibrational lifetimes τ_{exp}. Being very close to the dynamics obtained from the electronic friction approach, we base this analysis on the simple textbook model of a linearly damped harmonic oscillator with constant damping. Averaging the oscillating energy loss rate over a vibrational period we thus obtain

$$\gamma_{eh\text{-pairs}}(t) \approx \frac{E_{\mathrm{vib}}}{\tau_{\mathrm{exp}} \left(1 - \zeta^2\right)} \, \mathrm{e}^{-2\zeta \omega_{\mathrm{vib}} t}, \qquad (17)$$

where $\zeta = (2\tau_{\mathrm{exp}} \omega_{\mathrm{vib}})^{-1}$ is the damping ratio. For the same reasons as given in section III A 4 the most consistent comparison with the theory presented in our work is then the initial energy dissipation rate at $t = 0$.

C. Perturbative Excitation Spectra

1. Trajectories

In general, the trajectory $\boldsymbol{Q}(t)$ is represented by a $3N$ dimensional vector, where N is the number of atoms the admolecule consists of. Surface motion is considered to be negligible for present purposes, but could be included in future applications. As has already been explained in section III A, focusing on the stretch-mode dynamics of CO allows to reduce this dimensionality to only include the adsorbate atoms' Cartesian z-coordinates $\boldsymbol{R}_z$. Moreover, neglecting the PES-induced coupling from stretch to FT_z mode for one vibrational period, a convenient one-dimensional descriptor of the actual dynamics is the stretch amplitude $Q_{\mathrm{stretch}}(t)$ of the two-dimensional position vector in normalmode space defined as

$$\begin{pmatrix} Q_{\mathrm{stretch}}(t) \\ Q_{\mathrm{FT}_z}(t) \end{pmatrix} = \boldsymbol{U}^T \boldsymbol{M}^{1/2} \left(\boldsymbol{R}_z(t) - \boldsymbol{R}_z(\tau_{\mathrm{eq}}) \right). \qquad (18)$$

Here, $\boldsymbol{U}$ is the matrix consisting of the normalmode vectors that diagonalizes the mass-weighted force constant matrix, and $M_{ij}^{1/2} = \sqrt{m_i} \delta_{ij} \delta_{\alpha\beta}$.

We assign the trajectory energy as pure kinetic energy such that the resulting velocity vector is perfectly aligned with the
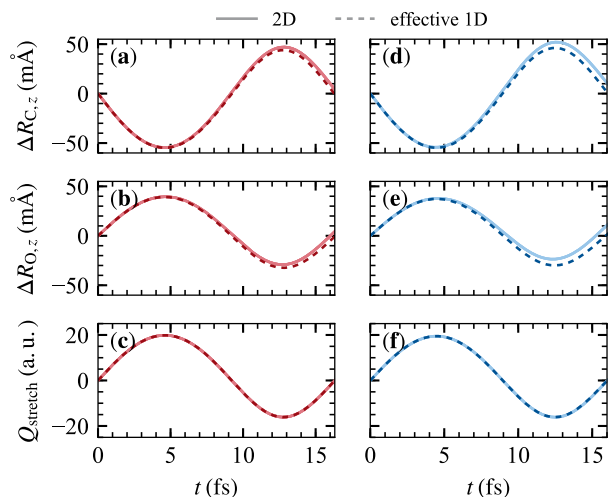

FIG. 2. Frictionless trajectories for $E_{\mathrm{vib}} = \frac{3}{2} \hbar \omega_{\mathrm{vib}}$ generated with the effective one-dimensional PES (dashed lines) as compared to those from the actual two-dimensional PES (drawn lines) for (a)–(c) CO on Cu(100) and (d)–(f) Pt(111). Please note that there are drawn lines for frictionless 2D-trajectories as well as 2D-trajectories including different electronic friction tensors as detailed in section III A 2. Yet, the frictional damping effect is negligible over one vibrational period, which is why one cannot distinguish them from each other. Obviously, the effective one-dimensional propagation in normalmode space yields a convincing description of the respective atomic Cartesian displacements ΔR_z. The projection of the Cartesian displacements into normalmode space yields virtually identical amplitudes as indicated in (c) and (f).

stretch mode vector obtained from a prior normalmode analysis of the PES detailed in section III A 1. We then numerically propagate trajectories according to the forces from this PES but neglect FT_z-mode components of the force vector. This procedure thus yields an effective propagation in a one-dimensional cut of the PES aligned with the stretch mode. We did not use direct forces from the full PES in section III A 1 as the minute though existing potential-induced coupling from the stretch mode to the frustrated translation in z-direction yields a motion pattern that is a superposition of both modes. Hence, to obtain a completely closed trajectory (same start and end configuration) as fundamentally required for the perturbative treatment of adsorbate vibrations, the resulting integration times would be much longer than in our decoupled and thus effectively one-dimensional approximation.

We have carefully verified this approximation to still yield very accurate trajectories. This is visualized in Fig. 2. There is obviously only a minute deviation of the atomic cartesian displacements as compared the a propagation on the "full" PES from section III A 1. Moreover, by comparing the frictionless trajectory from the "true" PES with the frictional counterparts we note that the dissipative effect of the frictional force within any model is virtually non-existing compared to the mode coupling effect of the underlying PES. All in all, these findings justify our approximation of an unperturbed trajectory for an

isolated, uncoupled stretch-mode.

2. Perturbation Potential

Instead of directly evaluating the gradient of the perturbation potential matrix elements as suggested from

$$\lambda_{ij}(t_n) = \int_0^{t_n} \left\langle j \left| \nabla_{\boldsymbol{Q}} \hat{v}_{\text{pert}} \left(\boldsymbol{Q}(t)\right) \right| i \right\rangle \cdot \dot{\boldsymbol{Q}}(t)\, e^{i\frac{\epsilon_{ji}}{\hbar}t}\, dt, \tag{19}$$

Meyer and Reuter [8] proposed a very efficient interpolation-approach which we also adapt here. At first the elements

$$V_{ij} = \langle j | \hat{v}_{\text{eff}}\left(\boldsymbol{Q}(t)\right) | i \rangle \tag{20}$$

are evaluated from static DFT calculations on a grid along the trajectory. Here, $\hat{v}_{\text{eff}}\left(\boldsymbol{Q}(t)\right)$ is the effective Kohn-Sham (KS) single particle potential at the respective snapshots. Afterwards, the elements are interpolated along $\boldsymbol{Q}(t)$ to give an analytical expression $M_{ij}\left(\boldsymbol{Q}(t)\right)$. The derivative of this interpolated expression with respect to $\boldsymbol{Q}(t)$ then yields a good approximation

$$\begin{aligned}\frac{\partial M_{ij}\left(\boldsymbol{Q}(t)\right)}{\partial \boldsymbol{Q}} &\approx \frac{\partial}{\partial \boldsymbol{Q}} \left\langle j \left| \hat{v}_{\text{eff}}\left(\boldsymbol{Q}(t)\right) \right| i \right\rangle \\ &= \frac{\partial}{\partial \boldsymbol{Q}} \left\langle j \left| \hat{v}_{\text{pert}}\left(\boldsymbol{Q}(t)\right) \right| i \right\rangle \end{aligned} \tag{21}$$

for the matrix elements required for the calculation of the excitation spectra. Note that the static contribution $\hat{v}_{\text{eff}}(\boldsymbol{Q}_0)$ to the perturbation potential $\hat{v}_{\text{pert}}\left(\boldsymbol{Q}(t)\right) = \hat{v}_{\text{eff}}\left(\boldsymbol{Q}(t)\right) - \hat{v}_{\text{eff}}(\boldsymbol{Q}_0)$ vanishes when taking the derivative. Furthermore the derivatives from Eq. (21) are analytically known as soon as the matrix elements M_{ij} are interpolated along $\boldsymbol{Q}(t)$ using e.g. cubic splines. Finally, the dressed matrix elements can be written as

$$\lambda_{ij}(t_n) \approx \int_0^{t_n} \left(\frac{\partial}{\partial \boldsymbol{Q}} M_{ij}\left(\boldsymbol{Q}(t)\right) \right) \cdot \dot{\boldsymbol{Q}}(t)\, e^{i\frac{\epsilon_{ji}}{\hbar}t}\, dt. \tag{22}$$

We evaluate the matrix elements from Eq. (20) on a dense grid of $\Delta Q_{\text{stretch}} = 0.1$ a.u. spacing using density functional theory (DFT) as implemented through a custom extension [8, 24] to the CASTEP code [9]. Exchange-correlation effects are treated within the generalized gradient approximation (GGA) using the functional by Perdew, Burke and Ernzerhoff (PBE) [10]. The geometrical setup of the respective slabs is the same as detailed in section III A 1. However, in order to avoid artificial overlap between orthonormal eigenstates we do not use ultrasoft pseudopotentials (USPPs) here but rather resort to optimized norm-conserving Vanderbilt pseudopotentials (ONCVPPs) [25, 26] that in turn require a significantly higher plane wave cut-off energy of 1000 eV to yield properly converged results. Yet, as visualized in Fig. 3 we find that the actual total electronic energies E_{el} determining the vibrational dynamics are virtually identical for both settings.

Moreover, as compared to the calculations mentioned in section III A 1 and Ref. 4 we tighten the convergence criteria for the total electronic energy in the SCF cycle from
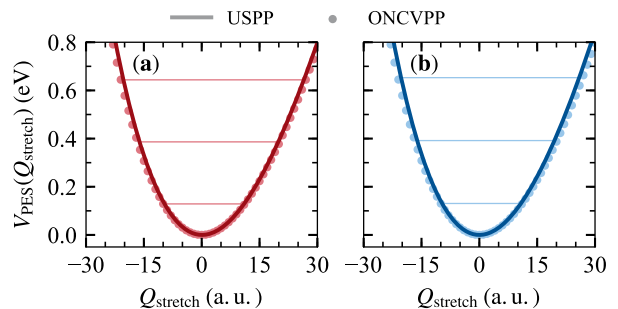

FIG. 3. Comparison of the electronic energies $V_{\text{PES}} = E_{\text{el}}(Q_{\text{stretch}}) - \min\{E_{\text{el}}(Q_{\text{stretch}})\}$ for CO on (a) Cu(100) and (b) Pt(111) as obtained from the calculations of the matrix elements in Eq. (20) using optimized norm-conserving Vanderbilt pseudopotentials (ONCVPPs), and a cut along the stretch mode direction of the PES detailed in section III A 1 based on ultrasoft pseudopotentials (USPPs). Horizontal lines indicate vibrational levels.

1×10^{-5} meV/atom to 1×10^{-8} meV/atom, and use a significantly denser sampling of reciprocal space in terms of a $(40 \times 40 \times 1)$ and $(20 \times 20 \times 1)$ grid of Monkhorst-Pack $\boldsymbol{k}$-points [27] for CO on Cu(100) and Pt(111), respectively. We further replace the sampling δ-function in the numerical evaluation of the spectra with a Gaussian function of broadening width $\sigma = 25$ meV.

3. Long-time Spectra

When evaluating long-time spectra we face the problem of sampling the metallic continuum on a finite grid. This means that even though we are using an extremely dense $\boldsymbol{k}$-point grid we cannot correctly represent the actual resonant frequencies. Hence we integrate the transition matrix elements to times t_n which are large enough such that the energy dissipation rate has reached a plateau, but small enough such that we avoid numerical instabilities. Figure 4 depicts the corresponding energy dissipation rate

$$\gamma_{eh\text{-pairs}} = \frac{1}{t_n} \int_0^{\infty} \epsilon\, P_{\text{ex}}(\epsilon; t_n)\, d\epsilon\ . \tag{23}$$

We thus approach the long-time limit δ-function from Eq. (6) through the progressively sharper nascent $\tilde{\delta}$-function in Eq. (5). The width of the main peak of this function centered around ω_{vib} is given through $\Delta E = 2\pi\hbar/t_n$ [6]. As shown in Fig. 4, the maximum stable integration time for both systems is $t_n \approx 320$ fs which results in $\Delta E \approx 13$ meV. We note that this value is a fraction of the smearing widths required to numerically converge recently published ODF calculations [19].

4. Connection and Differences to Vibrational Lifetime Theories

The matrix elements occuring in Eq. (19) suggest a close relationship of our approach with the vibrational lifetime theory by Hellsing and Persson [28] based on linear response. A
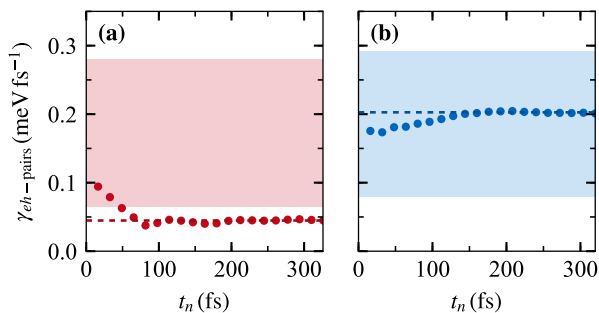
FIG. 4. Energy dissipation rate $\gamma_{eh\text{-pairs}}$ according to Eq. (23) as a function of the integration length $t_n = nT$ for CO on (a) Cu(100) and (b) Pt(111). The horizontal line marks the average over the last 10 data points. The shaded region indicates the range of values we obtain from our MD simulations with electronic friction over one vibrational period (cf. section III A).

respective generalization of this concept to any kind of motion has been shown by Trail and coworkers [2] which, again, underscores the close connection of electronic friction and vibrational damping. This approach can be shown to be equivalent [29] to the one by Head-Gordon and Tully (HGT) for the vibrational relaxation rates based on perturbation theory [30]. Here, the authors themselves demonstrated the respective connection to electronic friction in their seminal work on molecular dynamics with electronic friction [5]. To stress the differences to our approach, we will focus on the HGT theory for the sake of conceptual similarity. Thereby we will only sketch fundamental differences and refer the reader to Refs. 19, 30, and 31 for a nice derivation of the HGT approach, as well as to Ref. [8] for a detailed derivation of our approach.

The difference between our method and these quantum vibrational lifetime theories is a question of *different perspectives*. Within our approach, we consider a time-resolved one-way coupling between nuclear and electronic degrees of freedom, and thus a *driven electronic system*. That is, the nuclear motion is considered as an external perturbation to the electronic system, given through a classical trajectory and concomitant time-dependent changes in the electronic Hamiltonian. The perturbation thus acts only in the electronic subspace, and we consider the nuclear motion to be classical and independent of the electron dynamics, as detailed in section III C 1. Our approach is thus very much in the spirit of the classical path and Redfield method for mixed quantum-classical dynamics (see, e.g., Ref. 32) in order to evaluate the effect of non-adiabatic coupling on the electronic system along the unperturbed nuclear path. Ultimately, this allows to investigate the effects of electronic coherence, but also to explicitly resolve the respective excitation spectrum.

In turn, the HGT approach to vibrational lifetimes considers the non-adiabatic coupling between adiabatic vibronic states, i.e., single-configurational products of nuclear (vibrational) states and electronic Born-Oppenheimer states for the equilibrium configuration. Based on Fermi's Golden Rule, the objective is the decay rate of the first excited vibrational state into

any state in the continuum of vibronic states associated with the vibrational ground state. Focus here is thus not on the electronic excitations induced by the nuclear motion, but rather on the effect of the non-adiabatic coupling on the nuclear vibrations. There is thus no resolved spectrum (just a sum over couplings yielding a decay rate), and no explicit time-dependence of the perturbation as the Golden Rule is a $t \to \infty$ limit, cf. Eq. (6).

In HGT-theory, the nuclear wave functions are taken to be stationary quantum harmonic oscillator wave functions, whereas our approach considers a more rigorous kind of periodic motion, notably invoking spatially varying perturbation matrix elements as detailed the main manuscript and section II B. Moreover, the HGT perturbation is given as matrix element of the nuclear kinetic energy operator between vibronic states, and consequently acts in both the nuclear and electronic subspace, which are thus mutually coupled to each other. A de-excitation in the one subspace requires an excitation in the other subspace. We further note that the sole position-dependence of the friction coefficient/lifetime expression is a manifestation of the Markov approximation.

[1] J. R. Trail, M. C. Graham, D. M. Bird, M. Persson, and S. Holloway, Phys. Rev. Lett. **88**, 166802 (2002).

[2] J. R. Trail, D. M. Bird, M. Persson, and S. Holloway, J. Chem. Phys. **119**, 4539 (2003).

[3] A. C. Luntz, M. Persson, and G. O. Sitz, J. Chem. Phys. **124**, 091101 (2006).

[4] S. P. Rittmeyer, J. Meyer, J. I. Juaristi, and K. Reuter, Phys. Rev. Lett. **115**, 046102 (2015).

[5] M. Head-Gordon and J. C. Tully, J. Chem. Phys. **103**, 10137 (1995).

[6] G. Schatz and M. Ratner, *Quantum Mechanics in Chemistry*, 1st ed., Dover Books on Chemistry Series (Dover Publications, Mineola, NY, 2002).

[7] M. Timmer and P. Kratzer, Phys. Rev. B **79**, 165407 (2009).

[8] J. Meyer and K. Reuter, New J. Phys. **13**, 085010 (2011).

[9] S. J. Clark, M. D. Segall, C. J. Pickard, P. J. Hasnip, M. I. J. Probert, K. Refson, and M. C. Payne, Z. Kristallogr. **220**, 567 (2005).

[10] J. P. Perdew, K. Burke, and M. Ernzerhof, Phys. Rev. Lett. **77**, 3865 (1996); **78**, 1396 (1997).

[11] D. Vanderbilt, Phys. Rev. B **41**, 7892 (1990).

[12] T. L. Ferrell and R. H. Ritchie, Phys. Rev. B **16**, 115 (1977).

[13] P. Echenique, R. Nieminen, and R. Ritchie, Solid State Commun. **37**, 779 (1981).

[14] P. M. Echenique, R. M. Nieminen, J. C. Ashley, and R. H. Ritchie, Phys. Rev. A **33**, 897 (1986).

[15] M. J. Puska and R. M. Nieminen, Phys. Rev. B **27**, 6121 (1983).

[16] F. Hirshfeld, Theor. Chim. Acta **44**, 129 (1977).

[17] J. I. Juaristi, M. Alducin, R. Díez Muiño, H. F. Busnengo, and A. Salin, Phys. Rev. Lett. **100**, 116102 (2008).

[18] M. Askerka, R. J. Maurer, V. S. Batista, and J. C. Tully, Phys. Rev. Lett. **116**, 217601 (2016).

[19] R. J. Maurer, M. Askerka, V. S. Batista, and J. C. Tully, Phys. Rev. B **94**, 115432 (2016).

[20] G. Bussi and M. Parrinello, Phys. Rev. E **75**, 056707 (2007).

[21] B. Leimkuhler and C. Matthews, Appl. Math. Res. Express **2013**, 34 (2013).

[22] D. A. Sivak, J. D. Chodera, and G. E. Crooks, J. Phys. Chem. B **118**, 6466 (2014).

[23] The transformation matrix U is orthogonal, i.e., $U^{-1} = U^T$ since $\tilde{\eta}$ is real-symmetric by construction [18].

[24] J. Meyer, *Ab initio Modeling of Energy Dissipation during Chemical Reactions at Transition Metal Surfaces*, Phd thesis, Freie Universität Berlin, Germany (2012).

[25] D. R. Hamann, Phys. Rev. B **88**, 085117 (2013).

[26] M. Schlipf and F. Gygi, Comp. Phys. Comm. **196**, 36 (2015).

[27] H. J. Monkhorst and J. D. Pack, Phys. Rev. B **13**, 5188 (1976).

[28] B. Hellsing and M. Persson, Phys. Scr. **29**, 360 (1984).

[29] N. Lorente and M. Persson, Faraday Discuss. **117**, 277 (2000).

[30] M. Head-Gordon and J. C. Tully, J. Chem. Phys. **96**, 3939 (1992).

[31] V. Krishna and J. C. Tully, J. Chem. Phys. **125**, 054706 (2006).

[32] J. C. Tully, Faraday Discuss. **110**, 407 (1998).